THESIS FOR THE DEGREE OF DOCTOR OF PHILOSOPHY

Fatigue improvement of steel bridges with high-frequency mechanical impact treatment

POJA SHAMS-HAKIMI

Department of Architecture and Civil Engineering
Division of Structural Engineering
Lightweight Structures
CHALMERS UNIVERSITY OF TECHNOLOGY
Gothenburg, Sweden 2020

Fatigue improvement of steel bridges with high-frequency mechanical impact treatment
POJA SHAMS-HAKIMI
ISBN 978-91-7905-251-5

Doktorsavhandlingar vid Chalmers tekniska högskola
Ny serie nr 4718
ISSN 0346-718X

Department of Architecture and Civil Engineering
Division of Structural Engineering, Lightweight Structures
Chalmers University of Technology
SE-412 96 Gothenburg
Sweden
Telephone: + 46 (0)31-772 1000

Cover:
Aquarelle painting of a suspension bridge created by Caroline Shams Hakimi.

Chalmers Reproservice
Gothenburg, Sweden, 2020

To Caroline, Miryam, Meysam
and my father

Fatigue improvement of steel bridges with high-frequency mechanical impact treatment

POJA SHAMS-HAKIMI
Department of Architecture and Civil Engineering
Division of Structural Engineering, Lightweight Structures
Chalmers University of Technology

ABSTRACT

This thesis investigates the performance of fatigue-improved welds with high-frequency mechanical impact (HFMI) for application on new bridges. Fatigue strength improvement with HFMI can enable lightweight design of bridges and allow the utilisation of the benefits of high-strength steels. Studies of various bridge types were performed in this thesis showing that 20% material saving is possible in the main load-carrying members through post-weld treatment and the use of increased steel grades ($f_y > 355$ MPa) where necessary. Limitations of the application of HFMI treatment on bridges were also identified, related to the degree of improvement and choice of steel grade.

Experimental work of HFMI-treated joints with thick main plates relevant for bridges is scarce in the literature and comprehensive studies on the thickness effect are few. Therefore, the thickness effect was studied based on an established database of 582 fatigue test results of different types of HFMI-treated joints, collected from 28 studies. It was shown that the thickness effect becomes weaker than what is recommended for as-welded joints as a result of HMFI treatment. Fatigue experiments were conducted on a typical fatigue-prone detail in steel bridges with load-carrying plates of 40 and 60 mm which showed a significant fatigue strength improvement after HFMI treatment, exceeding recommended fatigue strengths given by the International Institute of Welding. Based on the fatigue experiments, a weak thickness effect was derived for non-load-carrying transverse attachment joints where the attachment and weld sizes are kept constant.

The performance of HFMI-treated welds in composite steel and concrete road bridges was studied through a state-of-the-art review and simulations of variable amplitude in-service stresses in four case-study bridges in Sweden. It was shown that, in such bridges, very high and varying stress ratios are present due to a high portion self-weight stresses, which constitute up to 50% of the highest total stresses. Furthermore, it was revealed that the fatigue-critical locations in HFMI-treated bridges remain unchanged compared with conventional bridges and that compressive overloads pose no detrimental effect that requires additional attention in the fatigue assessment. Variable amplitude experiments with a bridge spectrum load from the case studies were conducted, including both low and high mean stress tests. The low mean stress tests performed equally or better than the constant amplitude fatigue strength, confirming that bridge loads do not pose any additional damaging effect for non-load-carrying transverse attachment specimens. The high mean stress tests clearly reflected the detrimental effect of high tensile self-weight stresses and enabled verification and development of approaches to consider these effects in design.

Keywords: fatigue; thickness effect; variable amplitude; bridge; steel; HFMI;

Preface

The work in this thesis was carried out between January 2015 and December 2019 in Gothenburg, Sweden, as a collaboration between the company ELU Konsult AB, WSP Sverige AB and the Division of Structural Engineering at Chalmers University of Technology. The extended summary of this thesis is a modification and extension of the author's Licentiate thesis [1]. The funding was provided by the Swedish Transport Administration, the Norwegian Public Road Administration as well as by Vinnova and Formas.

I want to express my gratitude and appreciation to my supervisor, Associate Professor Mohammad Al-Emrani, for his professional engagement throughout the five years of this project, but also the tremendous support on a personal level. Special thanks to Doctor Fredrik Carlsson whose help was invaluable for the completion of this thesis. I would also like to thank my co-supervisors during this period, Doctor Farshid Zamiri, Assistant Professor Halid Can Yıldırım and Doctor Asma Manai.

Many thanks to all the partners in the Vinnova project: Joakim Hedegård and Christof Schneider from Swerea KIMAB for valuable discussions and for performing the weld scanning in the experimental part of this thesis, Mattias Clarin from SSAB for providing the steel materials for the test specimens, Tennce Carlsson from Lecor Stålteknik AB for manufacturing the specimens and Paul Lefevre from SONATS for performing the HFMI treatment and the residual stress measurement. Special thanks to Professor Zuheir Barsoum and his co-workers, Doctor Mansoor Khurshid and Mister Ahmad Mahmoudi for performing parts of the fatigue experiments at the Royal Institute of Technology in Stockholm.

To my wife, Caroline, I am grateful for all your love, support and perseverance. To my father, I thank you for always believing in me. Finally, I take this opportunity to express my love for my five- and seven-year-old kids, Meysam and Miryam. You guys are the best!

Gothenburg, 2020
Poja Shams-Hakimi

LIST OF PUBLICATIONS

This thesis is based on the work contained in the following papers:

Paper I

P. Shams Hakimi, A. Mosiello, K. Kostakakis, och M. Al-Emrani, ”Fatigue life improvement of welded bridge details using high frequency mechanical impact (HFMI) treatment”, in The 13th Nordic Steel Construction Conference (NSCC.2015). Tampere University of Technology, Tampere, Finland, 2015, s. 201–202.

Paper II

P. Shams-Hakimi, H. C. Yıldırım, och M. Al-Emrani, ”The thickness effect of welded details improved by high-frequency mechanical impact treatment”, *International Journal of Fatigue*, vol. 99, Part 1, s. 111–124, 2017, doi: http://doi.org/10.1016/j.ijfatigue.2017.02.023.

Paper III

P. Shams-Hakimi, F. Zamiri, M. Al-Emrani, och Z. Barsoum, ”Experimental study of transverse attachment joints with 40 and 60 mm thick main plates, improved by high-frequency mechanical impact treatment (HFMI)”, *Engineering Structures*, vol. 155, s. 251–266, 2018, doi: http://doi.org/10.1016/j.engstruct.2017.11.035.

Paper IV

P. Shams-Hakimi, F. Carlsson, and M. Al-Emrani, “Assessment of in-service stresses in steel bridges for high-frequency mechanical impact applications,” submitted to *Engineering Structures, 2020.*

Paper V

P. Shams-Hakimi and M. Al-Emrani, “High-cycle variable amplitude fatigue experiments and a design framework for bridge welds treated by high-frequency mechanical impact,” submitted to *Engineering Structures, 2020.*

Author's contributions to jointly published papers

The contribution of the author of this thesis to the appended papers is described here.

I. Responsible for planning and writing the paper, performing the literature review and the parametric study. The co-authors performed the feasibility studies, reviewed the work and provided comments.

II. Responsible for planning and writing the paper, performing the literature review, analysing the experimental data and performing the numerical analyses. The co-authors reviewed the work and provided comments.

III. Responsible for planning and writing the paper, executing 60% of the fatigue experiments, performing the microstructural investigation, analysing the experimental results and performing the fracture mechanics calculations. The co-authors reviewed the work, provided comments and performed 40% of the fatigue testing.

IV. Responsible for planning and writing the paper, performing the literature review, simulating the traffic response and analysing the results. The co-authors reviewed the work, provided comments and helped with the probabilistic part.

V. Responsible for planning and writing the paper, performing the fatigue experiments, analysing the results and developing the design framework. The co-author reviewed the work, provided comments and helped with the design framework development.

CONTENTS

Extended Summary

1 Introduction

1.1 Background

Fatigue damage evolves under cyclic loading at levels lower than the elastic limit of the material and results in cracks that initially can be difficult to detect. Under adverse situations and if not detected, such cracks can develop rapidly and cause failure in structures. This makes fatigue often the governing criterion in the design of steel bridges, especially considering the long service lives of 80 to 120 years during which bridge elements are subjected to millions of load cycles. Fatigue damage emanates at sites where geometric changes give rise to stress concentration. Weldments are examples of such sites and constitute the most susceptible parts of bridges to fatigue damage. Despite the disadvantages with regards to fatigue, welding is the predominant joining method in steel bridges.

With the introduction of the Eurocodes as design standards for bridges in Sweden, the fatigue limit state has been found to govern the design to a greater extent than before, such that new bridge designs require more material. This has led to the loss of competitiveness of steel and composite steel/concrete bridges. Yet, these types of bridges possess advantages such as high strength to weight ratio, the possibility of pre-manufacturing and quick assembly as well as launching methods that are essential in certain circumstances. Utilising existing technologies to solve the fatigue problem would, therefore, imply obvious advantages and potentially reduce the material consumption in such bridges.

Post-weld fatigue improvement techniques can substantially increase the endurable number of load cycles in structures by improving the fatigue properties of weldments in which the fatigue cracks emanate from the weld toe; the transition region between base and weld material. Such techniques include *stress concentration reducing* or *residual stress-based* methods. The stress concentration reducing techniques involve grinding or TIG re-melting of the weld toe, improving the fatigue strength through enlarged transition radius. The residual stress-based methods mainly rely on either removing the tensile residual stresses from welding or even introducing compressive residual stresses which delay the formation and propagation of fatigue cracks. Such techniques include post-weld heat treatment, shot peening, needle/hammer peening or the more recent high-frequency mechanical impact treatment.

High-frequency mechanical impact (HFMI) treatment has proven to be one of the most efficient techniques for fatigue enhancement [2]–[5], yielding the greatest improvement

in the high-cycle regime, where the fatigue load consists of relatively small stress ranges, such as in bridges. This treatment improves the fatigue strength at the weld toe through high-frequency impacts (>90 Hz) of indenters made of high-strength steel, normally attached to hand-held tools. The improvement mechanisms involve 1) introduction of compressive residual stresses through plastic deformation, which reduces the effective part of the stress range causing fatigue damage, 2) smoothening of the weld toe, which decreases stress concentration and 3) strain hardening of the material through plastic deformation, which increases the material's resistance against crack initiation. HFMI tool manufacturers use brand names such as Ultrasonic Impact Treatment (UIT), Ultrasonic Needle Peening (UNP), Ultrasonic Peening (UP), High-frequency Impact Treatment (HiFIT) and Pneumatic Impact Treatment (PIT). In general, all these HFMI tools produce equivalent improvement of the fatigue strength at the weld toe [6][7]. An example of an HFMI tool and indenters is shown in Figure 1.

Figure 1. An example of an HFMI tool and indenters [8].

In 2016, the International Institute of Welding (IIW) adopted the HFMI technique by providing fatigue assessment and quality assurance recommendations for this post-weld treatment method [9]. The IIW specifies that the improvement recommendations are valid for the fatigue strength of the weld toe in steel materials with yield stresses from $f_y = 235$ to 960 MPa and plate thicknesses between $t = 5$ and 50 mm [9]. The recommendations are based on studies that show a change of slope of the SN curve, m, from 3 to 5 [10], material strength dependence [11] and influence of variable amplitude loading [6][12] on the fatigue strength after HFMI treatment. Furthermore, conditions are given for the stress ratio, R (S_{min}/S_{max}), as well as the maximum and minimum stress which have an important influence on the fatigue strength after HFMI treatment [7][13]–[15].

This thesis mainly aims at studying aspects of HFMI treatment that are relevant for bridge applications. Two main topics of investigation were chosen; 1) the influence of

main plate thickness on the fatigue strength of HFMI-treated joints and 2) the performance of these joints under realistic load conditions in bridges. Although the IIW treats the effect of thickness on fatigue strength, the research on which these recommendations were based does not cover HFMI-treated joints. In fact, no systematic and detailed investigation of the thickness effect with a large enough sample size of fatigue experiments exists in the literature for HFMI-treated joints. Since relatively thick plates are common in bridges and can be expected in HFMI-improved bridges as well, a thorough understanding of the influence of HFMI treatment on the thickness effect is justified.

The fatigue performance under realistic in-service loading can be sensitive to the different characteristics of the load, especially for HFMI-treated joints. For each field of application, it is necessary to build up enough results of variable amplitude spectrum load fatigue experiments to safely propose guidelines and recommendations. There are currently just a handful of experimental studies available with variable amplitude loads relevant for bridges. Furthermore, no research or guidance exists currently on the treatment of variable amplitude loads with high overall mean stresses and where the mean stresses and stress ratios vary, which is the case in bridges.

1.2 Aim and objectives

The overall aim of this thesis is to investigate the fatigue performance of HFMI-treated welds under conditions applicable to bridges. To that end, the following research questions in the form of objectives have been defined for this project.

1) To study the potential benefit of HFMI treatment on common bridge types in terms of material saving and to identify limitations of using HFMI in bridge applications in terms of the degree of improvement and steel grades.

2) To study the influence of thickness on the fatigue strength, based on existing experimental fatigue results published in the literature of HFMI-treated joints.

3) To investigate the degree of fatigue strength improvement by HFMI for a typical fatigue-prone bridge detail with large main plate thicknesses and relevant material yield stresses, through experimental work and analytical models.

4) To quantify and characterise realistic in-service stresses in bridges and assess the performance of HFMI-treated welds with respect to these load conditions.

5) To experimentally evaluate the performance of HFMI-treated welds subjected to variable amplitude bridge loads and to quantify the severity of the mean stress effect under spectrum loading.

6) To propose design procedures for fatigue strength prediction and the treatment of high and varying mean stresses and stress ratios under variable amplitude loading.

1.3 Method and scientific approach

The scientific approach comprised literature reviews, experimental work and the use of analytical models and numerical tools. The two main literature reviews in this thesis were related to the effects of thickness and variable amplitude loading on the fatigue performance of HFMI-treated welds. The thickness effect was assessed based on published experimental fatigue test results of HFMI-treated joints with the nominal stress approach. Numerical analyses with the effective notch stress approach were also performed to further investigate the thickness effect. Additional fatigue experiments were conducted under four-point bending of non-load-carrying transverse attachment details with large main plate thicknesses which were lacking in the literature. Crack growth analyses with linear elastic fracture mechanics were employed to modify the experimental results to represent axial loading. Traffic measurement data (BWIM) were used to simulate in-service stresses in bridges and to quantify and characterise these stresses for the assessment of HFMI-treated welds. To that end, various case-study bridges were used, which enabled calculation of realistic stress magnitudes and evaluation of mean stresses from real permanent loads (i.e. from self-weight). A critical spectrum load from the above study was used in fatigue testing to investigate the performance of HFMI-treated welds under these conditions and to quantify the mean stress effect. The results from the tests were used to develop and verify a design framework.

1.4 Limitations

- This thesis focuses on fatigue improvement with HFMI treatment to provide the necessary knowledge and design recommendations for the implementation of this method in the design of new bridges. Thereby, the scope does not include aspects of repair or retrofitting of existing structures.

- All the bridge investigations in this thesis include conventional girder bridges. Other types of bridges such as bridges with box girders or truss bridges are not investigated. This implies that the investigated bridges also involved conventional construction methods. Special construction methods such as the launching of steel sections are therefore not included.

- The investigations of the effect of thickness on fatigue strength are limited to low mean stress and constant amplitude fatigue loading.

- The simulated in-service bridge stresses, the variable amplitude fatigue experiments and some of the related design procedure proposals are limited to the investigated traffic pool which is relevant for Swedish conditions.

1.5 Outline of the thesis

This thesis is mainly based on one conference paper and four journal papers. Additional work which has not been published in papers is also included. The extended summary of this thesis is a modification and extension of the author's Licentiate thesis [1]. The outline of the thesis is as follows.

Chapter 1: This chapter gives background and justification of the research and defines the problem statements in the form of objectives. The chapter is an adaptation from [1].

Chapter 2: The fatigue behaviour of welded joints is described in this chapter, followed by a general description of the thickness effect and influence of loading, and how HFMI treatment affects fatigue behaviour. The chapter is an adaptation from [1].

Chapter 3: Based on a literature review and an established database in Paper II, the thickness effect in HFMI-treated joints is assessed in this chapter, section 3.3, fulfilling objective 2. Section 3.3 is an adaptation from [1]. Furthermore, the database is used to derive characteristic fatigue strengths for some common weldments and the involved methodologies are then adopted as design procedure proposals in chapter 7.

Chapter 4: Objective 1 is treated in this chapter which regards fatigue aspects in bridges and the potential benefits and limitations of HFMI application for bridges. Results from Paper I in the form of a parametric study are included in this chapter. The chapter is an adaptation from [1].

Chapter 5: Experimental results from Paper III are presented in a condensed format in this chapter in fulfilment of objective 3. The chapter is an adaptation from [1].

Chapter 6: Investigations related to realistic in-service loads and the performance of HFMI-treated joints under such loads is included in this chapter in fulfilment of objectives 4 and 5, based on the work performed in Paper IV and V.

Chapter 7: This chapter provides design procedure proposals related to the investigated topics in this thesis and fulfils objective 6.

Chapter 8: The main conclusions of the five papers are summarised in this chapter followed by suggestions for further research.

2 Fatigue of welded joints

Fatigue is a damaging process that occurs progressively in metallic components and structures which are subjected to repeated stress cycles. The damage process can start from the very first cycle, for stresses far below the elastic limit of the material. This process involves several stages, but a common simplification is to divide the total fatigue life into two phases; (macro) crack initiation and (macro) crack propagation until failure [16].

The position of final fatigue failure is decided by the weakest link in the material. In a plain metallic plate, the weakest link is often an inhomogeneity on the surface or at the plate edge. The surface roughness and the method of cutting are therefore important factors for the fatigue strength of plain components [17]. In a component without notches, the number of cycles to initiate a macro-crack dominates the fatigue life, and the fatigue limit, below which fatigue failure will not occur, is approximately one-third of the ultimate strength [18], $0.3f_u$. Due to the absence of notches, the macro-crack propagation rate is relatively low.

In notched components with holes or sharp edges, the position of fatigue failure is normally at the site of highest stress concentration. Still, the fatigue crack initiation phase can constitute a significant portion of the fatigue life, but the fatigue limit is reduced to approximately $0.3f_u/K_t$, where K_t is a factor by which the nominal stresses are magnified at the notch. The crack propagation rate is higher than in plain components due to the presence of stress concentration.

In welded components, the transition between weld and base material is the weakest link, since, in addition to high stress concentration, tensile residual stresses are present from the cooling process after welding. Furthermore, weld defects such as undercuts, porosities, inclusions or spatter can also exist in the weld toe region, acting as sharp notches and crack-like defects. As a result, the crack initiation phase constitutes a minor part of the total fatigue life and, in addition to the notch effect, the tensile residual stresses contribute to an increased crack propagation rate. A consequence of welding is, therefore, a dramatic decrement in fatigue strength, as illustrated in Figure 2 with *SN* curves. Because the fatigue life of welded components is mainly governed by macro-crack propagation, the second consequence of welding is that the fatigue strength becomes relatively independent of the material strength, see Figure 3 for sharp notches.

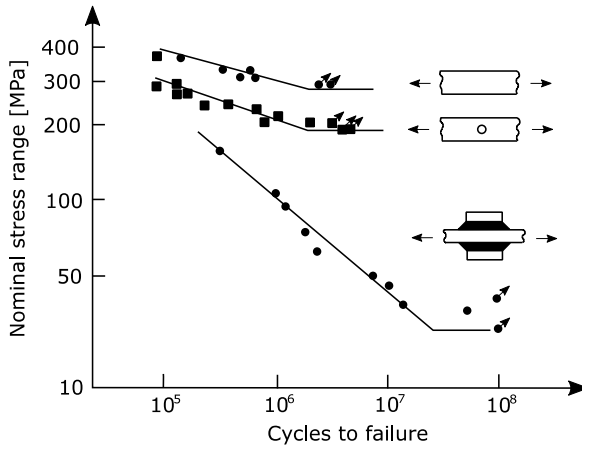

Figure 2. Fatigue strength decrement due to notches and welds adapted from [19].

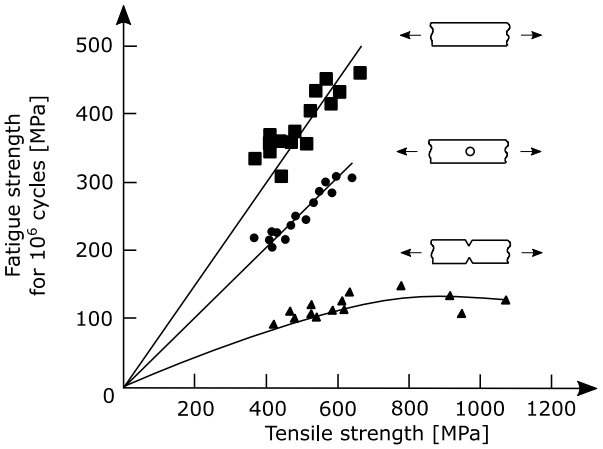

Figure 3. Fatigue strength dependence on material strength adapted from [20].

In principle, HFMI treatment of welded joints results in similar fatigue behaviour as that of specimens with round notches and no welds, as shown in Figure 2 and Figure 3. The *SN* curve of HFMI-improved joints is situated at higher stress ranges, typically with a shallower slope and higher fatigue limit than for as-welded (AW) joints. Also, the fatigue strength of HFMI-treated joints is dependent on material strength. The greatest improvement is obtained in high-cycle fatigue whereas, in low cycle fatigue, the difference in fatigue strength compared with the AW state might be negligible, see e.g. [4][13].

Figure 4 shows the design *SN* curves of HFMI-treated specimens according to the IIW [9], with the fatigue strength at two million cycles (FAT class) of the corresponding AW details in parentheses. The depicted HFMI FAT classes apply for $f_y < 355$ MPa and low mean stress loading ($R = 0.1$). The curves for the AW details are shown according to Eurocode 3 (EC3), as this standard is relevant in many countries for bridge design [21]. According to the IIW, weldments with other FAT classes than between 50 to 90 are not allowed for HFMI treatment. This is because, below FAT 50, weldments possess an increased risk of fatigue cracking from the weld root, whereas, above FAT 90, the fatigue resistance is either determined by other locations than the weld toe, or, it already includes improvements, such as for flush ground butt welds.

The depicted second slopes of both the AW and HFMI curves in Figure 4, m_2, are only valid for variable amplitude (VA) loading. For constant amplitude (CA) loading, Eurocode only provides the first slope and prescribes infinite life after 5 million cycles (the constant amplitude fatigue limit). Instead of infinite life, the IIW CA curve changes slope to $m_2 = 22$ after 10 million cycles. Furthermore, beyond 100 million cycles, Eurocode prescribes infinite life for VA loading (the cut-off limit), whereas no such limit is provided by the IIW.

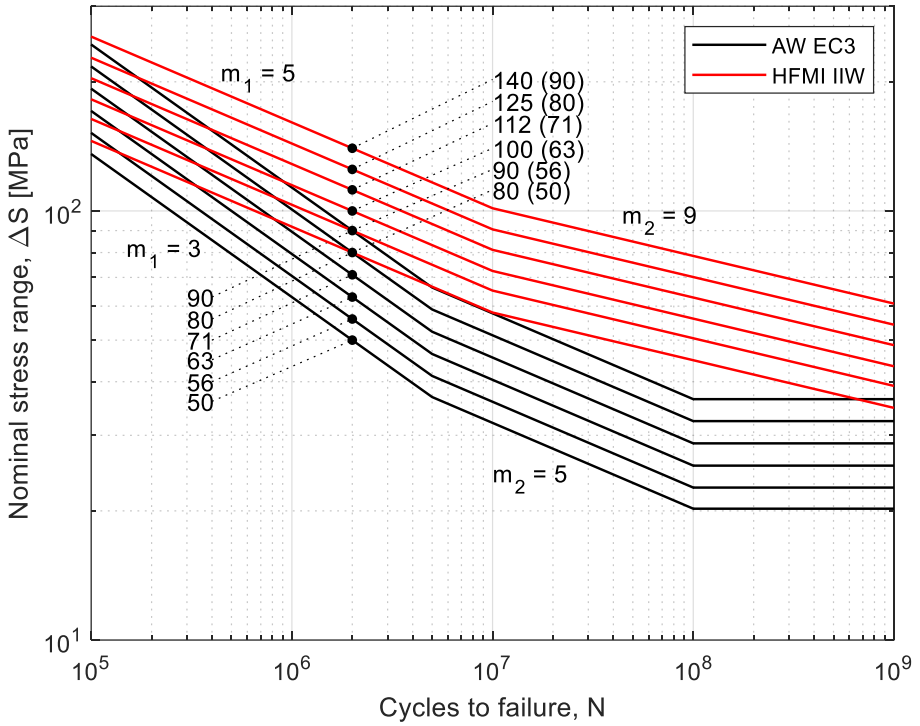

Figure 4. The Eurocode 3 [21] version of as-welded (AW) SN curves of weldments allowed for HFMI treatment and the corresponding SN curves after HFMI treatment for $f_y < 355$ MPa and $R = 0.1$ loading according to the IIW [9].

2.1 Influence of loading

The fatigue strength of AW joints is usually considered to be independent of load conditions, such as high mean or maximum loads since high tensile residual stresses are assumed to already exist locally at the weld toe [22]. This makes the local mean stress insensitive to changes in the applied mean load. Due to the concentration of stresses at the weld toe, maximum loads can cause local yielding and relax the existing residual stresses, even for nominal stresses below the elastic limit. This results in a beneficial effect in the AW condition. Thus, local yielding due to unforeseen overload events in VA loading is not of concern when dealing with AW joints [23].

In contrast, the fatigue strength of HFMI-treated weld toes is highly reliant on the induced compressive residual stresses and is therefore sensitive to the load conditions. An increase in tensile mean load reduces the compressive residual stresses momentarily, making the following load cycles more damaging. Overloads in VA loading can permanently reduce the fatigue strength through residual stress relaxation, which poses further challenges compared with AW joints. Compressive loads are of special importance since when superimposed to the existing compressive residual stresses cause local yielding at a lower magnitude compared with tensile loads. This may be harmless if the following load cycles continue to be compressive or of low mean stress, however, subsequent loading with high tensile mean stresses is, of course, detrimental [24]–[26].

Stress limitations to guarantee the integrity of the induced residual stresses are provided by the IIW in the format of maximum permissible stress range as a function of stress ratio [9]. This is equivalent with limitation of tensile stresses to $S_{max} \leq 0.8f_y$ for $R \geq$ -0.125 and gradually decreasing stress limitations for both tensile and compressive stresses for $R <$ -0.125 ($\Delta S \leq 0.9f_y$). The boundary stress ratio of $R =$ -0.125 is simply where the maximum stresses intersect at $0.8f_y$ for the two criteria.

An alternative description of the IIW stress limitations is given here. Figure 5 shows a shaded area for permissible stresses, bounded by a solid line which constitutes the maximum permissible stresses, and a dashed line which limits the compressive stresses for $R <$ -0.125. The IIW states that these limitations are valid in both CA and VA loading. However, it is not clear if these limitations are valid even if the mean stress changes in the same loading, for example, if it is allowed for an HFMI-treated weld to first be subjected to $\Delta S = 0.9f_y$ with $R =$ -1 and, subsequently, to $S_{max} = 0.8f_y$ with $R = 0.5$.

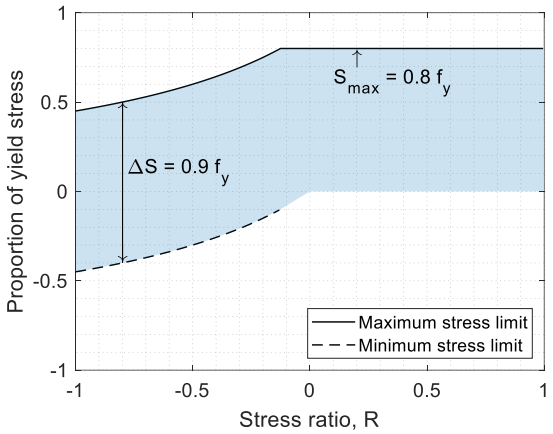

Figure 5. Limitation of stresses adapted from the IIW [9].

The fatigue strength of HFMI-treated specimens has commonly been established through CA experiments at a fixed stress ratio of $R = 0.1$, covering low mean stresses. Some high mean stress investigations also exist, which have typically included CA experiments of $R = 0.5$ loading, showing a considerable decrease in fatigue strength compared with $R = 0.1$. A practical approach to consider this effect is provided by the IIW [9] as penalties on the FAT class for various stress ratios in a table format, see Table 1. For VA loading, where stress ranges may be associated with different stress ratios, the IIW does not provide recommendations. Chapter 6 in this thesis, as well as Paper IV and V, investigate this matter more.

Table 1. Fatigue strength reduction for increased stress ratios, according to the IIW [9].

Stress ratio	*FAT class reduction*
$R \leq 0.15$	No reduction
$0.15 < R \leq 0.28$	Reduction by one class
$0.28 < R \leq 0.40$	Reduction by two classes
$0.40 < R \leq 0.52$	Reduction by three classes

2.2 Influence of thickness

The thickness effect entails fatigue strength reduction for an increase of load-carrying plate thickness. The thickness effect is part of a more general phenomenon called the size effect in which additional geometric quantities that influence the fatigue strength are included. The size effect can be divided into three categories: the statistical, technological and geometric size effects [27][28].

- The statistical size effect reflects a decrement of fatigue strength due to a higher probability of the existence of defects in a larger material volume or component. In welded joints, the statistical size effect is governed by the weld length, since fatigue cracking usually starts from the weld toe [29].
- The technological size effect regards the effect of size during the manufacturing process. Commonly, welding of larger components induces higher tensile residual stresses which reduce the fatigue strength. Also, the manufacturing process of thicker plates may give rise to greater variations in grain size through the thickness direction and reduced yield stresses [28].
- The geometric size effect includes the influence of geometry on the stress state during loading. Taking a non-load-carrying transverse attachment detail as an example, the influencing geometric parameters on the fatigue strength are main plate thickness (t_1), weld size (l) and attachment plate thickness (t_2), see Figure 6. Increasing any of these dimensions results in increased stress concentration at the weld toe, thereby shortening the fatigue crack initiation life, or in the case of welded joints, resulting in faster crack growth during the early propagation phase [29][30]. Aside from increasing the stress concentration, an increased main plate thickness also reduces the rate of which stresses decrease through the thickness, i.e. the stress gradient, Figure 6a. For thicker main plates, a lower stress gradient results in larger stresses near the surface of the weld toe, which shortens the crack propagation life. Besides, a similar stress gradient effect arises when a component is subjected to bending, which manifests in a more severe thickness effect.

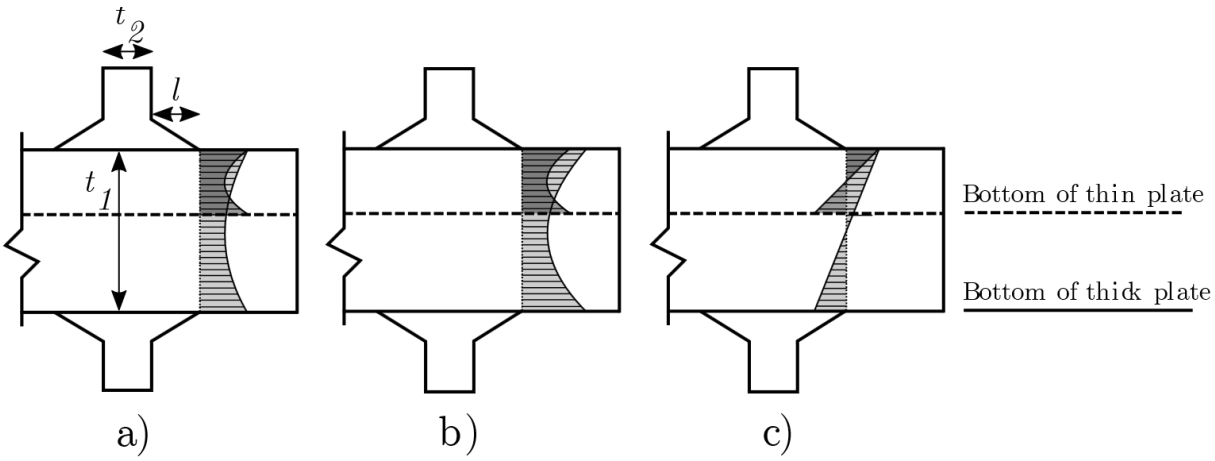

Figure 6. Geometric thickness effect due to a) stress gradient and b) stress concentration. c) Effect of bending.

Gurney's approach [31] is a well-established method for treating the thickness effect and is adopted in several design codes and guidelines [29]. With this approach, fatigue test results can be evaluated in terms of stress-thickness (S-t) curves. Equation (1) describes the function of the S-t curve. The fatigue strength, ΔS_m, corresponding to thickness, t, can be found from the S-t curve, which is defined for a reference fatigue strength, ΔS_{ref}, and thickness, t_{ref}. The exponent, n, also referred to as thickness correction exponent describes the slope of the S-t curve and is a measure of the severity of the thickness effect. With this approach, Equation (1) can be used to reduce the fatigue strength of details with plate thicknesses greater than t_{ref}. The value of t_{ref} is often set to 25 mm in design codes [29].

$$\Delta S_m = \Delta S_{ref} \left(\frac{t_{ref}}{t}\right)^n \quad (1)$$

Paper II in this thesis elaborates more on the thickness effect through a literature review and provides new information about the thickness effect of different types of welded joints improved by HFMI treatment. Section 3.3 in this thesis gives a summary of the results of Paper II.

3 SN curves for HFMI

A database of experimental fatigue test results of HFMI-treated joints was established in Paper II to evaluate the thickness effect. The same database has been used in this thesis to establish characteristic *SN* curves for transverse butt welds (B) and joints with non-load-carrying transverse (C & T) and longitudinal attachments (L), which were loaded in axial tension under stress ratios of $0 \leq R \leq 0.1$. Table 2 gives an overview of the database. The database included 582 fatigue test results of small-scale specimens from 28 different studies. Runouts and results above five million cycles were excluded as well as failure modes which were explicitly reported elsewhere than the weld toe. Two methods of statistical evaluation were central in this study. The first was the calculation of prediction limits for the characteristic *SN* curves which followed the best practice guide of Schneider and Maddox [32]. The second was the *multiple regression with dummy variables* (*MRD*), which allows for the evaluation of a parameter that is common for different categorical groups [33][34]. See Paper II for more details and section 3.1 for an example of the implementation of the *MRD*-method.

Table 2. Experimental studies of HFMI-treated joints included in the database.

Ref	*Authors*	*Detail*	f_y *[MPa]*	*R*	*t [mm]*	*k*
[35]	Abdullah et al., 2012	B	349	0.1	5	2
[36]	Hrabowski et al., 2014	B	960	0.1	8	8
[37]	Huo et al., 2000	B	267	0.1	8	8
[38]	Janosch et al., 1996	B	763	0.1	9.5	8
[39]	Kuhlmann and Günther, 2009	B, C	355 - 690	0.1	12	17
[40]	Leitner et al., 2014	B, T, L	355 - 960	0.1	5	91
[41]	Ummenhofer et al., 2006	B, T	407, 520	0.1	8 - 30	21
[7]	Ummenhofer et al., 2011	B, L	434, 719	0.1	16, 30	108
[13]	Wang et al., 2009	B, L	390, 700	0.05, 0.1	8	19
[42]	Weich, 2008	B, L	434, 719	0.1	16	132
[43]	Deguchi et al., 2012	C, L	355	0	16	5
[44]	Ermolaeva and Hermans, 2014	C	690	0.1	20	8
[45]	Han et al., 2009	C	352	0.1	16	7
[5]	Iwata et al., 2015	C	317 - 374	0.05	10 - 50	13
[46]	Kuhlmann et al., 2005	C	355, 460	0.1	12	12
[47]	Kuhlmann et al., 2006	C	690	0.1	12	3
[48]	Okawa et al., 2012	C	520	0.1	20	3
[49]	Tehrani Yekta, 2012	C	350	0.1	9.5	13
[50]	Zhao et al., 2016	C	345	0.1	10	5
[51]	Haagensen et al., 1998	L	780	0.1	6	4
[52]	Haagensen and Alnes, 2005	L	350, 700	0.1	8	15
[53]	Huo et al., 2005	L	390	0.1	8	4
[54]	Lihavainen and Marquis, 2004	L	355	0.1	8	10
[55]	Lihavainen et al., 2004	L	355	0.1	5	5
[56]	Marquis and Björk, 2008	L	700	0.1	8	5
[57]	Martinez et al., 1997	L	398, 780	0.1	12	12
[58]	Vanrostenberghe et al., 2015	L	690 - 960	0.1	5 - 20	38
[59]	Wu and Wang, 2012	L	272	0.1	8	6

B = butt weld, C = double-sided transverse attachment, T = single-sided transverse attachment, L = longitudinal attachment, t = main plate thickness, k = number of specimens

3.1 The SN slope

An example of an area of use of the *MRD*-method is demonstrated in this section. The method is used to find the *SN* slope, m, which gives the best fit accounting for all the test series in the HFMI database as separate categorical groups. The group distinction is necessary or else, a simple regression analysis of all data points would give a wrong slope, see Figure 7a. The grouping was made so that all influential parameters were equal within each group, such as detail type, yield stress, thickness and other geometries, resulting in 80 different groups. With the *MRD*-method, a common slope of $m = 4.94$ was found for all groups. In Figure 7b, the individual *SN* slopes of each group are plotted in an ordered bar diagram together with the average value of m as well as the value obtained with the *MRD*-method. Figure 7c and d show the free slopes and the fixed slope from *MRD*, respectively, in *SN* diagrams. Some of the groups contained too few data points which resulted in invalid slope values. In the fatigue part of Eurocode, a sample size of at least ten was used in the statistical evaluations [21]. Excluding all groups with less than ten data points gave $m = 4.78$ with *MRD*.

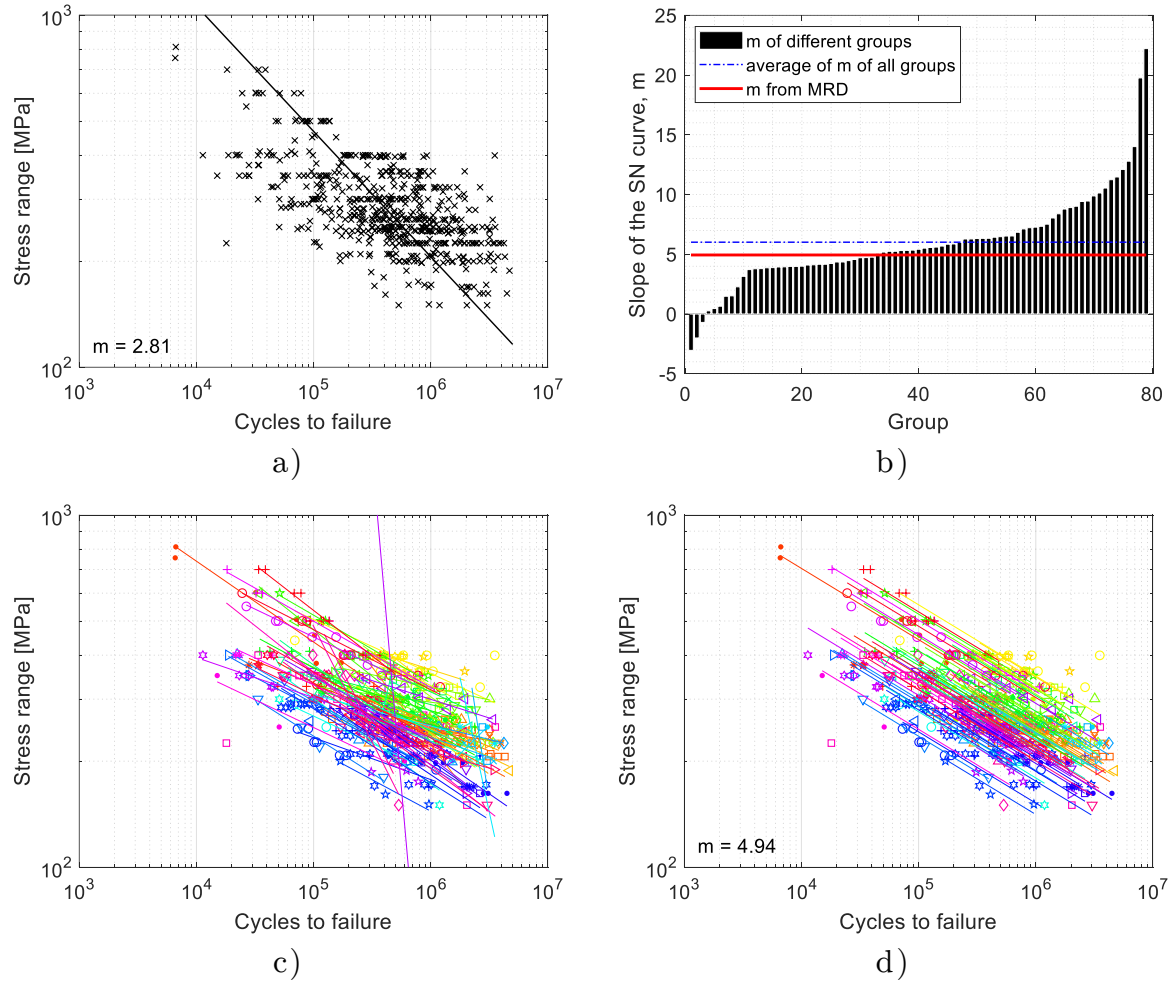

Figure 7. Finding the appropriate SN slope for the HFMI-treated specimens in the database. a) The consequence of using simple regression. b) SN slopes of individual groups compared with the average and the one from the MRD-method. c) The free slopes and d) the fixed slope from the MRD-method for all groups.

3.2 The yield stress effect

To arrive at representative *SN* curves for HFMI-treated welds, the influence of yield stress and main plate thickness were first quantified. Subsequently, that information was used to adjust the *SN* data to describe reference values for those parameters. In this section, the *MRD*-method was used to isolate the effect of yield stress and evaluate the slope of yield stress versus fatigue strength, β_1, see Figure 8. The fatigue strength of each data point was calculated assuming an *SN* slope of $m = 5$. Before evaluation of the thickness effect, the fatigue data were adjusted to represent a reference yield stress of $f_{y,0} = 355$ MPa, by linear interpolation according to Equation (2). With this equation, the stress range of each data point, ΔS_i, was adjusted depending on the yield stress of that data point, $f_{y,i}$, and the yield stress effect of that detail, β_1. More information is found in Paper II.

$$\Delta S_{\beta,i} = \Delta S_i - \beta_1 \left(f_{y,i} - f_{y,0} \right) \tag{2}$$

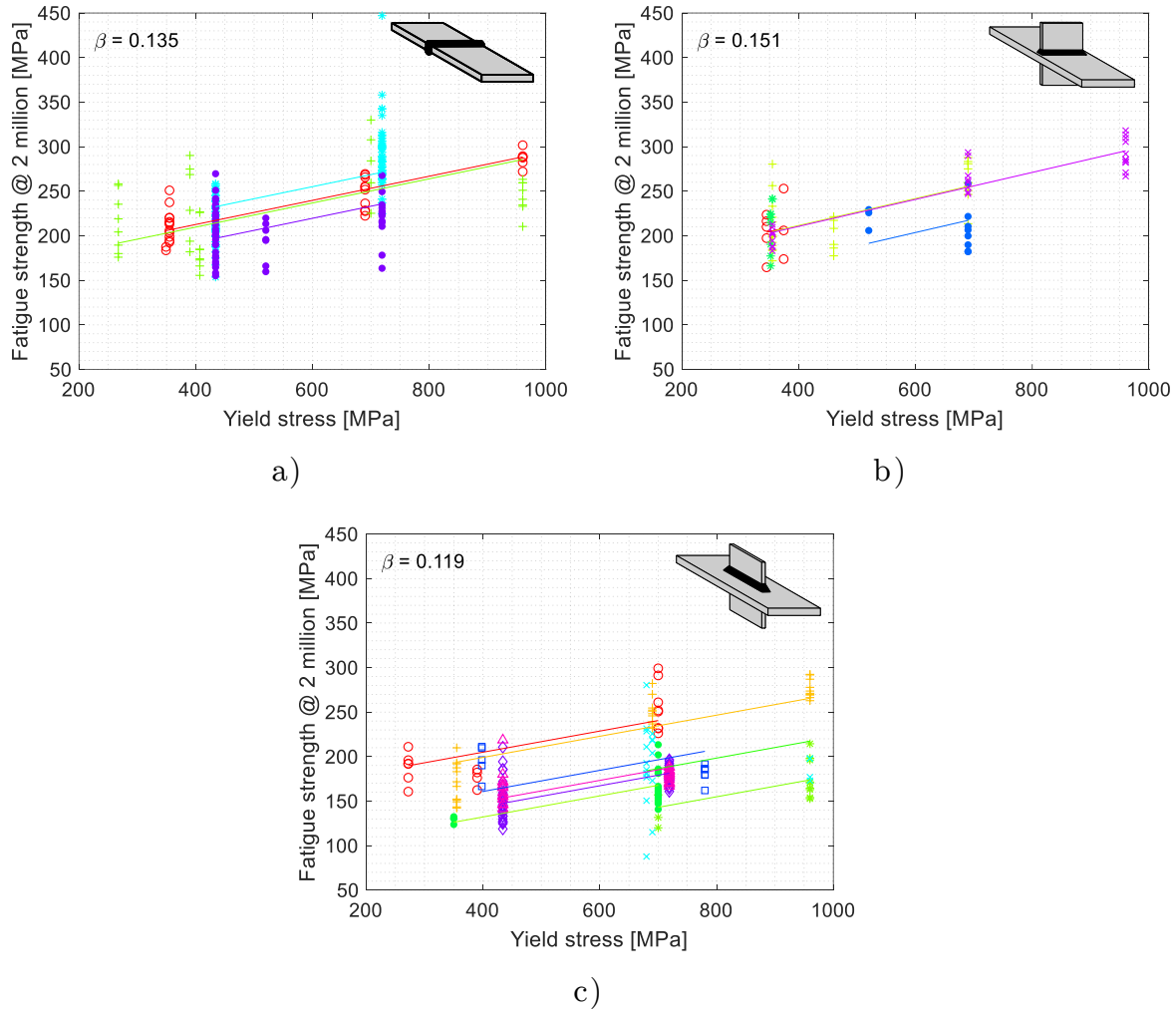

Figure 8. The yield stress effect of HFMI-treated joints. a) butt welds grouped by thickness, b) transverse attachments grouped by main plate thickness and single/double-sided attachments and c) longitudinal attachments grouped by attachment length and main plate thickness.

3.3 The thickness effect

This section covers the topic of thickness effect of HFMI-treated welds which is one of the main subjects of this thesis. Therefore, more elaborations are made here, including comparisons to literature reviews and provisions in standards. The IIW recommends a thickness correction exponent of $n = 0.2$ for joints improved by any post-weld treatment method, e.g. grinding, TIG re-melting or the peening methods [9][60]. This exponent is, however, based on fatigue test data of only toe ground joints [61]. For joints in the as-welded (AW) state, the recommended exponent is $n = 0.3$ for transverse and longitudinal attachments and $n = 0.2$ for transverse butt welds [61].

In Paper II, a review of thickness-effect studies of AW joints was performed to better understand by which mechanisms HFMI treatment could influence the thickness effect. The review indicated that the thickness effect of AW butt joints is technological since the thickness influence could be eliminated by both stress-relieving and high mean stress loading, according to [62][63]. For AW longitudinal attachment joints, most of the reviewed studies indicated that the thickness effect is negligible, with thickness correction exponents close to zero. Fracture mechanics calculations performed by Gurney [31] even showed a "reverse" thickness effect (negative n) in longitudinal attachment joints and it was suggested not to reduce the fatigue strength due to thickness increase. Studies of AW transverse attachment joints showed thickness correction exponents between $n = 0.2$ and 0.3 for proportional scaling, i.e. proportional size increase of attachment and weld with respect to main plate thickness. In cases where attachment and weld sizes were kept constant, increasing the main plate thickness resulted in thickness correction exponents of only $n = 0.05$-0.1 [64]–[66].

Here, the yield stress adjusted data from the previous section was used to evaluate the thickness correction exponent, n, for HFMI-treated joints. Through this approach, variations in fatigue strength from yield stress were eliminated and the thickness correction exponent could be found correctly. Equation (1) entails that n is the slope of the linear relationship of thickness versus fatigue strength in a log-log scale. The obtained thickness correction exponents are shown in Figure 9. Although the experiments in the database were conducted with low mean stresses, the butt weld joints showed a weak thickness effect with $n = 0.055$, suggesting that peening eliminates the presumed technological thickness effect observed in the AW state. For the two remaining details, the *MRD*-method was again utilised to obtain a common thickness correction exponent for groups where the detail geometries differed significantly. In here, different groups were established for double- (cruciform) and single-sided (T-joints) transverse attachments and for various lengths of longitudinal attachments. An exponent of $n = 0.207$ was obtained for the transverse attachment joints, close to the thickness correction exponent recommended by the IIW. For the longitudinal attachments, a relatively strong reverse thickness effect was observed with $n = -0.188$. It was concluded in Paper II that thickness correction should not be made for longitudinal attachments and that the current recommendation of $n = 0.2$ can be over-conservative for HFMI-treated butt

welds. Overall, HFMI-treated joints show a weaker thickness effect than what is recommended by the IIW [61] for AW joints, resulting in an additional source of improvement for thicker plates.

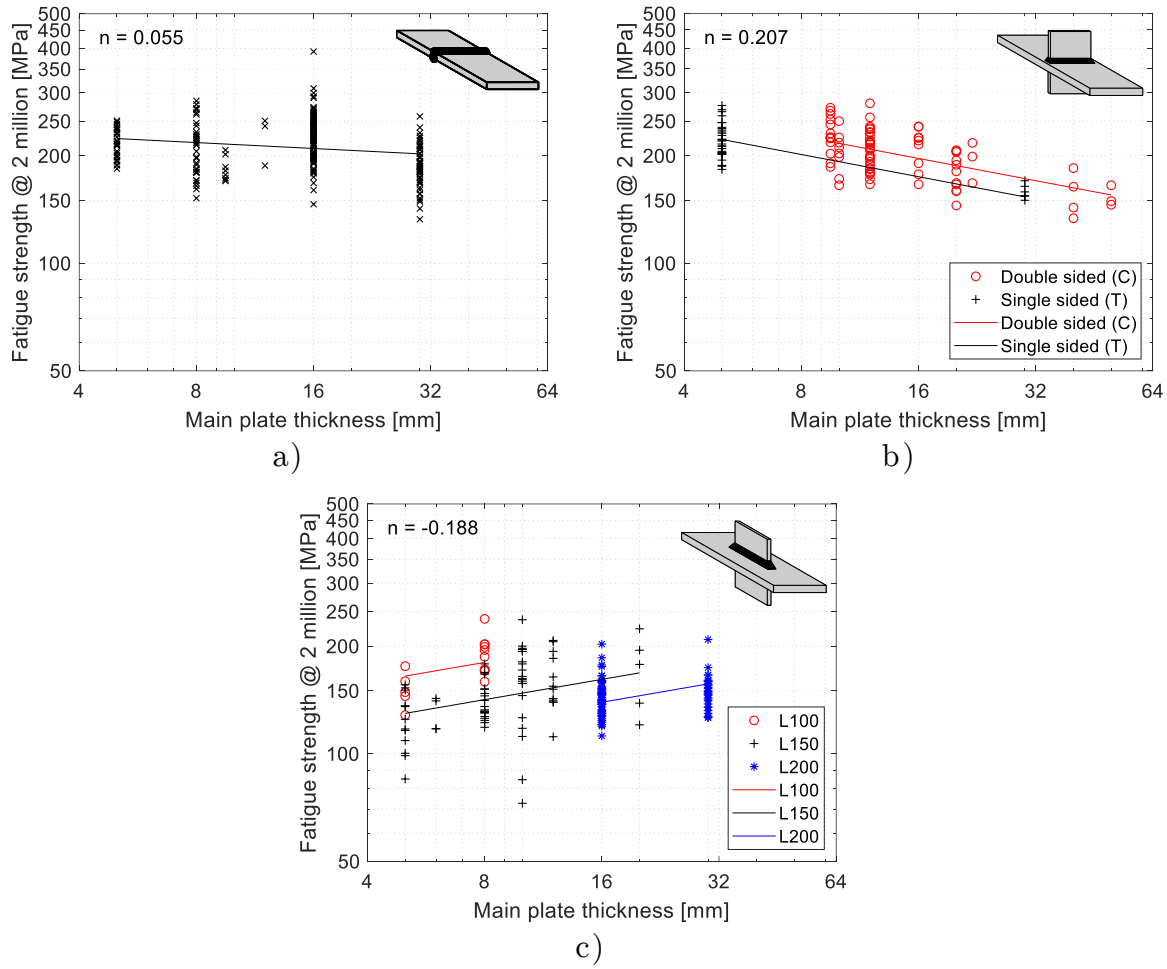

Figure 9. Thickness effect of HFMI-treated joints. a) butt welds, b) transverse attachments grouped by single/double-sided attachments and c) longitudinal attachments grouped by attachment length.

The yield stress adjusted data were further modified with respect to thickness for the butt weld and transverse attachment joints to represent a reference thickness. The thickness adjustment of the data involved enlargement of the stress range of each data point which had thickness $t_i > t_{ref}$, according to Equation (3). In this thesis, reference thicknesses were found by minimising the standard deviation of the *SN* data. No thickness correction was made for the longitudinal attachments since a t_{ref} could not be found that minimised the standard deviation. Instead, an alternative approach was implemented for this detail which is described in the next section.

$$\Delta S_{\beta n,i} = \Delta S_{\beta,i} \left(\frac{t_i}{t_{ref}} \right)^n \tag{3}$$

3.4 The SN curves

The obtained *SN* curves are depicted in Figure 10. See Paper II for comparison with the *SN* curves of the original unmodified data. For the butt weld and transverse attachment details, the *SN* curves can be further adapted to become compatible with design codes by changing the reference thicknesses to 25 mm through a simple thickness correction with Equation (1). This will be done in chapter 7, which presents a proposal for design procedure.

In Figure 10c, the longitudinal attachment data was only adjusted for yield stress but variations in thickness and attachment length remained. Most of the data (78%) comprised attachment lengths ≥ 100 mm, which corresponds to the greatest length that the Eurocode distinguishes for this detail in the AW condition [21]. Accordingly, it can be stated that the derived *SN* curve for the longitudinal attachment details applies for attachment lengths of 100 mm and greater. Especially, since the exclusion of the data with shorter attachment lengths than 100 mm only reduced the mean, leaving the characteristic strength unchanged. However, the strength in Figure 10c should be accompanied with a lower limit on the thickness due to the reverse thickness effect which entails reduced fatigue strength for thinner plates. For this purpose, the longitudinal attachment data was first thickness corrected to 5 mm (i.e. the smallest in the pool), resulting in a low characteristic strength of FAT 86. Subsequently, this strength was thickness corrected according to Equation (1), with n = -0.188, to find the thickness that corresponded to FAT 109, as in Figure 10c. This approach gave a lower limit on the thickness of t_{lim} = 17 mm.

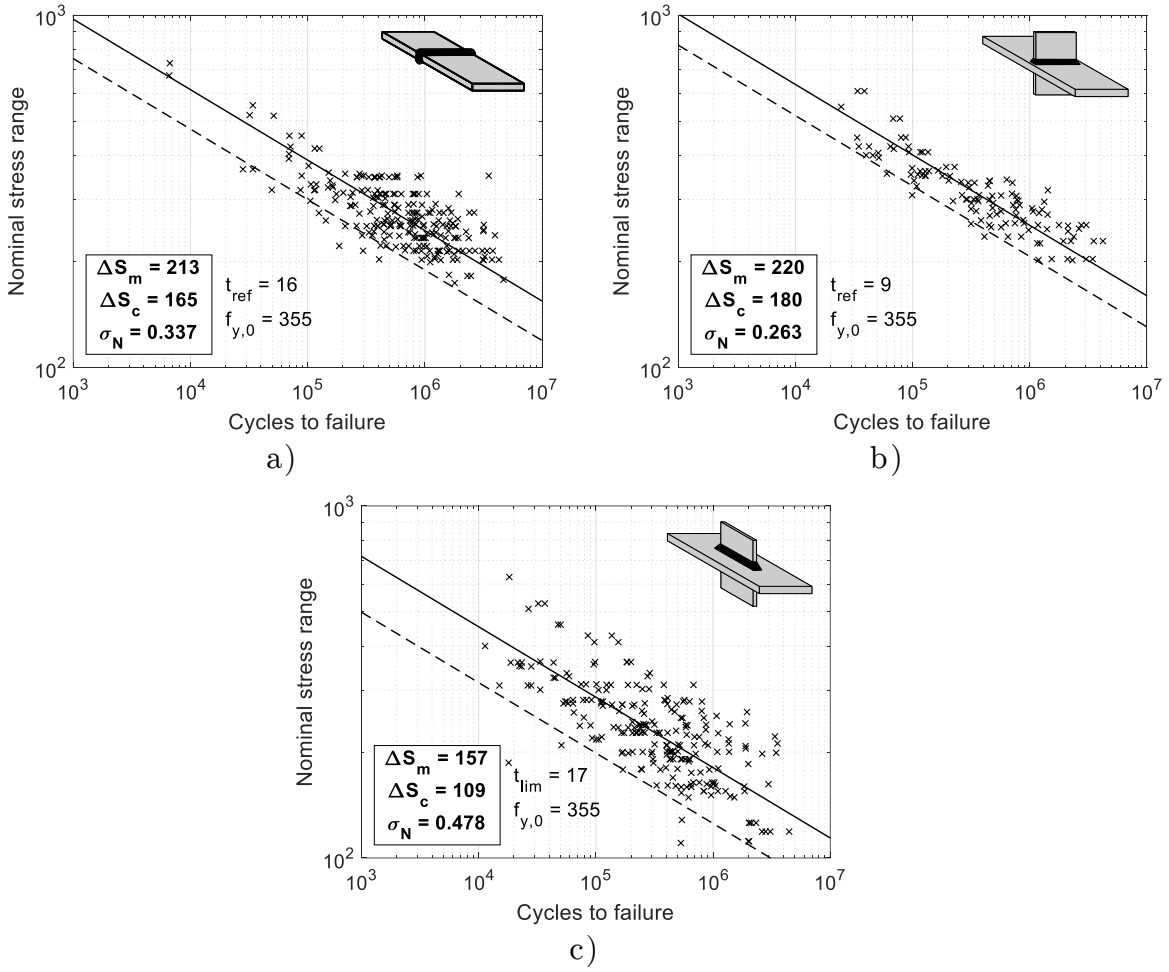

Figure 10. Derived SN curves for HFMI-treated details for a reference yield stress of $f_{y,0}$ = 355 MPa and various reference (or limiting) thicknesses. The SN slopes are fixed to m = 5. ΔS_m and ΔS_c are the mean (50%) and characteristic (95%) fatigue strengths, respectively, and σ_N is the standard deviation.

4 Material saving potential in bridges

In the design of bridges, several criteria regarding the functionality and capacity of the structure expressed as design limit states must be considered. The ultimate limit state (ULS) covers the resistance against exceptionally heavy short-term loads such as overloaded trucks or high-speed train passages including dynamic effects. In the ULS, the structural integrity is permanently lost which is referred to as a structural failure. Failure modes in this limit state include yielding of the material or instability phenomena such as local or global buckling. The fatigue limit state (FLS) is closely related to the ULS in terms of permanent loss of structural integrity if fatigue cracks arise. However, the fatigue process occurs over time and for much lower loads than the ULS, thus, a separate limit state for fatigue is appropriate. Lastly, the serviceability limit state (SLS) must be considered, involving anything that may compromise the functionality of the bridge without affecting the structural integrity. Vertical deflection is included in this category. Limiting vertical deflection is of importance for safe traffic passage under bridges and, in the case of railway bridges, for the proper functionality of the rails.

The most common types of steel bridges consist of two or more welded I-beams (girders), acting as the main load-carrying members, and a deck structure which distributes the loads to the girders. Depending on the type of traffic and possible requirements on the self-weight, the deck can be made of either steel or concrete (i.e. composite). Railway bridges of steel often have decks consisting of stiffened steel plates, whereas, the simplest steel road bridges are commonly made with concrete decks. While the fatigue-prone details in such bridges can be relatively limited in number, their design against fatigue requires a significant amount of extra material in the girder flanges compared with the other design limit states, in order to reduce stresses and endure the long service lives. One such fatigue-prone detail is often the inevitable weld between vertical web stiffeners and the flanges, see Figure 11a. Eurocode 3 provides a fatigue strength of FAT 71-80 for this detail [21]. For longer bridges, butt welding of bridge segments is necessary (FAT 80-90), sometimes in conjunction with cope-holes (FAT 71).

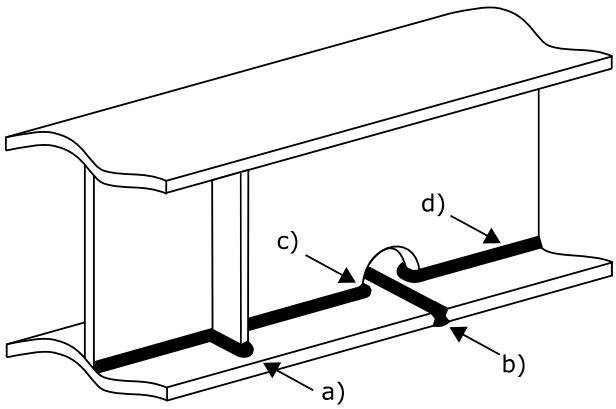

Figure 11. Typical weldments in bridges. a) non-load-carrying transverse attachment, b) butt weld, c) cope-hole and d) longitudinal flange-to-web weld.

Experience shows that the FLS often governs the design of railway bridges by a significant margin and competes with the ULS in the design of road bridges. Hence, the benefits of HFMI application on new bridge designs can be substantial, especially in conjunction with the use of higher steel grades. There are, however, design criteria which are not affected by HFMI treatment or the use of higher steels grades, which will limit the extent of material saving. For instance, during the construction phase of road bridges, the steel girders must withstand the weight of the wet concrete, which does not contribute to the load-carrying capacity. During this stage, lateral-torsional buckling of the compression flanges is critical. Such instability failures are not influenced by increased steel grades and can, therefore, restrict the extent of material saving. The same applies to vertical deflection in bridges, which are also not steel grade dependent. Moreover, the maximum fatigue strength is limited by the strength of the longitudinal flange-to-web welds (FAT 125), which are unsuitable for HFMI treatment since fatigue cracks may start from inner weld defects in such details.

Considering all design aspects and limitations mentioned above, the following sections provide the percentage steel saving in the main load-carrying members of several bridges if they had been designed with improved fatigue strengths corresponding to a three to four FAT class increase. Although the effectiveness of HFMI treatment is highly dependent on the mean stress, this effect is neglected in this section. This is because several investigations indicate that the detrimental effects of a static tensile mean stress (i.e. from self-weight) can be bypassed if the treatment is performed while that mean stress already is active [43], [67]–[74]. In practice, this corresponds to HFMI treatment on-site, after the erection of bridges and application of all permanent loads.

4.1 Parametric study

A parametric study of fictitious simply supported railway bridges was conducted in Paper I to quantify the potential of material saving following post-weld treatment. Span lengths ranging between $10 \leq L \leq 30$ meters were included in the study and the bridges were verified for ULS, FLS and SLS by following the Eurocodes [21][75][76]. The ULS checks included calculations for bending, shear and bending-shear interaction including local buckling. The FLS check was conducted for heavy traffic mix of trains with a partial safety factor of $\gamma_{Mf} = 1.35$ and a service life of 100 years, with the linear damage accumulation method. A weldment in the mid-span with detail category FAT 71 was assumed in the lower flanges as the fatigue critical detail. To be conservative, fatigue improvement was considered with an increase of three FAT classes, resulting in FAT 100, with the slope of the SN curve equal to $m = 3$. For the SLS condition, a limitation of vertical deflection of $L/800$ was used. Figure 12 displays a typical cross-section of a railway bridge included in this study.

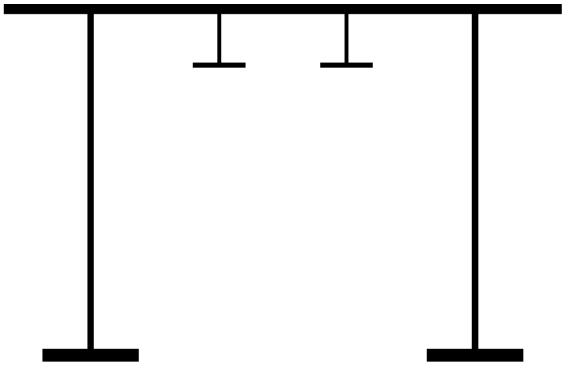

Figure 12. A typical cross-section of a railway bridge included in the parametric study.

Initial bridge designs were produced with a steel grade of S355 (minimum yield stress of 355 MPa) without post-weld treatment, referred to as *Original designs*. The flange thicknesses were kept constant, equal to 35 and 45 mm for the upper and lower flanges respectively, while the web heights varied to meet the design requirements for the different span lengths. After application of post-weld treatment and implementation of higher steel grade, S460, the upper and lower flange thicknesses could be reduced to 20 and 30 mm, respectively, including minor changes of the bottom flange widths. In Figure 13, the utilisation ratios (UR) for the different limit states are presented as a function of span length for each step of the calculations. The UR is defined as the ratio of load effect to resistance such that a UR < 1.0 implies fulfilment of the requirements of the limit state. From Figure 13a, it is apparent that FLS is most dominant for shorter span lengths. As can be seen in Figure 13b, a significant decrease in the UR of FLS occurs after post-weld treatment and ULS becomes the dominant design criterion. Increasing the material strength to S460 reduces the UR of ULS to the same level as SLS, indicating that greater material strengths are unnecessary, see Figure 13c. Finally, the UR's of the new designs with reduced flange thicknesses are depicted in Figure 13d, showing that there remains more potential for material saving for the shorter spans if a greater fatigue strength improvement or a greater slope is assumed, e.g. $m = 5$. Table 3 summarises the percentage of material saving in the beams as a result of post-weld treatment and the use of a higher steel grade.

Table 3. Material reduction of bridge cross-sections in the parametric study.

L = 10 m	*L = 15 m*	*L = 20 m*	*L = 25 m*	*L = 30 m*
31%	26%	25%	23%	21%

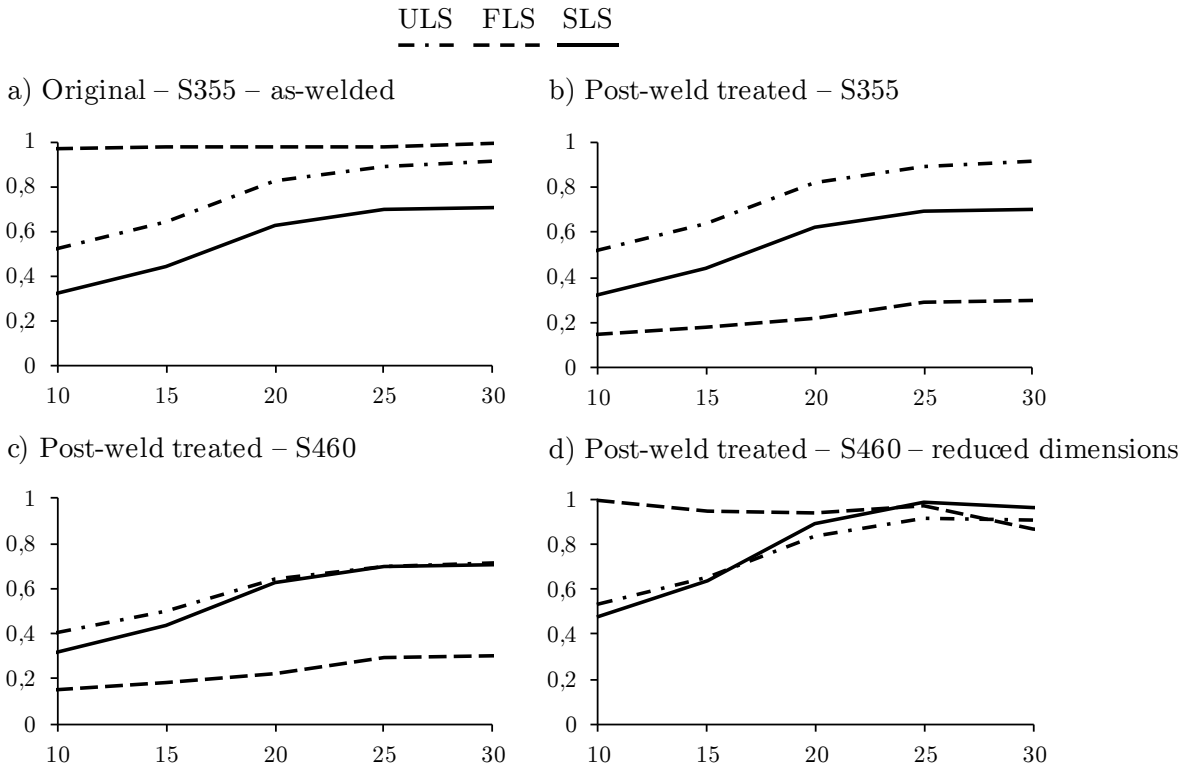

Figure 13. Utilisation ratios for different design limit states in the parametric study of simply supported railway bridges.

4.2 Case studies

In addition to the parametric study, case studies were performed on three different bridges that have been built in Sweden without post-weld treatment. They consisted of a simply supported railway bridge and two road bridges; one simply supported and one continuous. All three bridges were designed according to the Eurocode standards with the damage equivalent factor (lambda) method for fatigue stress assessment [76]. The bridges were re-designed with smaller flange thicknesses after accounting for post-weld treatment and increased material strength where necessary, thereafter, the material saving was assessed. Unlike the parametric study, the obtained material saving here is more accurate since the existing design calculations were re-used. Consequently, the calculated material saving was more representative and isolated to only the effect of fatigue strength improvement and the potential use of higher steel grades.

Simply supported Railway Bridge

The railway bridge comprised 15 identical 10 m long simply supported segments, each made of two I-beams with a common top flange as the deck. The original flange thicknesses were 30 mm at the top and 45 mm in the bottom, with a bottom flange width of 600 mm, see Figure 14. The steel grade was S355 and the fatigue critical detail was a non-load-carrying transverse attachment joint in the mid-span, FAT 80. An increase of three FAT classes, retaining the same steel grade, allowed for thickness reduction in the flanges which resulted in 17% material saving in the beams, corresponding to 30

tonnes of steel for the entire bridge. The treatment length was estimated to about 30 m in total. An estimation of the stress ratio with the load model 71 according to Eurocode [75] gave $R = 0.08$. The real stress ratio is not a constant value, since it may vary depending on load magnitude. Although an improvement of more than three FAT classes could be achieved, the limitation of vertical deflection did not allow for more material reduction in this case. The utilisation ratios for the design limit states are summarised in Table 4.

Figure 14. The railway bridge (during construction). Original flange dimensions and the dimensions after HFMI treatment in parenthesis. Red lines indicate HFMI-treated areas.

Table 4. The utilisation ratios for the original design and the new design with post-weld treatment.

Utilisation	*ULS*	*FLS*	*SLS*
Original	0.63	1.00	0.82
New	0.79	0.96	1.00

Simply supported Road Bridge

The simply supported road bridge (Figure 15) spanned 32 m and consisted of three different segments of steel I-beams with various flange dimensions to optimise the material utilisation. The top flange thicknesses were 20 mm in the two outer segments and 25 mm in the middle one, whereas the bottom flanges were made of 25 mm in the outer and 32 mm in the middle. The deck was made of concrete which acted compositely with two I-beams through shear studs. A steel grade of S355 was used in the top flanges and webs, whereas S420 steel was used in the bottom flanges. The ultimate and fatigue limit states governed equally in this design. Due to the heavy concrete deck, a high stress ratio of at least $R = 0.65$ was estimated for the critical details with the fatigue load model 3 of Eurocode [76].

The calculations for post-weld treatment was performed with two alternatives. For both alternatives, the top flange thicknesses could not be reduced due to limited lateral torsional buckling capacity during the construction phase, thus, the material saving was only a result of bottom flange thickness reduction. For alternative 1, only a non-load-carrying transverse attachment in the mid-span was assumed post-weld treated, an approximate treatment length of 2 m. Thereby, butt welds that joined the three

bridge segments were left in the AW state in the calculations. Decreasing the bottom flange thicknesses in the middle segment to 15 mm and increasing the yield stress to 620 MPa resulted in a material saving of 10%, corresponding to 2.5 tonnes of steel. This assumed a FAT class increase from FAT 80 to FAT 125. In alternative 2, the butt welds were treated in addition to the transverse attachments, assuming the same FAT classes and a total treatment length of 16 m. A material saving of 22% in the beams was realised by reducing the bottom flange thicknesses to 15 and 11 mm in the middle and outer segments, respectively, and increasing the yield stress to 620 MPa. This corresponded to 5.4 tonnes of steel saving. In this case, the fatigue strength of the flange-to-web welds (Figure 11d) was the limiting factor for material saving. Table 5 gives a summary of the utilisation ratios. More details on this study are available in [77].

Figure 15. The simply supported road bridge.

Table 5. The utilisation ratios for the original design and the new designs with post-weld treatment.

Utilisation	*ULS*	*FLS*	*SLS*
Original	0.89	0.89	0.54
New, Alt. 1	0.97	0.96	0.78
New, Alt. 2	0.98	0.97	0.85

Continuous Road Bridge

The last bridge was a continuously supported composite road bridge with five spans and a total length of 130 m, see Figure 16. Like the simply supported road bridge, this bridge consisted of two I-beams with varying flange thicknesses in composite action with a concrete deck. The stress ratio was estimated to a somewhat lower value in this bridge compared with the simply supported case, with $R = 0.52$. The steel grade was S355 in all parts. Around 40 critical details in the form of transverse attachments from vertical stiffeners and cross bracings as well as in-situ and workshop butt welds required post-weld treatment. The total treatment length was approximated to 154 m for the whole bridge. The welded details were all FAT 80 in the AW state and were assumed to FAT 125 after treatment. The steel grade was increased to S460 for the new design. Typical examples of some thickness reductions were 40 to 30 mm in the bottom and 30 to 20 mm in the top flanges over the supports. In the mid-spans, the top flanges were kept relatively unchanged due to the risk of buckling in the construction phase, whereas the bottom flange thicknesses were typically reduced from 40 to 20 mm. As a simplification, the bending moment distribution of the original design was reused in the new design. In total, 23% material was saved in the beams, which corresponds to 30 tonnes of steel. Table 6 shows the maximum utilisation ratios. The fatigue strength of the AW flange-to-web welds was the limiting factor for further material saving in this bridge.

Figure 16. The continuous road bridge (during construction).

Table 6. The utilisation ratios for the original design and the new design with post-weld treatment.

Utilisation	*ULS*	*FLS*	*SLS*
Original, support	1.00	0.41	-
Original, span	0.87	0.96	0.34
New, support	1.00	0.51	-
New, span	0.99	0.98	0.47

4.3 Summary and remarks

In this section, summarising points and some additional remarks are listed related to the fatigue design of some commonly built bridge types in Sweden and the feasibility of post-weld treatment in these contexts. The points may not apply for other bridge types than those investigated here, such as truss bridges where the static systems are significantly different or road bridges with orthotropic steel decks where complex weldments exist.

- A material saving of around 20% can be achieved in the main load-carrying members of bridges through post-weld treatment and potentially the use of higher steel grades, depending on the type of bridge and circumstances of the specific case.

- When bridges are made lighter by using thinner plates, the fatigue performance increases due to less thickness effect. Also, HFMI-treated welds possess milder thickness effect than what is recommended for as-welded joints, as described in section 3.3, which implies further efficiency. Thinner plates can also dramatically reduce welding effort, particularly in case of butt welds.

- Transverse non-load-carrying attachments and butt welds usually make up the fatigue critical details in the investigated bridge types. In these details, cracking occurs at the weld toe. However, if treated, root failure might become a competing failure mode to the treated weld toe. One way of solving this issue is to use full-penetration welds.

- It is recalled that the use of increased steel grades can be restricted by vertical deflection in the case of railway bridges, and instability phenomena such as global buckling during the construction phase of composite road bridges. Furthermore, fatigue failure of other non-treatable welds can become governing, such as the longitudinal flange-to-web welds (FAT 125), making higher steel grades unnecessary.

- Various steel grades were used for the calculations of the parametric and case-study bridges after post-weld treatment, making a generalisation of suitable steel grades difficult. For the investigated railway bridges S355 and S460 were used and higher grades was limited by vertical deflection criteria. For the composite road bridges S460 and S620 were used, limited by the fatigue criteria of the flange-to-web welds.

- Important questions remain regarding the treatment of the mean stress effect if HFMI would have been performed before the application of self-weight stresses, e.g. at a workshop. Furthermore, the risk of residual stress relaxation due to overloads in real in-service loading requires assessment. These questions are investigated in chapter 6.

5 Constant amplitude experiments

Fatigue experiments were conducted on 40 and 60 mm non-load-carrying transverse attachment joints under four-point bending to establish constant amplitude (CA) *SN* curves, both in AW and HFMI-treated states. In conjunction with the CA experiments, weld toe scanning, residual stress measurements and microstructural investigations were performed. Fracture mechanics calculations were used to investigate the corresponding fatigue strengths under axial loading. This chapter presents a summary of the investigations and results. For detailed information, see Paper III.

A total of six test series were produced for fatigue experiments, two of AW and four of HFMI-treated specimens, see Table 7. Due to availability in the inventory of the steel producer, the delivered steel plates varied somewhat between different series. For instance, a thickness of 38 mm was delivered for series 1 instead of 40 mm and a steel grade of S500 for series 2 instead of S460. The S500 steel had similar mechanical properties as the S460 steel of the same thickness. The specimen geometry and loading arrangement is shown in Figure 17. The specimen geometries were chosen to represent a typical weldment in bridges; a vertical web stiffener welded to a flange.

The welding was performed by Lecor Stålteknik AB with flux-cored arc welding and the same welding procedures were performed for all series. The welds were made with full penetration to avoid root failure. The specimens to be improved by HFMI treatment were ground before peening to achieve a weld quality class B according to ISO 5817 [78]. The AW specimens in series 1 and 2, however, were not ground. All specimens were welded in an upright position, resulting in a smooth transition from the main plate to weld metal, see Figure 17. HFMI treatment was performed with a single indenter of radius 3 mm with an average treatment speed of 200-300 mm/min.

Table 7. Test series and mechanical properties. The number of tested specimens indicated with k.

Series	*Specimens*	*t [mm]*	*Steel grade*	f_y *[MPa]*	f_u *[MPa]*	*Elongation [%]*	*k*
1	460-38-AW	38	S460M	562	659	22	7
2	500-60-AW	60	S500G2M	471	596	25	6
3	355-40-HFMI	40	S355K2+N	382	531	25	10
4	460-40-HFMI	40	S460M	566	639	23	11
5	355-60-HFMI	60	S355K2+N	361	532	25	10
6	460-60-HFMI	60	S460G2M Z35	494	597	26	10

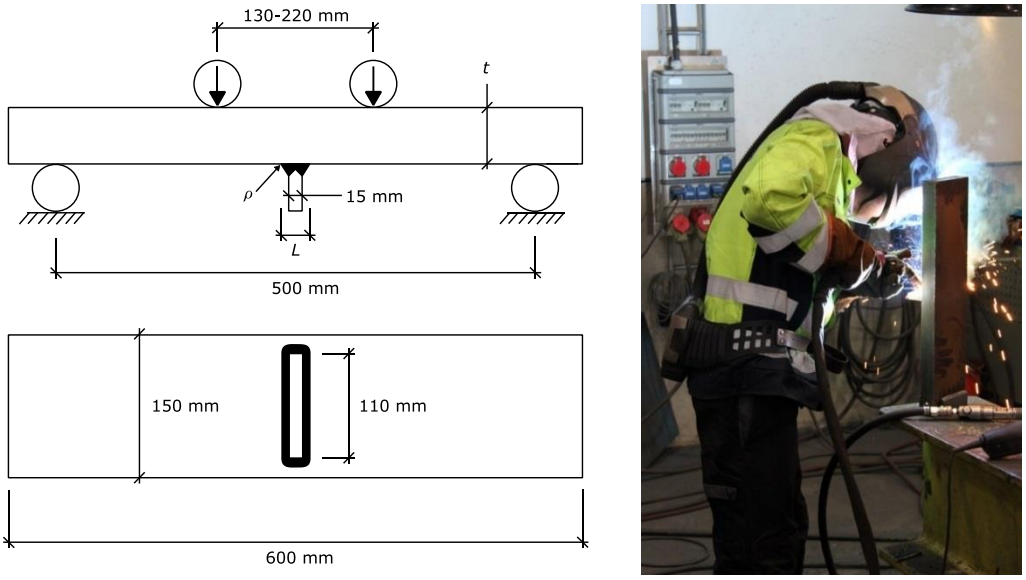

Figure 17. Test specimen dimensions, loading arrangement and a picture of the manufacturing.

5.1 Fatigue experiments

Fatigue testing was performed with a target stress ratio of $R = 0.1$, although, some variations occurred between the tests within $0.01 \leq R \leq 0.21$, see Appendix of Paper III. The loading frequency varied depending on load level, between 3-20 Hz. For the HFMI series, 27 out of 41 specimens failed from the weld toe, with the failure defined as a half thickness crack. The rest were runouts. All 13 AW specimens failed from the weld toe. Figure 18 shows the obtained fatigue strengths in terms of mean *SN* curves with a 50% probability of failure, excluding runouts. The characteristic design curve for these specimens is FAT 80 in the AW state according to both the Eurocode and the IIW ([21][61]). For the HFMI-treated state, FAT 140 is valid according to the IIW recommendations for yield stresses between 355 to 550 MPa [9]. No data points fell below the corresponding characteristic design curves.

The obtained fatigue strengths for the AW series were exceptionally high. This was probably due to the upright positioning during manufacturing which resulted in large toe radii. The low residual stresses as indicated by the residual stress measurements in the next section could also have contributed to the high fatigue strengths of the AW series. However, the residual stress measurements were performed on ground specimens before HFMI treatment, where grinding could have affected the residual stresses to become different from an AW specimen. Evaluation of the thickness effect of the HFMI-treated specimens was performed by implementing yield stress adjustment and, subsequently, deriving n for all HFMI specimens in one group, see Paper III. A thickness correction exponent of $n = 0.135$ was obtained, which lies close to reported values of $n = 0.1$ for AW joints with constant attachment and weld sizes. The difference may qualitatively be explained by the effect of bending which can result in stronger thickness effect.

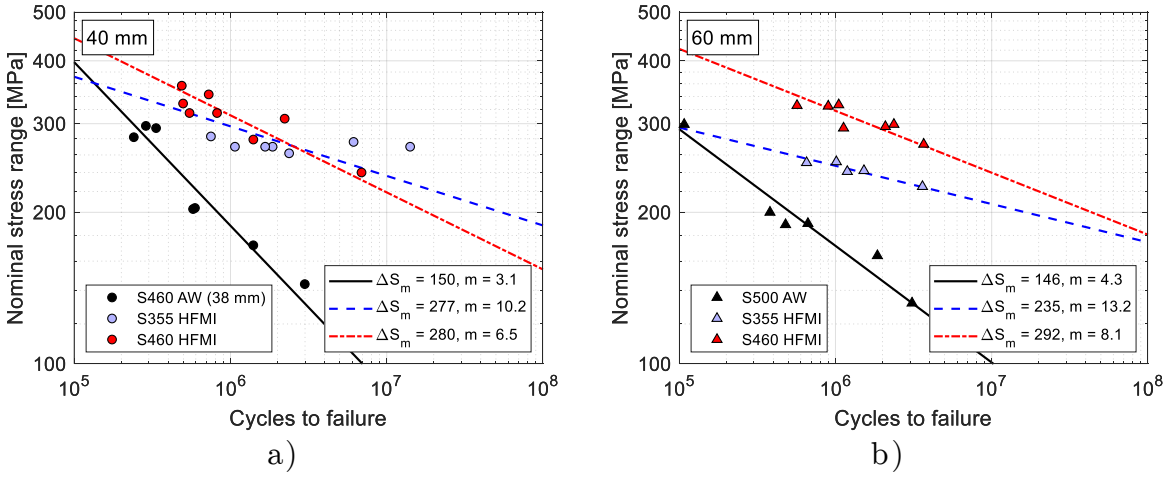

Figure 18. Mean SN curves of all CA test series. a) includes the 40 mm specimens and b) includes the 60 mm specimens.

5.2 Crack growth analyses

Because the recommended FAT classes for HFMI joints are based on axially tested specimens and the obtained results were situated much higher above the design curves, linear elastic fracture mechanics (LEFM) calculations were performed to assess the difference in crack growth between bending and axial loading. With the help of this assessment, the obtained experimental fatigue strengths could be modified to represent axial loading. To calculate the number of cycles in the crack propagation phase, N_p, Equation (4) according to Paris' law was used, where the range of the stress intensity factor, ΔK, was replaced with ΔK_{eff} to account for crack closure and residual stress effects. The material constants C (N, mm), and m_{LEFM} were taken as $1.8 \cdot 10^{-13}$ and 3, respectively, by following the IIW document XIII-2370r1-11-XV-1376r1-11, which is an update of the LEFM chapters in [61]. The initial crack depth was chosen to $a_0 = 0.1$ mm and the final crack depth at failure, a_f, to half of the main plate thickness. More elaboration on the choice of a_0 is made in Paper III.

$$N_p = \int_{a_0}^{a_f} \frac{da}{C\Delta K_{eff}{}^{m_{LEFM}}} \tag{4}$$

The effective range of the stress intensity factor, ΔK_{eff}, was calculated according to Equation (5), as suggested by Bremen [79].

$$\begin{aligned} \Delta K_{eff} &= K_{app,max} - K_{op} \text{ if } K_{op} > K_{app,min} \\ \Delta K_{eff} &= K_{app,max} - K_{app,min} \text{ if } K_{op} \leq K_{app,min} \end{aligned} \tag{5}$$

The crack opening stress intensity factor, K_{op}, accounts for both crack closure, according to [79], as well as the effects of residual stresses, as shown in Equation (6):

$$K_{op} = min\left(\frac{0.2}{1 - R_{eff}}, 0.28\right) \cdot \left(K_{app,max} + K_{res}\right) \tag{6}$$

where R_{eff} is an effective stress ratio according to Equation (7).

$$R_{eff} = \frac{K_{app,min} + K_{res}}{K_{app,max} + K_{res}} \tag{7}$$

The weight function method was chosen for calculation of the stress intensity factors, with the general form as shown in Equation (8). Closed-form solutions for semi-elliptical surface cracks in finite plates presented in [80] and [81] were used for the weight functions, $m(x,a)$.

$$K = \int_0^a \sigma(x) \cdot m(x,a) \cdot dx \tag{8}$$

The chosen weight functions required the crack development at the surface, c, for which an empirical model of the crack shape, a/c, was chosen according to [82]. The initial crack shape, a_0/c_0, was chosen based on comparisons to the experiments, on which more elaboration is made in Paper III. For calculation of the minimum and maximum applied stress intensities, the stress distributions, $\sigma(x)$, were computed for each series with the finite element method, including the actual geometries and toe radii. An example of the stress distribution for test series 1 is shown in Figure 19. The residual stresses were assumed to zero for the calculations of AW specimens, whereas for HFMI-treated specimens, compressive residual stresses were assumed near the surface as shown in Figure 20, based on the residual stress measurements. To convert the fatigue strengths to axial loading, first, the number of cycles calculated for the propagation phase in bending was subtracted from the total number of cycles obtained from the experiments. This can be considered as the crack initiation life. Subsequently, the number of cycles for crack propagation under axial loading was calculated and added to the initiation life to obtain the total fatigue life under axial loading. New *SN* curves were constructed with the modified data and it was shown that the effect of loading mode on the fatigue strength was negligible for the specimen geometries studied in here. The modification procedure above assumes that the loading mode does not affect the crack initiation life of the specimens.

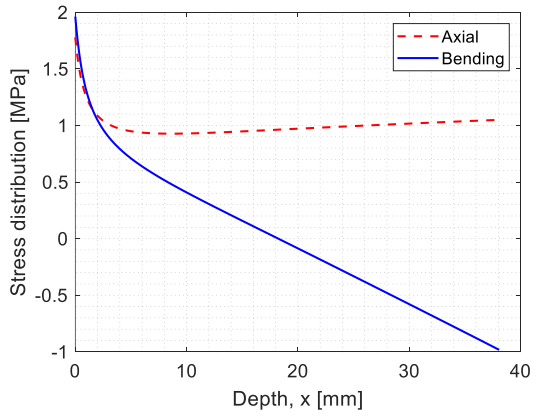

Figure 19. Stress distribution for 1 MPa nominal stress for series 1.

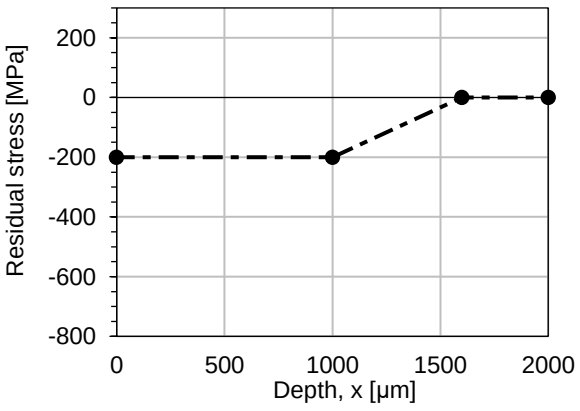

Figure 20. Assumed residual stress distribution for HFMI-treated specimens in LEFM calculations.

5.3 Other related experiments

A microstructural investigation was performed with optical microscopy with the largest magnification of 50 times. Two HFMI-treated specimens were included of steel grades S355K2+N and S460M. It was observed that in the two investigated samples, HFMI treatment was predominantly performed on the weld materials, causing some degree of observable grain elongation through plastic deformation. However, better images were considered necessary for accurate conclusions. In the regions unaffected by peening, the weld microstructures were similar for the two steel grades. The base materials were of ferritic-pearlitic microstructure in the S355K2+N steel whereas the S460M steel had significantly smaller grains with a bainitic microstructure. Further observations were that the treated surfaces appeared smoother than the base material surfaces, indicating that the surface roughness could have reduced by the treatment.

Weld scanning was performed by Swerea KIMAB with a laser measurement device. Hundreds of two-dimensional profiles were produced along each weld of all specimens, with a spacing less than 1 mm. An algorithm developed by Stenberg et al. [83] was then used to quantify the weld toe radii and weld toe distances. Due to the upright position of the specimens during welding, large toe radii were produced for the AW series. The weld toe radii of all the HFMI series were less than the AW series, about the same radius as the pin radius, 3 mm. Furthermore, the radii of series 3 were larger compared with the other HFMI series, presumably due to over-treatment. The weld toe distances were approximately twice the attachment thickness in all cases.

Residual stress measurements were performed by the company SONATS on four different specimens with 40 mm main plate thickness and two different steel grades, S355 and S460. Measurements of stresses in the transverse direction to the weld revealed zero or compressive stresses for non-treatment (ground) weld toes and significantly compressive stresses for HFMI-treated weld toes. The transverse residual stresses became approximately -250 to -300 MPa at the surface, gradually decreasing to zero at depths of about 1500 μm. The difference between residual stresses in the transverse direction for the two steel grades was relatively small, however, more compressive for the S460 specimen in the depths of 200-900 μm. These results should be treated qualitatively since no corrections were made for surface removal, which could have relaxed the stresses.

6 Variable amplitude investigations

Due to the risk of detrimental residual stress relaxation, the performance of HFMI-treated welds under variable amplitude (VA) loading has been the subject of many investigations in the past. For the same purpose, several studies have also explored the effect of a few preloads with exceptionally high stress peaks (both tensile and compressive) before CA fatigue loading with lower stresses. Paper IV gives a review of these investigations, provides new VA loads typical for bridges in Sweden achieved through traffic simulations and points out the key differences compared with the past investigations. This chapter gives a summary of Paper IV and presents the VA experiments of Paper V, covering the main topics of mean stress effect and performance compared with the CA fatigue strength.

6.1 Literature review

The effect of load-induced residual stress relaxation has in the most idealised manner been investigated through static preloading of small-scale specimens before CA fatigue loading [7][26][43][48][84][85]. The review of these studies clearly showed that compressive preloads are more detrimental compared with tensile ones and indicated that this effect is strongest for longitudinal attachments, such that conformity to the IIW strengths could be lost for high preloads. Transverse attachment specimens also showed fatigue strength decrement, however, these tests still conformed with the IIW fatigue strengths [9], even for higher preloads than for the longitudinal stiffeners, see Figure 21. Butt welds were shown to be insensitive to preloads. These findings point to a trend of higher sensitivity to residual stress relaxation due to notch intensity. This justifies the need for more specific stress limitation requirements than what is provided by the IIW today [9], see section 2.1.

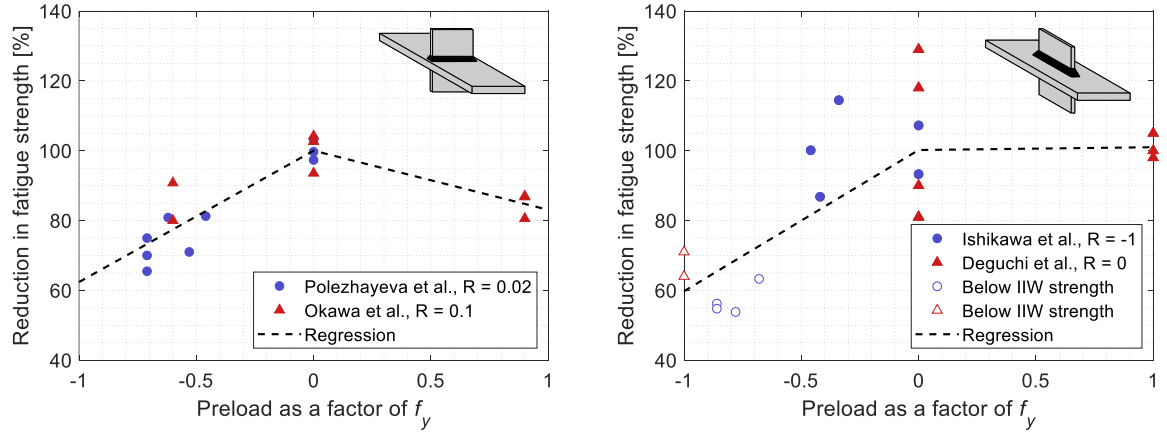

Figure 21. Fatigue strength with fixed SN slope of $m = 5$ as a function of the degree of preload. Regression lines show the fatigue strength reduction due to preloads. Fatigue strength with zero preload is 100 %.

Regarding the fatigue performance under VA loading, similar observations as for the preload studies are made related to notch intensity. Experimental VA studies have mostly found a worsened performance for longitudinal attachment details compared with their CA strengths ([6][56][86]–[90]), whereas for transverse attachments, similar or even longer fatigue lives were obtained ([48][91]–[94]). An overview of these studies is given in Table 8.

Usually assessed based on Palmgren-Miner's linear damage summation, VA loading can be compared with CA fatigue strengths with a single equivalent stress range accounting for the damaging effects of all stress ranges included in the load spectrum. This equivalent stress range does not, however, account for the added damaging effect if the largest loads in the spectrum cause residual stress relaxation. Hence, this overload effect, as well as the influence of other parameters on the fatigue life, have usually been quantified by the real damage sum, D_{real}. This damage sum is useful in cases where the VA fatigue strength deviates from the CA and is equal to the ratio of the number of cycles to failure from the VA experiment to the expected (calculated) number cycles to failure, $D_{real} = N_{exp}/N_{calc}$. The expected number of cycles is calculated with the CA fatigue strength together with, e.g., the Palmgren-Miner's equivalent stress range.

The real damage sum of most VA experiments involving longitudinal attachment details varied between 0.2-0.4 in the reviewed studies, whereas, transverse attachment details often failed with real damage sums of around 1.0 or higher. However, all experiments conformed with the fatigue strengths provided by the IIW [9]. The low damage sums of longitudinal attachments were often attributed to residual stress relaxation or the influence of fluctuating mean stresses. In cases with fluctuating mean stress, the IIW provides a specified damage of $D_{spec} = 0.2$ at failure, for AW joints [61]. According to Sonsino [95][96], fluctuating mean stresses can in severe conditions cause added damaging effects which cannot be accounted for with conventional mean stress corrections and neither is it considered in Palmgren-Miner's equivalent stress range.

Previous investigations of the fatigue performance of HFMI-treated joints under VA loading have mostly used theoretical probability density functions to produce stress ranges spectra and usually involved low mean stress and stress ratios with constant values, see Table 8. The only studies including varying stress ratios and mean stresses have been conducted by Tai and Miki [86][87] and Ghahremani et al. [91][92]. These were also the only VA studies made with reference to bridges. Furthermore, Ghahremani et al. [91][92] performed the only testing with empirical spectra of realistic in-service bridge loads. Low overall mean stresses were used in almost all these experiments, except for two data points [86]. The investigated mean stress properties, including fluctuating mean stress, were considered uninfluential [86][87][91][92].

Table 8. Reviewed VA studies. T = transverse, L = longitudinal attachments.

Ref	*Load type*	*Detail*
[86][87]	Spectrum: Weibull (bridge), R = Varying (fluctuating mean, only tension)	L
[91][92]	Spectrum: Empirical (bridge), R = Varying (fluctuating mean, only tension)	T
[48]	Block: Storm pattern (offshore), R = Varying (constant mean, 100 MPa including compression)	T
[6][56] [88]	Spectrum: log linear/Gauss like, R = -1 (constant mean, 0 MPa)	L
[93]	Spectrum: Gauss like (crane), R = 0.1 (fluctuating mean)	T
[89]	Spectrum: log linear, R = 0.1 (fluctuating mean)	L
[90]	Block: case specific, R ≈ 0.1 (constant mean, 0.55*S_{max})	L
[94]	Block: case specific, R = 0.1 (fluctuating mean)	T

6.2 Realistic in-service bridge stresses

In Paper IV, design calculations of four case-study bridges that have been built in Sweden were used in conjunction with measured traffic data to simulate realistic in-service stresses. To investigate unfavourable conditions for HFMI-treated welds, composite steel and concrete road bridges were chosen. Such bridges experience high mean stresses from the self-weight of the concrete decks, which in combination with the stresses from traffic produce very high stress ratios. In addition, overloads are considered more severe in road bridges due to lesser control of excessively loaded trucks, variability in the transverse position as well as the occurrence of meeting and following trucks on the bridge. The four case-study bridges are depicted in Figure 22. Bridges 1 and 2 were the same road bridges studied in section 4.2.

The bridges were all designed according to the Eurocodes, using the same partial safety factors and load models in the fatigue designs, without any post-weld treatments. They were designed for a traffic intensity of N_{obs} = 50,000 heavy vehicles per year and service lives of 80 years, except Bridge 2, which was designed for 120 years. To obtain realistic self-weights, the contributions of steel girders, concrete deck and pavement were included in this study. Bending moment influence lines were generated at sections with a spacing of ≤ 1 m for all bridges to obtain in-service stresses at all locations. The influence lines accounted for variations in bending stiffness coming from shear lag, cracking of the concrete deck and variations in steel girder sections. More information on the bridges is provided in Appendix A.

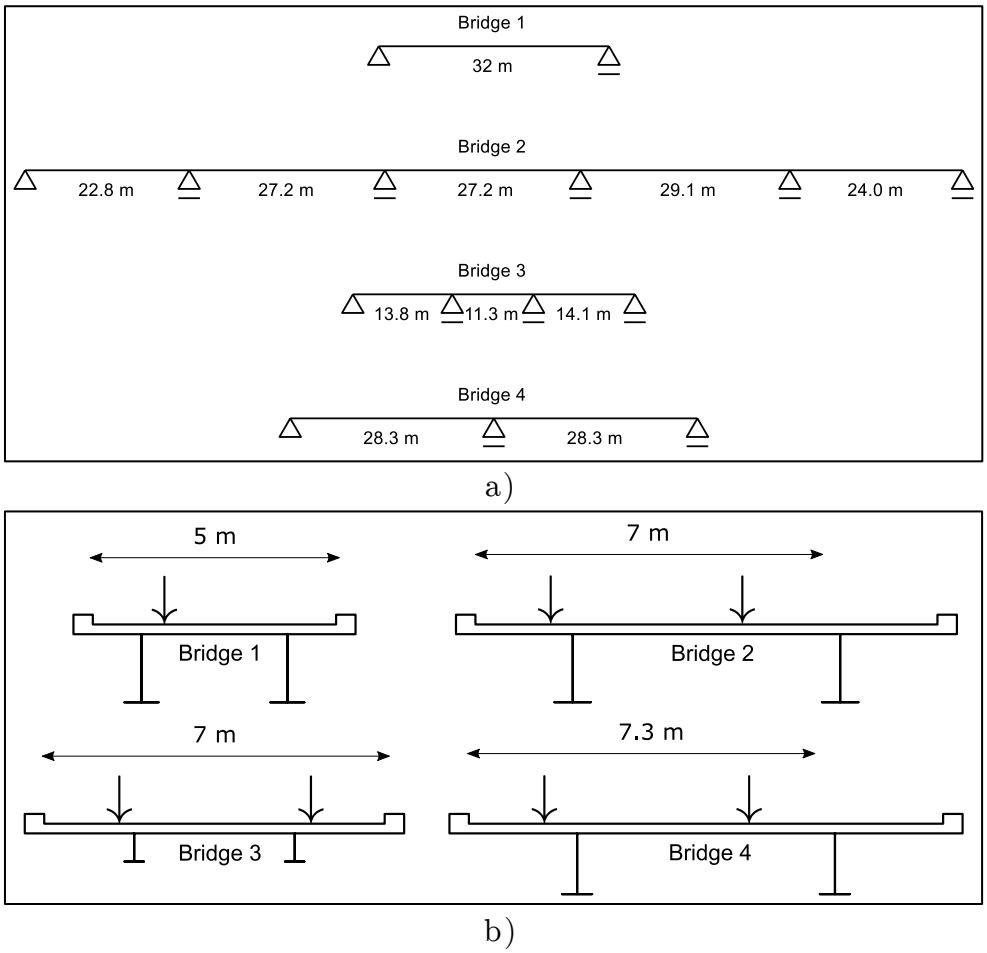

Figure 22. Investigated case-study bridges, each including two I-beams working in composite action with a concrete deck. a) span lengths and b) cross-sections, including expected traffic positions per lane (vertical arrows). Horizontal arrows indicate the portion of the bridge dedicated to road traffic.

A database including 55,000 unique trucks measured at 12 different locations in Sweden was used for the traffic simulations. Detailed information on the database has previously been published by Carlsson [97][98]. Carlsson showed that the traffic data from different locations were reasonably similar and representative of Swedish traffic. The trucks were run one by one over the influence lines with a fixed transverse position (centre of traffic lanes), resulting in normal stress variations over time. Rainflow analysis in accordance with [99] was performed on the stress-time histories to obtain stress ranges with corresponding mean stresses.

Table 9 provides nominal stress results in the most damage-critical sections of the bridges in the AW state, which in all cases occurred near mid-spans at the bottom flanges. Effects of the simultaneous presence of two trucks and variability in positions transverse to the travel direction were studied separately due to their stochastic nature. The effects of the stochastic events on the stresses are given in parenthesis in Table 9. Including these effects, the following characteristics were found: 1) maximum stresses constitute 40-70 % of the yield stresses, 2) the self-weight stresses make up 30-50 % of the maximum stresses and, 3) the ratio of equivalent stress ranges to maximum stress ranges vary between 0.3-0.4.

Table 9. Nominal stress results from bending for critical bridge sections in the AW state. Values in parentheses refer to the effects of the most unfavourable stochastic events.

Bridge	*Design life [Years]*	f_y *[MPa]*	S_{self} *[MPa]*	S_{max} *[MPa]*	ΔS_{max} *[MPa]*	ΔS_{eq3} *[MPa]*	$\Delta S_{eq3,5}$ *[MPa]*
1	80	400	123	241 (+10%)	117 (+20%)	47	49
2	120	345	65	135 (+9%)	82 (+17%)	32	38
3	80	335	68	189 (+9%)	131 (+14%)	41	43
4	80	400	112	216 (+10%)	127 (+16%)	49	50

f_y – yield stress accounting for thickness according to EN-10025-2
S_{self} – stress from self-weight
S_{max} – highest stress peak in the load sequence including self-weight and traffic load
ΔS_{max} – largest stress range in the load sequence
ΔS_{eq3} – single-slope (m = 3) equivalent stress range
$\Delta S_{eq3,5}$ – double-slope (m = 3 & 5) equivalent stress range assuming FAT 80

Two simultaneous trucks on bridges and variable transverse position of traffic can in extreme cases result in higher maximum stresses compared with single trucks travelling with fixed transverse position. Stresses from such events are of interest for comparison to the yield stress in bridges to avoid residual stress relaxation. For this purpose, Monte Carlo simulations of these events were performed in Paper IV, corresponding to 100 times the design lives of the case-study bridges, to capture the most unfavourable cases. For each of the investigated event types, a percentage increase of the stress ranges and maximum stresses was obtained. For Bridges 1 and 3, transverse position resulted in the largest stress increase, whereas for Bridges 2 and 4, meeting truck events were decisive, see Table 9. No interaction between the different event types was considered. Furthermore, no meaningful influence on damage was found for any of the event types. Appendix B provides more information on the modelling of these events.

Bridges with enhanced fatigue strength will possess smaller steel cross-sections and therefore be associated with increased stresses compared with conventional bridges. If not limited by the ULS or SLS, the increased stresses will ultimately be determined by the fatigue strength of the flange-to-web welds (FAT 125), as discussed in chapter 4. Considering that transverse attachments and butt welds (FAT 80) were critical in the original bridges, the stresses in "optimised" HFMI-treated bridges can, at most, be estimated with a factor of $\eta = 125/80 = 1.56$ on the original stresses, see Figure 23. This generates the same FLS utilisation ratio for the optimised case as for the original one. Needless to say, other design limit states or the performance of the HFMI-treated welds, themselves, may restrict the elevation of stresses to lower values. Thus, magnification of the stresses from Table 9 with $\eta = 1.56$ represents the highest possible stresses in HFMI-treated bridges and is used for further evaluations. Table 10 provides some characteristic load quantities relevant for HFM-treated bridges. The percentage increase in maximum stresses and stress ranges due to the stochastic events from Table 9 also apply for the results in Table 10. For more information on these results, see Paper IV.

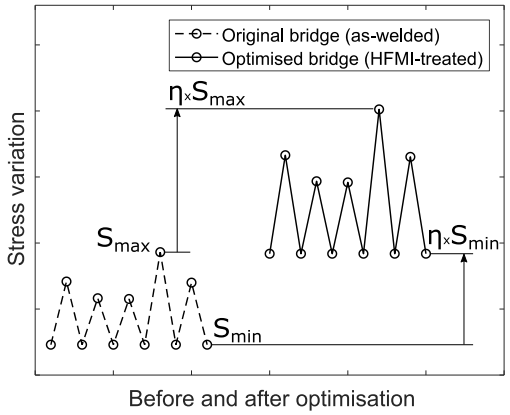

Figure 23. Schematic illustration of the elevation of stresses by η in HFMI-treated bridges.

The mid-span of the simply supported bridge (Bridge 1) involved the most unfavourable spectrum shape as well as the highest stress ratios compared with the most damage-critical sections in the other bridges, see Figure 24. All other sections, including non-damage critical sections, were also studied to ensure that the mid-span of Bridge 1 included the worst load case, even if normalised stress ranges were considered. It was found that neither the spectrum shape nor the stress ratios exceeded those in the mid-span of Bridge 1. At the damage-critical sections, which occurred near the mid-spans in all the bridges and involved solely tensile stresses, the smallest stress range cycles had the highest stress ratios and vice versa. This meant that the mean stresses were non-constant. In Paper IV and V, the topic of varying mean stress is treated and in section 6.3, a method of considering it in fatigue assessment is presented.

Table 10. Results of some characteristic load quantities for critical sections in HFMI-treated bridges, η = 1.56. Stresses are nominal (MPa).

Bridge	*Section*	R_{avg}	R_{max}	*R'*	S_{self}	S_{min}	S_{max}	ΔS_{max}	ΔS_{eq5}	$\Delta S_{eq5,9}$
1	16.0 m	0.76	0.88	0.51	192	192	375	183	82	81
2	92.5 m	0.70	0.84	0.39	102	83	211	128	53	59
3	5.0 m	0.65	0.85	0.31	107	90	294	204	72	73
4	42.6 m	0.72	0.86	0.41	174	139	337	198	85	84

R_{avg} – average stress ratio in the load sequence
R_{max} – highest stress ratio in the load sequence
R' – stress ratio of the largest stress range in the load sequence
S_{min} – lowest stress valley in the load sequence including self-weight and traffic load
ΔS_{eq5} – single-slope (m = 5) equivalent stress range
$\Delta S_{eq5,9}$ – double-slope (m = 5 & 9) equivalent stress range assuming FAT 140

In Paper IV, the bridge sections in which compressive stresses arose were also studied, from the viewpoint of residual stress relaxation. In the investigated bridges, such sections occurred in regions with constant and low overall mean stresses and lower stress ranges compared with the damage-critical sections. It was found that if tensile stresses fulfil the requirement given by the IIW (Figure 5), the compressive stresses will constitute very small proportions of the yield stress. By considering this and comparing the stress levels to those from the reviewed preload studies, the compressive stresses were regarded as benign, not requiring further assessment.

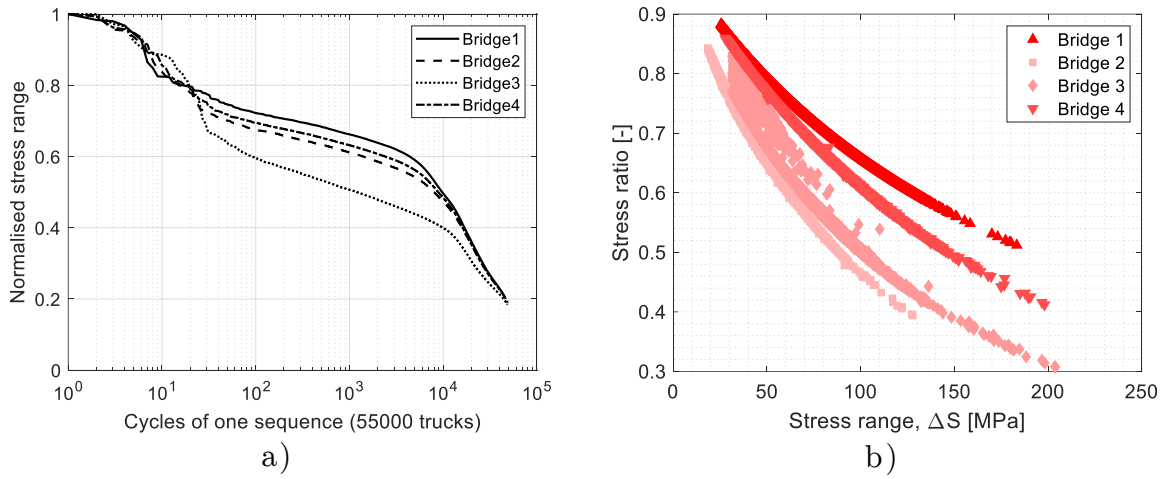

Figure 24. a) Normalised stress range spectra and b) stress range versus stress ratio relationships for the critical sections in HFMI-treated bridges.

6.3 Fatigue experiments

Based on the assessments in the previous section, the load history of the mid-span of Bridge 1 was chosen for the VA fatigue experiments (Figure 25), which were executed with cycle-by-cycle random sequence spectrum loading with frequencies between 10-20 Hz. The same load setup as in Figure 17 for the CA experiments was used. A total of 12 transverse attachment specimens were tested with HFMI-treated joints, coming from the same batch as test series 4 in Table 7. All specimens failed at the weld toe, with failure defined as a half thickness crack.

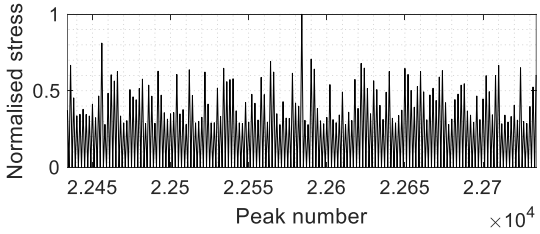

Figure 25. A normalised sequence sample of the VA loading centred around the highest peak load with minimum stresses equal to zero.

The first questions to be answered by the experiments were whether a bridge VA load, including varying mean stresses, would have any negative influence on the fatigue performance of the studied specimens, compared with the CA strength. Such negative influences could potentially arise from residual stress relaxation caused by the highest stress peaks or from mean stress fluctuations in severe cases [95][96]. For this purpose, a series of four HFMI specimens with low overall mean stresses (LM), i.e. average stress ratios of approximately $R = 0.1$ were tested and compared with the CA $R = 0.1$ fatigue strengths obtained from section 5.1 (test series 4). Palmgren-Miner's equivalent stress range according to Equation (9) was used for this comparison, with the SN slope $m = 6.5$. In this equation, ΔS_i is the stress range of the i^{th} load cycle in the spectrum and n_i, the number of occurrences associated to that cycle.

$$\Delta S_{eq} = \sqrt[m]{\frac{\sum(n_i \cdot \Delta S_i{}^m)}{\sum n_i}} \tag{9}$$

The second question was related to the treatment of high mean stresses and stress ratios which vary with the stress range as in Figure 24b. The challenge is that, on the one hand, no single *SN* curve is valid when the stress ratios vary, thus, the penalty method of IIW (Table 1) cannot be used directly. On the other hand, Palmgren-Miner's equivalent stress range (Equation (9)) does not account for the mean stress. The aim was, therefore, to quantify the mean stress effect under spectrum loading by considering the stress ratio of each load cycle individually and performing a mean stress correction for each cycle according to a predetermined relationship. It was assumed that a continuous representation of the IIW stress ratio penalties (Table 1) could be used for this relationship, including extrapolation of the IIW method to $R = 1.0$. However, instead of reducing the *fatigue strength* as suggested by the IIW, the *stress ranges* were enlarged with a corresponding factor according to Figure 26. In other words, each FAT class reduction was represented by a factor of approximately 1.125 on the stress range. Hence, Equation (10) and (11) could be used to express the VA loading with a modified equivalent stress range to be compared with the CA $R = 0.1$ fatigue strength. Three high mean (HM) test series with different stress levels were tested for this purpose, HM1, HM2 and HM3. In addition, one test specimen (HM4-1) was compressively pre-loaded five times with -480 MPa, before fatigue testing under similar stress levels as in Bridge 1 to simulate unfavourable conditions during the construction phase. The results are summarised in Figure 27 and Table 11.

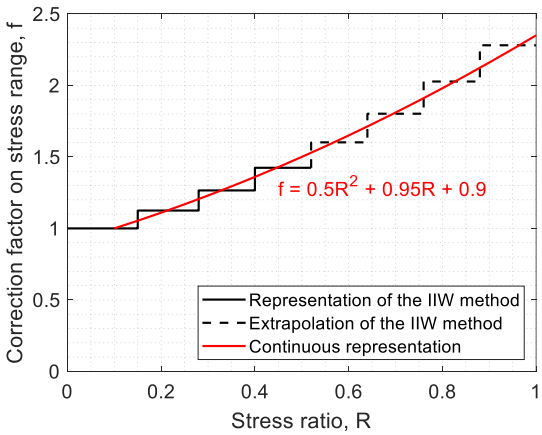

Figure 26. Illustration of the continuous mean stress correction implemented in here and the underlying stepwise method.

$$\Delta S_{eq,R} = \sqrt[m]{\frac{\sum(n_i \cdot (\Delta S_i \cdot f_i)^m)}{\sum n_i}} \tag{10}$$

$$\begin{aligned} f_i &= 0.5R_i^2 + 0.95R_i + 0.9 \quad for\ 0.1 \leq R_i < 1.0 \\ f_i &= 1.0 \qquad\qquad\qquad\qquad otherwise \end{aligned} \tag{11}$$

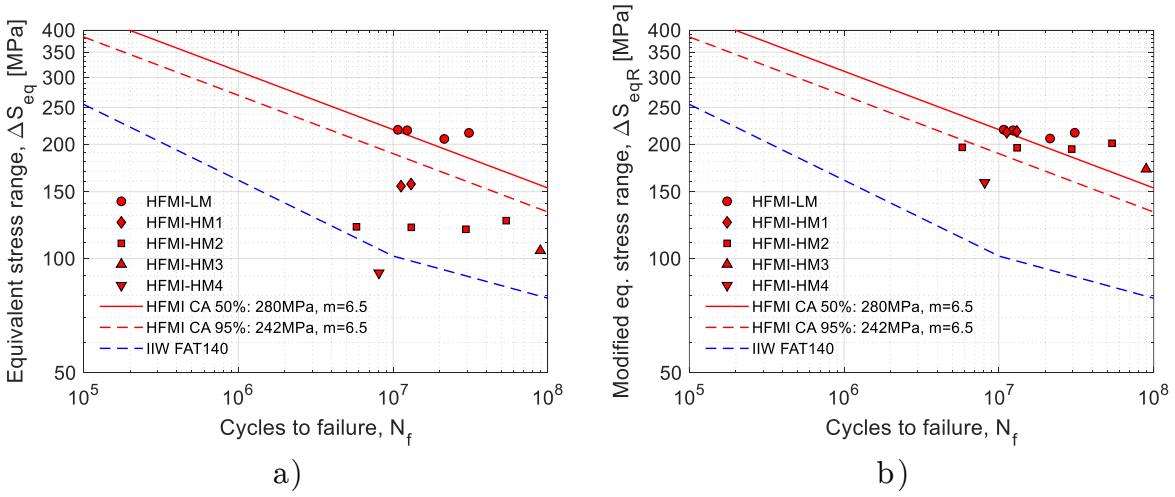

Figure 27. a) Equivalent stress ranges with single-slope Palmgren-Miner's sum according to Equation (9) and b) modified equivalent stress ranges according to Equation (10) to include the mean stress effect, compared with the experimental CA $R = 0.1$ curves from section 5.1.

Table 11. Results of the VA fatigue experiments.

Specimen	S_{max}	S_{min}	ΔS_{max}	ΔS_{min}	ΔS_{eq}	$\Delta S_{eq,R}$	R_{max}	R_{min}	R_{avg}	Nf	Description
HFMI-LM-1	435	17	418	106	218,4	218,5	0,14	0,04	0,10	10 732 297	Low mean
HFMI-LM-2	435	20	415	104	217,7	217,7	0,16	0,05	0,09	12 330 575	Low mean
HFMI-LM-3	419	23	396	98	206,6	207,1	0,19	0,05	0,12	21 393 484	Low mean
HFMI-LM-4	427	21	407	103	214,3	214,5	0,17	0,05	0,11	30 892 827	Low mean
HFMI-HM1-1	426	126	300	68	155,1	215,1	0,65	0,30	0,52	11 244 773	High mean level 1
HFMI-HM1-2	429	126	303	69	157,1	216,2	0,65	0,29	0,52	13 052 850	High mean level 1
HFMI-HM2-1	427	194	234	55	121,2	196,3	0,78	0,45	0,67	5 796 948	High mean level 2
HFMI-HM2-2	424	192	232	56	120,8	195,8	0,77	0,45	0,67	13 096 410	High mean level 2
HFMI-HM2-3	424	193	231	56	119,4	194,3	0,78	0,46	0,67	29 530 032	High mean level 2
HFMI-HM2-4	428	191	237	59	125,8	201,2	0,76	0,45	0,66	53 752 303	High mean level 2
HFMI-HM3-1	388	188	200	51	104,9	172,0	0,79	0,48	0,68	89 302 861	High mean with realistic stress ranges
HFMI-HM4-1	375	195	179	41	91,6	158,5	0,83	0,52	0,74	8 092 180	Five preloads of -480 MPa then high mean with realistic stress ranges

As can be seen in Figure 27, all tests in the LM series performed equally or better than the CA $R = 0.1$ strength. The obtained real damage sums were all above 1.0 with the average value of 1.6 for the LM test series. Thus, the bridge VA loading in it-self, including its characteristics, was not detrimental for the fatigue performance, meaning that no other damaging effect aside from the stress ranges, which is captured by Equation (9), took place during the loading. On the other hand, the HM1, HM2 and HM3 series performed worse than the CA $R = 0.1$ strength, as seen in Figure 27a. This was mainly due to the high mean stresses which are not captured by Equation (9), but also, because of the large scatter in the HM2 series. More elaboration on the cause of this scatter was made in Paper V. It is noted from Figure 27a, however, that the HM2

results still were situated above the characteristic design curve of FAT 140 as suggested by the IIW for $R = 0.1$ loading, even though the average stress ratios were far greater.

From Figure 27b, it is observed that a representation of the HM data with Equation (10) and (11) allowed for a direct comparison to the CA $R = 0.1$ strength. Excluding HM4-1 which was preloaded, an average real damage sum of 1.4 was obtained. This shows that the assumed mean stress correction together with the modified equivalent stress range appropriately account for the stress ranges as well as the high and varying mean stresses, and that no other damaging effects other than these took place. Finally, it is seen in Figure 27 that the fatigue performance of the HM4-1 specimen decreased dramatically due to the five compressive preloads. Seeing that large scatters can occur, it is concluded that compressive preloads of this magnitude is unacceptable and must be avoided after HFMI treatment.

6.4 Treatment of mean stress

This section further explores the validity of the mean stress correction according to Equation (11) and presents a new method to consider the mean stress effect in VA loading for design purposes. A summary of the work of generalising the method for Swedish road bridges is presented and verified against the VA experiments as well as the case-study bridges from section 6.2. The result is then used to propose a design framework in chapter 7.

Since the establishment of the IIW method for stress ratio consideration, several fatigue tests with stress ratios $R \geq 0.5$ have been published. Here, it is investigated if the extrapolation of the IIW method can be justified, besides what was shown by the VA experiments in the previous section. Yonezawa et al. [100] studied longitudinal attachment specimens with different steel grades under CA loading with various stress ratios between $-0.5 \leq R \leq 0.8$. In Figure 28, a comparison of the results from [100] is made with mean stress correction according to Equation (11), by assuming the same fatigue strength at $R = 0.1$ and dividing it by f for higher R values.

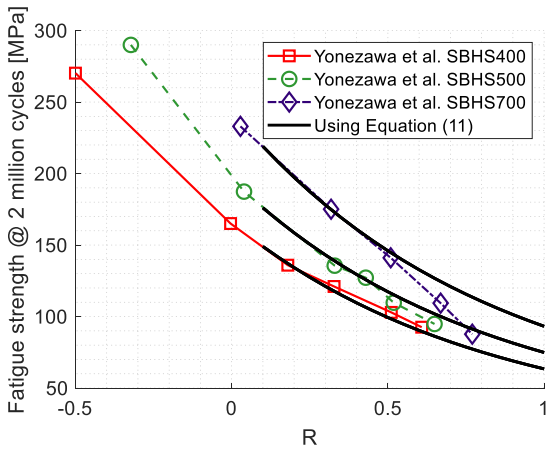

Figure 28. Comparison of mean stress correction according to Equation (11) with experimental results from [100].

It is observed that for the lower steel grades, mean stress correction with Equation (11) predicted the results very well and followed the same trends as the experiments. On the other hand, for the highest steel grade, the decline in strength was stronger for $R \geq 0.5$ such that Equation (11) over-predicted the strengths. This over-prediction occurred since the fatigue strength at $R = 0.1$ was very high. In design situations, however, the characteristic fatigue strength at $R = 0.1$ will be significantly lower as presented in section 3.4, Figure 10. Therefore, situations where Equation (11) over-predicts the fatigue strength due to high steel grades are not expected to be a concern in design. With the comparison in Figure 28 and the VA fatigue experiments conducted in this thesis, Equation (11) is thought to be reasonable and valid for $R > 0.5$.

As was shown by the VA experiments, it was possible to properly capture the effect of varying mean stresses under spectrum loading with the modified equivalent stress range, $\Delta S_{eq,R}$ from Equation (10), in conjunction with the mean stress correction from Equation (11). Hence, for spectrum loads where the mean stress and stress ratio is non-constant, the ratio of $\Delta S_{eq,R}/\Delta S_{eq}$ can with advantage be utilised to represent the severity of the mean stress effect. Generalising this ratio for different design applications and spectra could provide a simplified method for engineers to consider the mean stress effect without detailed knowledge about the real VA load. Since design codes, such as the Eurocodes, provide basic methods to obtain equivalent stress ranges [76], ΔS_{eq}, and since the real VA fatigue load seldom is available in the design stage of structures, a generalised version of $\Delta S_{eq,R}/\Delta S_{eq}$ can simply be used to magnify ΔS_{eq}.

In Paper V, the ratio of $\Delta S_{eq,R}/\Delta S_{eq}$ was denoted as a new factor, λ_{HFMI}, according to Equation (12). It was realised that in order to capture the severity of the mean stress effect in a spectrum load, λ_{HFMI} needs to account for three main parameters; 1) the stress ratio content (variation) from the VA load, 2) the stress ratio contribution from the self-weight and 3) a mean stress correction relationship. Point 1) necessitates specific VA loads to be studied and incorporated. Here, the Swedish traffic pool from section 6.2 was used together with influence lines of different locations on prismatic beams with various span lengths. Both simply supported beams and symmetrical continuous double-span beams were studied. The contribution of self-weight stresses, point 2), was represented with the ratio Φ, according to Equation (13), where S_{sw} is the self-weight stress and ΔS_{max} is the largest stress range from traffic. Equation (11) was implemented for point 3). Clear relationships between Φ and λ_{HFMI} could be found for all the investigated influence lines, which included several beam locations between mid-span ($0.5L$) to mid-support ($1.0L$).

$$\lambda_{HFMI} = \frac{\Delta S_{eq,R}}{\Delta S_{eq}} \tag{12}$$

$$\Phi = \frac{S_{sw}}{\Delta S_{max}} \tag{13}$$

At each investigated beam location, one of the shortest span lengths produced the highest Φ-λ_{HFMI} relationship, whereas this relationship remained fairly constant for longer span lengths, see Figure 29. An explanation for this observation is provided in Paper V. To simplify the method and obtain conservative estimations of λ_{HFMI} in design, it was proposed in Paper V to distinguish only between two different locations on bridges; mid-span and mid-support sections, in the same manner as in Eurocode 3 [76]. For mid-span sections in bridges, the Φ-λ_{HFMI} relationship of the shortest span length of simply supported beams was proposed, and for mid-support sections, the shortest span length of the $0.85L$ location on continuous beams was proposed.

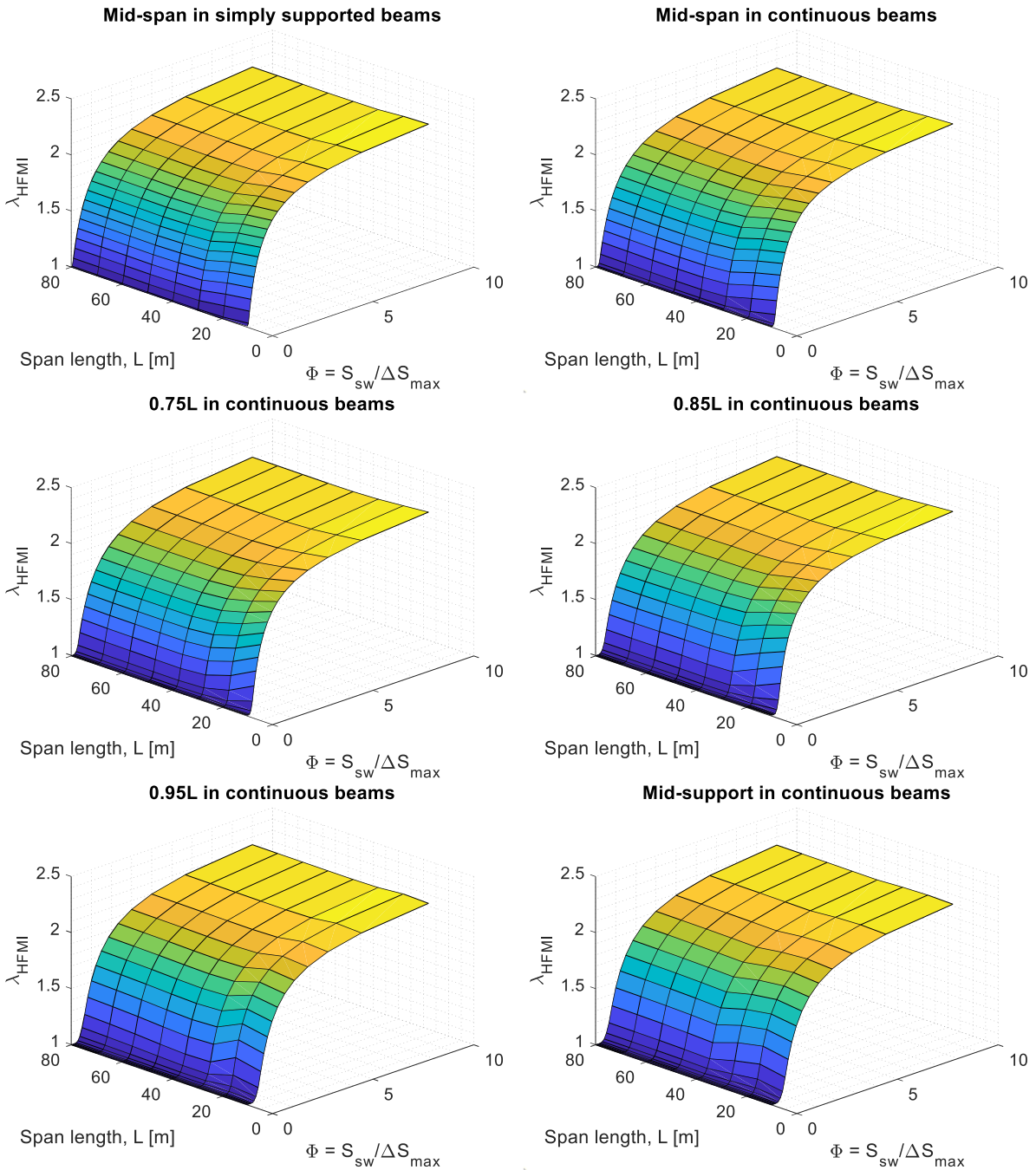

Figure 29. Influence of span length on the Φ-λ_{HFMI} relationship at different locations on the investigated beams.

In Figure 30, the proposed Φ-λ_{HFMI} relationships are compared with the actual Φ-λ_{HFMI} values of both the VA fatigue experiments and some of the bridge sections of the case-study bridges from section 6.2. Appendix C provides comparisons for all the bridge cross-sections. The conservatism observed in Figure 30a is because the data involved VA loads from span lengths greater than 10 m, which was the length chosen for the design curves. On the other hand, the data point of Bridge 3, which had the shortest span length of 13.8 m, was situated closest to the design curve. Expressions for the design curves are provided in section 7.2 together with a method to estimate ΔS_{max}, the largest stress range from traffic needed for calculating Φ.

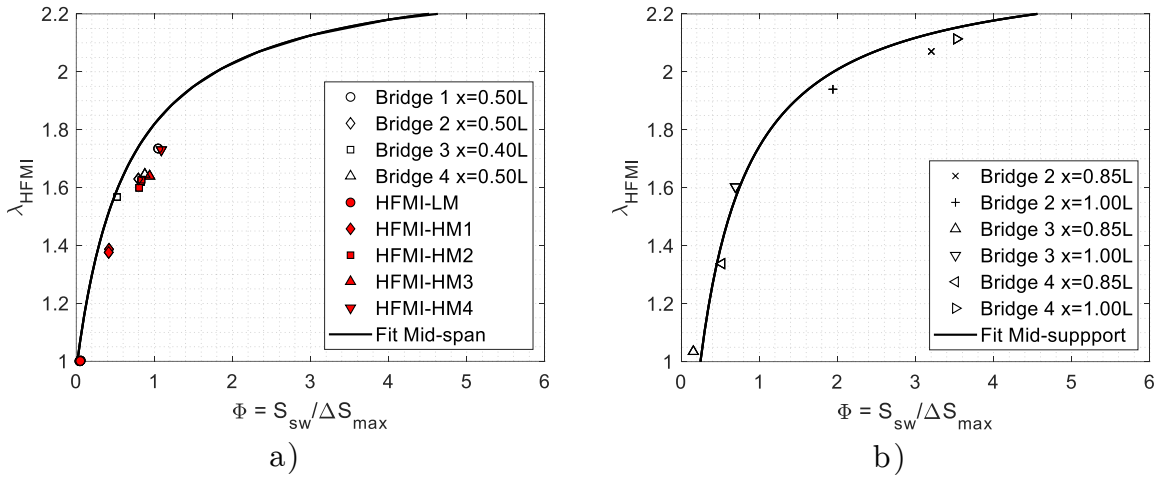

Figure 30. Exact Φ-λ_{HFMI} values of the VA experiments and some selected sections in the case-study bridges from section 6.2, compared with the proposed design curves. Graph a) is for mid-span and graph b) for mid-support sections.

7 Proposed design procedures

Based on the investigations made in this thesis, proposals for different aspects in the design of HFMI-treated joints is presented in this chapter. For constant amplitude (CA) loading, a model is proposed for predicting the fatigue strength of HFMI-treated specimens with various yield stresses, thicknesses and stress ratios, based on the results and methodology presented in chapter 3. For variable amplitude (VA) loading, a design framework is proposed which allows bridge designers to account for the effects of high and varying mean stresses without the need of cycle-by-cycle spectrum calculations.

7.1 Fatigue strength prediction

In chapter 3, characteristic fatigue strengths were established for transverse butt welds as well as for non-load-carrying transverse and longitudinal attachments, for CA $R = 0.1$ loading. These fatigue strengths are valid for a reference yield stress of 355 MPa and specific main plate thicknesses for the different types of weldments. This section proposes a model for predicting the fatigue strength for other yield stresses, main plate thicknesses and stress ratios. For the butt welds and transverse attachment specimens, strengths of 165 and 180 MPa were obtained for reference main plate thicknesses of 16 and 9 mm, respectively. For the longitudinal attachments, a characteristic fatigue strength of 109 MPa was considered valid for attachment lengths of ≥ 100 mm, which corresponded to a thickness of 17 mm. To represent the butt weld and transverse attachment data with a reference thickness of 25 mm for design, a correction according to Equation (1) is made using the same exponents as were obtained in section 3.3. For the butt welds and transverse attachments, the characteristic strengths become 161 and 146 MPa, respectively. The nearest FAT classes of 160 and 140 are proposed for the design of these weldments with rounded values for the thickness correction exponents. For the longitudinal attachment detail, the nearest lower FAT class of 100 is proposed. Following the same approach as in section 3.3 for this detail, a lower limit on thickness is required which becomes $t_{lim} = 11$ mm for FAT 100. For thinner plates down to 5 mm, a reduced FAT class of 90 is considered appropriate. Table 12 gives a summary of the proposed fatigue strengths.

For butt weld and transverse attachment joints with main plate thicknesses $t > t_{ref}$, the reference fatigue strengths from Table 12, $\Delta\sigma_{c,HFMI,ref}$, should be multiplied with f_t from Equation (14). For longitudinal attachment details, f_t should be set to 1.0.

$$\begin{aligned} f_t &= \left(\frac{25}{t}\right)^n \quad \textit{for transverse butt welds and transverse stiffeners} \\ f_t &= 1.0 \qquad \textit{for longitudinal attachments} \end{aligned} \tag{14}$$

Table 12. Proposed fatigue strengths, $\Delta\sigma_{c,HFMI,ref}$, for yield stress of 355 MPa and R = 0.1.

Detail	$\Delta\sigma_{c,HFMI,ref}$	*Thickness effect*
Transverse butt welds 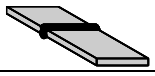	160	Correction exponent $n = 0.1$ $t_{ref} = 25$ mm
Non-load-carrying transverse attachments 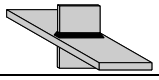	140	Correction exponent $n = 0.2$ $t_{ref} = 25$ mm
Non-load-carrying longitudinal attachments ($\geq$ 100 mm) 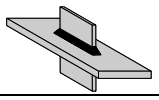	100	$t > 11$ mm
	90	$5 \leq t \leq 11$ mm

In section 3.2, linear relationships between the yield stress and fatigue strength according to Figure 8 was established for the three different joints types. An adaptation of Equation (2) for yield stress correction is given in Equation (15) which provides a factor to be multiplied with $\Delta\sigma_{c,HFMI,ref}$ to obtain the fatigue strength for any yield stress. The yield stress interval of $235 \leq f_y \leq 960$ MPa was covered in the database and is therefore valid here. A conservative value of $\beta_1 = 0.1$ is incorporated for design.

$$f_f = 1 + \frac{0.1(f_y - 355)}{\Delta\sigma_{c,HFMI,ref}} \quad for\ 235 \leq fy \leq 960\ MPa \tag{15}$$

To consider the stress ratio effect in CA fatigue loading, an adaptation of Equation (11) is given in Equation (16) for multiplication with $\Delta\sigma_{c,HFMI,ref}$.

$$\begin{aligned} f_R &= \frac{1}{0.5R^2 + 0.95R + 0.9} \quad && for\ 0.1 \leq R < 1.0 \\ f_R &= 1.0 && otherwise \end{aligned} \tag{16}$$

Finally, the proposed fatigue strengths in Table 12 can be modified according to Equation (17) to predict the fatigue strength for specific cases. Using this prediction model, the fatigue strength of all data included in the database and additional data with other stress ratios is predicted as shown in Figure 31. Only 16 data points out of 767 were over-predicted, corresponding to a failure probability of 2%. More detailed versions of Figure 31 and references for the additional data is provided in Appendix D.

$$\Delta\sigma_{c,HFMI} = f_t f_f f_R \Delta\sigma_{c,HFMI,ref} \tag{17}$$

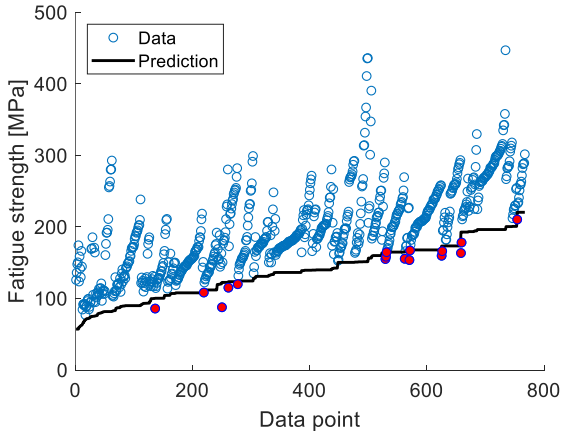

Figure 31. Prediction of fatigue strengths of experimental data with the proposed prediction model according to Equation (17). Colour-filled data points (16 of the 767 in total) indicate over-predicted results.

7.2 Variable amplitude framework

To consider the mean stress effect in spectrum loads with varying mean stresses and stress ratios, it was proposed in Paper V to magnify the Palmgren-Miner's equivalent stress range by the factor λ_{HFMI}. This factor is found by considering the ratio between self-weight stress and the maximum stress range from the VA load, ΔS_{max}, defined as the parameter Φ. For road bridges, Φ-λ_{HFMI} relationships were proposed for mid-span and mid-support sections as presented in Figure 32.

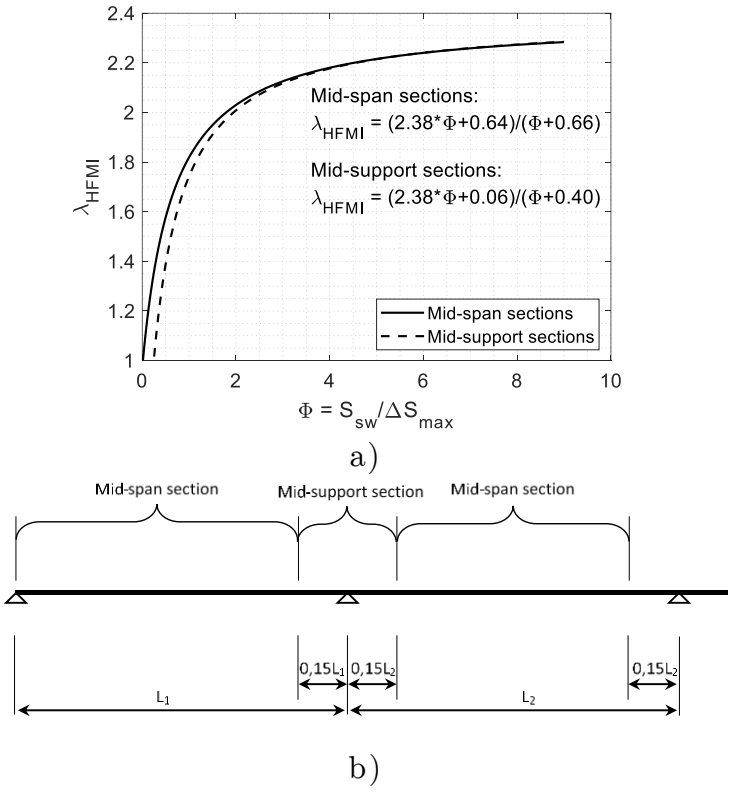

Figure 32. a) Φ-λ_{HFMI} curves proposed for use in the design of mid-span and mid-support sections and b) the definition of the regions where these sections are applicable, adapted from [76].

Since the most common fatigue assessment in the Eurocodes involves fatigue load model 3 (FLM3), the relationship of this load model to the real traffic was investigated and it was found that, for traffic loads in Swedish roads, ΔS_{max} could simply be replaced by $2\times\Delta S_p$, i.e. twice the FLM3 stress range. For more details on this topic, the reader is referred to Paper V. To estimate λ_{HFMI}, either Equation (18) or (19) should be used, depending on the bridge location, together with Equation (20), in which ΔS_p is the largest stress range generated by FLM3. These expressions are only valid for positive self-weight stresses, S_{sw}. If λ_{HFMI} smaller than 1.0 are obtained, they should be set to 1.0.

Mid-span:
$$\lambda_{HFMI} = \frac{2.38\Phi + 0.64}{\Phi + 0.66} \tag{18}$$

Mid-support:
$$\lambda_{HFMI} = \frac{2.38\Phi + 0.06}{\Phi + 0.40} \tag{19}$$

$$\Phi = \frac{S_{sw}}{2\Delta S_p} \tag{20}$$

Since the mean stress effect is included on the load side, the fatigue strength at two million cycles to be used in fatigue verification should be calculated according to Equation (21). The parameters involved in this Equation are defined in section 7.1.

$$\Delta\sigma_{c,HFMI} = f_t f_f \Delta\sigma_{c,HFMI,ref} \tag{21}$$

7.3 Calculation example

For of a vertical stiffener joint, welded to a beam flange with thickness 30 mm, which is made of steel S460, to be HFMI-treated after bridge erection, the following procedure should be followed. It is assumed that the yield stress is $f_y = 460$ MPa and that the self-weight stress is $S_{sw} = 100$ MPa. The equivalent stress range at two million cycles generated by the lambda method of the Eurocode, $\Delta S_{E,2}$, is assumed to be equal to the stress range generated by the FLM3, which is assumed to be $\Delta S_p = 90$ MPa. Starting with $\Delta\sigma_{c,HFMI,ref} = 140$ MPa, a thickness correction factor of $f_t = (25/30)^{0.2} = 0.96$ should be used together with a yield stress correction factor of $f_f = 1+(0.1[460\text{-}355]/140) = 1.08$. No stress ratio correction should be made for the fatigue strength since, in bridges, spectrum loads with varying mean stresses and stress ratios exist. This effect is instead covered on the load side. The fatigue strength at two million cycles becomes $\Delta\sigma_{c,HFMI} = 0.96\times1.08\times140 = 145$ MPa. Considering the self-weight ratio to the traffic load gives $\Phi = 100/(2\times90) = 0.56$. The λ_{HFMI} value for mid-span sections then becomes $\lambda_{HFMI} = (2.38\times0.56+0.64)/(0.56+0.66) = 1.62$. Assuming the safety factors of 1.35 and 1.0 on the resistance and load sides, respectively, gives a load of $1.0\times1.62\times90 = 146$ MPa and a resistance of $145/1.35 = 107$ MPa. As a result, the utilisation in the fatigue limit state becomes $146/107 = 1.36$, which is on the un-safe side. A bridge section as in this example would, therefore, require the HFMI treatment to be performed after the erection of the bridge, in which case the λ_{HFMI} could be set to 1.0, giving a utilisation factor of $90/107 = 0.84$. Needless to say, this would require more research on the topic of HFMI treatment under pre-existing tensile loads.

8 Conclusions

This thesis aimed to investigate the fatigue performance of high-frequency mechanical impact (HFMI) treated welded joints under conditions relevant for bridges. 1) Studies were conducted on the potential for material saving by post-weld treatment of bridge welds, 2) the thickness effect of HFMI-treated joints was investigated and 3) realistic in-service bridge loads were simulated to perform a detailed evaluation of the application of HFMI. Based on these findings, 4) the fatigue performance under realistic in-service bridge loads was assessed experimentally and 5) design procedures were proposed. Based on the studies in this thesis, the following main conclusions can be drawn.

- It was shown calculation wise that a material saving of around 20% is possible for the main load-carrying members of bridges. This could be achieved for a case-study railway bridge with only the application of post-weld treatment, without increasing the steel grade, which was S355 in the original design. In composite steel and concrete bridges, the post-weld treatment was calculated in conjunction with increased steel grades of S460 and S620.

- Longitudinal flange-to-web welds are common in bridges. These joints should not be post-weld treated and have a FAT class of 125 at the best in the as-welded state. This limits the fatigue strength improvement that can be utilised in the design of the main load-carrying members.

- Based on an established database of HFMI-treated specimens, the thickness correction exponent for butt welds was calculated to $n = 0.055$. For non-load-carrying transverse attachment joints, $n = 0.207$ was obtained. Non-load-carrying longitudinal attachment joints showed a reverse thickness effect of $n = -0.188$. These exponents are lower than what is given by the IIW for as-welded joints as well as for HFMI-treated joints in the cases of butt welds and longitudinal attachments. Hence, for these joint types, the IIW assumes an over-conservative thickness effect.

- For HFMI-treated non-load-carrying transverse attachment joints with constant attachment thickness and weld size, $n = 0.135$ was derived based on fatigue experiments conducted in this thesis. The fatigue test specimens comprised the main plate thicknesses of 40 and 60 mm and showed significantly greater fatigue strength compared with recommended values by the IIW under constant amplitude loading.

- The in-service stresses of four composite steel and concrete case-study bridges showed that the mean stresses and stress ratios are varying in realistic bridge

loads and that the permanent loads from self-weight stresses contribute to very high overall stress ratios. For such bridges, which are heavy, the full potential of material saving can only be realised if HFMI treatment is performed on-site, after the full application of all permanent loads.

- In the investigated case-study bridges, the highest stress peaks, including traffic and permanent loads, amounted to up to 70% of the yield stress in the fatigue damage-critical locations. Up to 50% of these stress peaks comprised stresses from permanent loads.

- Including the detrimental effect of high tensile permanent loads in the fatigue damage assessment showed that the damage-critical locations in HFMI-treated bridges remain unchanged compared with conventional bridges. The fatigue damage in mid-span regions was consistently and by a great margin higher compared with mid-support regions, even when accounting for cracking in the concrete deck over the mid-supports.

- Based on a literature review, it was deemed that compressive stress in bridges are benign when it comes to the consequences of residual stress relaxation. Compressive stresses only occur in low-damage locations with low overall mean stresses and constitute small proportions of the yield stress.

- Low mean stress variable amplitude fatigue experiments revealed that non-load-carrying transverse attachment specimens perform equally well as under constant amplitude loading, confirming similar observations in the literature. But it was experimentally shown that high minimum stresses (e.g. from self-weight) dramatically reduce the fatigue performance.

- A modified version of the Palmgren-Miner's equivalent stress range is proposed in which every stress range is magnified depending on the stress ratio of its cycle. A continuous expression is suggested for the magnification factor based on the IIW model for stress ratio penalties. Following this approach revealed very good agreement of the tested variable amplitude data with the constant amplitude strength for $R = 0.1$ loading.

- Based on the proposed method of stress ratio consideration, a design framework is also proposed allowing bridge designers to include the effect of mean stress under variable amplitude loading in a simple manner. This framework was verified against both the conducted experiments and the case-study bridges used in this thesis and was shown to produce reasonable results.

8.1 Suggestions for further research

The following subjects are proposed for further research.

- Application of HFMI treatment under pre-existing tensile loads, simulating the permanent loads, and subsequent fatigue testing with high mean stresses, both with constant and variable amplitude loading. Based on these findings, to propose design procedures for when HFMI treatment is performed under tensile loads.

- High mean stress constant amplitude fatigue tests with stress ratios of $0.5 < R \leq 0.9$ to complement existing results and to further examine the validity of the proposed mean stress correction method.

- Variable amplitude testing of longitudinal attachment details under the same bridge spectrum loads that were used here and investigation of whether the proposed design procedures would be valid in such cases.

- Investigation of road traffic from other countries in terms of mean stress severity in spectrum loading and comparison to the results in this thesis for further understanding and design methodology development.

- Using the proposed design framework to develop generalised expressions to consider the mean stress effect in other fields of application, such as for railway traffic, offshore structures and cranes.

References

[1] P. Shams-Hakimi, "Performance of high-frequency mechanical impact treatment for bridge application," 2017.

[2] K. J. Kirkhope, R. Bell, L. Caron, and R. I. Basu, "Weld detail fatigue life improvement techniques (No. SR-1379)," MIL Systems Engineering, Ottawa, Canada, SR-1379, 1996.

[3] E. S. Statnikov, V. O. Muktepavel, and A. Blomqvist, "Comparison of Ultrasonic Impact Treatment (UIT) and Other Fatigue Life Improvement Methods," *Weld. World*, vol. 46, no. 3–4, pp. 20–32, 2002, doi: 10.1007/BF03266368.

[4] M. M. Pedersen, M. O. Ø. Mouritsen, M. M. R. Hansen, M. J. G. Andersen, and M. J. Wenderby, "Comparison of Post-Weld Treatment of High-Strength Steel Welded Joints in Medium Cycle Fatigue," *Weld. World*, vol. 54, no. 7–8, pp. R208–R217, 2010.

[5] T. Iwata, T. Niwa, Y. Tanaka, T. Ando, and Y. Anai, "Thickness effect on fatigue strength of welded joint improved by HFMI." International Institute of Welding, 2015.

[6] H. C. Yildirim and G. B. Marquis, "A round robin study of high-frequency mechanical impact (HFMI)-treated welded joints subjected to variable amplitude loading," *Weld. World*, pp. 437–447, 2013, doi: 10.1007/s40194-013-0045-3.

[7] T. Ummenhofer *et al.*, *REFRESH–extension of the fatigue life of existing and new welded steel structures (Lebensdauerverlängerung bestehender und neuer geschweißter Stahlkonstruktionen)*. Düsseldorf, Germany: Forschungsvereinigung Stahlanwendung e.V. (FOSTA), 2010.

[8] "Ultrasonic Impact treatment - SONATS - SHOT PEENING - Needle Peening and metal forming." [Online]. Available: http://www.sonats-et.com/. [Accessed: 05-May-2017].

[9] G. B. Marquis and Z. Barsoum, *IIW Recommendations for the HFMI Treatment - For Improving the Fatigue Strength of Welded Joints*. Singapore: Springer Singapore, 2016.

[10] M. H. C. Yildirim and G. B. Marquis, "Overview of fatigue data for high frequency mechanical impact treated welded joints," *Weld. World*, vol. 56, no. 7–8, pp. 82–96, 2012.

[11] H. C. Yildirim and G. B. Marquis, "Fatigue strength improvement factors for high strength steel welded joints treated by high frequency mechanical impact," *Int. J. Fatigue*, vol. 44, pp. 168–176, 2012, doi: 10.1016/j.ijfatigue.2012.05.002.

[12] G. Marquis, "Failure modes and fatigue strength of improved HSS welds," *Eng. Fract. Mech.*, vol. 77, no. 11, pp. 2051–2062, 2010.

[13] T. Wang, D. Wang, L. Huo, and Y. Zhang, "Discussion on fatigue design of welded joints enhanced by ultrasonic peening treatment (UPT)," *Int. J. Fatigue*, vol. 31, no. 4, pp. 644–650, 2009, doi: 10.1016/j.ijfatigue.2008.03.030.

[14] H. Shimanuki and T. Okawa, "Effect of stress ratio on the enhancement of fatigue strength in high performance steel welded joints by ultrasonic impact treatment," *Int. J. Steel Struct.*, vol. 13, no. 1, pp. 155–161, 2013, doi: 10.1007/s13296-013-1014-9.

[15] E. Mikkola, "A study on effectiveness limitations of high-frequency mechanical impact," PhD thesis, Aalto University, 2016.

[16] J. Schijve, *Fatigue of structures and materials*. New York: Springer, 2008.

[17] T. Stenberg, E. Lindgren, Z. Barsoum, and I. Barmicho, "Fatigue assessment of cut edges in high strength steel - Influence of surface quality," *Mater. Werkst.*, vol. 48, no. 6, pp. 556–569, Jun. 2017, doi: 10.1002/mawe.201600707.

[18] P. J. Haagensen, "Chapter 11: Fatigue strength improvement methods," in *Fracture and Fatigue of Welded Joints and Structures*, Woodhead Publishing Ltd., 2011, pp. 297–329.

[19] S. J. Maddox, *Fatigue Strength of Welded Structures*, 2nd ed. Cambridge, UK: Abington Publishing, 1991.

[20] T. R. Gurney, *Fatigue of welded structures*, 2nd ed. Cambridge, UK: Cambridge University Press, 1979.

[21] Eurocode 3, "Design of steel structures - Part 1-9: Fatigue." European Committee for Standardization, 2005.

[22] C. Sonsino, "Damage accumulation under variable amplitude loading of welded medium- and high-strength steels," *Int. J. Fatigue*, vol. 26, no. 5, pp. 487–495, May 2004, doi: 10.1016/j.ijfatigue.2003.10.001.

[23] C. M. Sonsino, H. K. Fmann, R. Wagener, C. Fischer, and J. Eufinger, "Interpretation of Overload Effects Under Spectrum Loading of Welded High-Strength Steel Joints," *Weld. World*, vol. 55, no. 11–12, pp. 66–78, 2013, doi: 10.1007/BF03321544.

[24] M. Khurshid, Z. Barsoum, and G. Marquis, "Behavior of Compressive Residual Stresses in High Strength Steel Welds Induced by High Frequency Mechanical Impact Treatment," *J. Press. Vessel Technol.*, vol. 136, no. 4, p. 041404, Apr. 2014, doi: 10.1115/1.4026651.

[25] E. Mikkola and H. Remes, "Allowable stresses in high-frequency mechanical impact (HFMI)-treated joints subjected to variable amplitude loading," *Weld. World*, pp. 1–14, 2016, doi: 10.1007/s40194-016-0400-2.

[26] H. Polezhayeva, D. Howarth, M. Kumar, B. Ahmad, and M. E. Fitzpatrick, "The effect of compressive fatigue loads on fatigue strength of non-load carrying specimens subjected to ultrasonic impact treatment," *Weld. World*, vol. 59, no. 5, pp. 713–721, 2015, doi: 10.1007/s40194-015-0247-y.

[27] Niemi, Fricke, and Maddox, "Fatigue Analysis of Welded Components (Designer's guide to the structural hot-spot stress approach)." [IIW-XIII-1819-00], 2006.

[28] L. A. Costa Borges, "Size effects in the fatigue behaviour of tubular bridge joints (Thesis No. 4142)," EPFL, Lausanne, Switzerland, 2008.

[29] I. Lotsberg, "Assessment of the size effect for use in design standards for fatigue analysis," *Int. J. Fatigue*, vol. 66, pp. 86–100, Sep. 2014, doi: 10.1016/j.ijfatigue.2014.03.012.

[30] W. Fricke, "Recent developments and future challenges in fatigue strength assessment of welded joints," *Proc. Inst. Mech. Eng. Part C J. Mech. Eng. Sci.*, vol. 229, no. 7, pp. 1224–1239, May 2015, doi: 10.1177/0954406214550015.

[31] T. R. Gurney, "The influence of thickness on fatigue of welded joints - 10 years on (a review of british work)," in *Proc. Eighth Intn. Conference, Offshore Mechanics & Arctic Engng. (8th OMAE)*, The Netherlands, 1989.

[32] C. R. A. Schneider and S. J. Maddox, "Best practice guide on statistical analysis of fatigue data," *Weld. Inst. Rep.*, 2006.

[33] G. Wolf and B. Cartwright, "Rules for coding dummy variables in multiple regression.," *Psychol. Bull.*, vol. 81, no. 3, p. 173, 1974.

[34] S. Skrivanek, "The use of dummy variables in regression analysis," *More Steam LLC*, 2009.

[35] A. Abdullah, M. Malaki, and A. Eskandari, "Strength enhancement of the welded structures by ultrasonic peening," *Mater. Des.*, vol. 38, pp. 7–18, Jun. 2012, doi: 10.1016/j.matdes.2012.01.040.

[36] J. Hrabowski, S. Herion, T. Ummenhofer, and others, "Low-cycle Fatigue of Post Weld Treated Butt Welds Made of High-strength Steels," in *The Twenty-fourth International Ocean and Polar Engineering Conference*, 2014.

[37] L. X. Huo, D. Wang, Y. F. Zhang, and J. M. Chen, "Investigation on Improving Fatigue Properties of Welded Joints by Ultrasonic Peening Method," *Key Eng. Mater.*, vol. 183–187, pp. 1315–1320, 2000, doi: 10.4028/www.scientific.net/KEM.183-187.1315.

[38] J. J. Janosch, H. Koneczny, S. Debiez, E. C. Statnikov, V. J. Troufiakov, and P. P. Mikhee, "Improvement of fatigue strength in welded joints (in HSS and in aluminium alloys) by ultrasonic hammer peening," *Weld. WORLD-Lond.*-, vol. 37, pp. 72–83, 1996.

[39] U. Kuhlmann and H. P. Günther, "Experimentelle untersuchungen zur ermüdungssteigernden wirkung des PIT-verfahrens," *Vers. Univ. Stuttg. Inst. Für Konstr. Entwurf*, 2009.

[40] M. Leitner, M. Stoschka, and W. Eichlseder, "Fatigue enhancement of thin-walled, high-strength steel joints by high-frequency mechanical impact treatment," *Weld. World*, vol. 58, no. 1, pp. 29–39, Jan. 2014, doi: 10.1007/s40194-013-0097-4.

[41] T. Ummenhofer, I. Weich, and T. Nitchke-Pagel, "Extension of Life Time of Welded Fatigue Loaded Structures," presented at the International Society of Offshore and Polar Engineers, 2006.

[42] I. Weich, "Ermüdungsverhalten mechanisch nachbehandelter Schweißverbindungen in Abhängigkeit des Randschichtzustands (Fatigue behaviour of mechanical post weld treated welds depending on the edge layer condition)," Technischen Universität Carolo-Wilhelmina, Braunschweig, Germany, 2008.

[43] T. Deguchi *et al.*, "Fatigue strength improvement for ship structures by Ultrasonic Peening," *J. Mar. Sci. Technol.*, vol. 17, no. 3, pp. 360–369, 2012, doi: 10.1007/s00773-012-0172-3.

[44] N. S. Ermolaeva and M. J. Hermans, "Research on Post-weld Impact Treatments of High-strength Steel," in *The Twenty-fourth International Ocean and Polar Engineering Conference*, 2014.

[45] S.-H. Han, J.-W. Han, Y.-Y. Nam, and I.-H. Cho, "Fatigue life improvement for cruciform welded joint by mechanical surface treatment using hammer peening and ultrasonic nanocrystal surface modification," *Fatigue Fract. Eng. Mater. Struct.*, vol. 32, no. 7, pp. 573–579, Jul. 2009, doi: 10.1111/j.1460-2695.2009.01361.x.

[46] U. Kuhlmann, J. Bergmann, A. Dürr, R. Thumser, H.-P. Günther, and U. Gerth, "Erhöhung der Ermüdungsfestigkeit von geschwei\s sten höherfesten Baustählen durch Anwendung von Nachbehandlungsverfahren," *Stahlbau*, vol. 74, no. 5, pp. 358–365, 2005.

[47] U. Kuhlmann, A. Dürr, and H.-P. Günther, "Improvement of fatigue strength of welded high strength steels by application of post-weld treatment methods," in *IABSE Symposium Report*, 2006, vol. 92, pp. 25–32.

[48] T. Okawa, H. Shimanuki, Y. Funatsu, T. Nose, and Y. Sumi, "Effect of preload and stress ratio on fatigue strength of welded joints improved by ultrasonic impact treatment," *Weld. World*, vol. 57, no. 2, pp. 235–241, 2013.

[49] R. Tehrani Yekta, "Acceptance Criteria for Ultrasonic Impact Treatment of Highway Steel Bridges," University of Waterloo, 2012.

[50] X. Zhao, M. Wang, Z. Zhang, and Y. Liu, "The Effect of Ultrasonic Peening Treatment on Fatigue Performance of Welded Joints," *Materials*, vol. 9, no. 6, p. 471, Jun. 2016, doi: 10.3390/ma9060471.

[51] P. J. Haagensen, E. S. Statnikov, L. Martinez, and S. S. AB, "Introductory fatigue tests on welded joints in high strength steel and aluminium improved by various methods including ultrasonic impact treatment (UIT)," *IIW Doc*, vol. 13, pp. 1748–98, 1998.

[52] P. J. Haagensen and O. Alnes, "Progress Report on IIW WG2 Round Robin Fatigue Testing Program on 700 MPa and 350 MPa YS Steels." 2005.

[53] L. Huo, "Investigation of the fatigue behaviour of the welded joints treated by TIG dressing and ultrasonic peening under variable-amplitude load," *Int. J. Fatigue*, vol. 27, no. 1, pp. 95–101, Jan. 2005, doi: 10.1016/j.ijfatigue.2004.05.009.

[54] V.-M. Lihavainen and G. Marquis, "Estimation of fatigue life improvement for ultrasonic impact treated welded joints," in *ECF15, Stockolm 2004*, 2004.

[55] V.-M. Lihavainen, G. Marquis, and E. S. Statnikov, "Fatigue strength of a longitudinal attachment improved by ultrasonic impact treatment," *Weld. World*, vol. 48, no. 5–6, pp. 67–73, 2004.

[56] G. Marquis and T. Björk, "Variable amplitude fatigue strength of improved HSS welds," *Int. Inst. Weld. IIW Doc. XIII-2224-08*, 2008.

[57] L. Martinez, A. F. Blom, H. Trogen, and T. Dahle, "Fatigue behavior of steels with strength levels between 350 and 900 MPa. - Influence of post-weld treatments.pdf," in *Proceedings of the North European Engineering and Science COnference (NESCO)*, Stockholm, 1997.

[58] S. Vanrostenberghe *et al.*, "Improving the fatigue life of high strength steel welded structures by post weld treatments and specific filler material (FATWELDHSS) final report.," Luxembourg, 2015.

[59] L. C. Wu and D. P. Wang, "Effect of Welding Residual Stress on Fatigue Performance of the Welded Joints Treated by Ultrasonic Peening," *Adv. Mater. Res.*, vol. 418–420, pp. 337–341, 2012, doi: 10.4028/www.scientific.net/AMR.418-420.337.

[60] P. J. Haagensen and S. J. Maddox, "IIW recommendations on post weld fatigue life improvement of steel and aluminium structures," *IIW Doc. XIII-2200r7-07*, 2010.

[61] A. F. Hobbacher, *Recommendations for Fatigue Design of Welded Joints and Components (IIW document IIW-2259-15)*, 2nd ed. Switzerland: Springer International Publishing, 2016.

[62] A. Ohta, T. Mawari, and N. Suzuki, "Evaluation of effect of plate thickness on fatigue strength of butt welded joints by a test maintaining maximum stress at yield strength," *Eng. Fract. Mech.*, vol. 37, no. 5, pp. 987–993, Jan. 1990, doi: 10.1016/0013-7944(90)90022-9.

[63] A. Ohta, Y. Maeda, M. Nihei, and S. Nishijima, "Variable effects of stress relief on fatigue strength of butt welded joints with different plate thickness," *Int. J. Fract.*, vol. 24, no. 3, pp. R81–R87, Mar. 1984, doi: 10.1007/BF00032690.

[64] S. Berge, "On the effect of plate thickness in fatigue of welds," *Eng. Fract. Mech.*, vol. 21, no. 2, pp. 423–435, Jan. 1985, doi: 10.1016/0013-7944(85)90030-X.

[65] N. Yamamoto, M. Mouri, T. Okada, and T. Mori, "Analytical and Experimental Study on the Thickness Effect to Fatigue Strength," *ClassNK Tech. Bull.*, vol. 31, pp. 33–44, Dec. 2013.

[66] J. Yagi, S. Machida, M. Matoba, Y. Tomita, and I. Soya, "Thickness Effect Criterion for Fatigue Strength Evaluation of Welded Steel Structures," *J. Offshore Mech. Arct. Eng.*, vol. 115, no. 1, pp. 58–65, Feb. 1993, doi: 10.1115/1.2920090.

[67] J. W. Fisher, M. D. Sullivan, and A. W. Pense, "Improving fatigue strength and repairing fatigue damage, Dec. 1974," 1974.

[68] S. J. Maddox, "Fatigue of steel fillet welds hammer peened under load, Doc. IIW-1387, Welding in the World," vol. 41, pp. 343–349, 1998.

[69] S. Walbridge and A. Nussbaumer, "Benefits of post-weld treatment to improve tubular bridge fatigue performance," in *IABSE Symposium Report*, 2007, vol. 93, pp. 26–33.

[70] K. Ghahremani, "Predicting the Effectiveness of Post-Weld Treatments Applied under Load," 2010.

[71] S. J. Maddox, M. M. Doré, and S. D. Smith, "A case study of the use of ultrasonic peening for upgrading a welded steel structure," *Weld. World*, vol. 55, no. 9–10, pp. 56–67, 2011.

[72] X. Zhao, D. Wang, and L. Huo, "Analysis of the S–N curves of welded joints enhanced by ultrasonic peening treatment," *Mater. Des.*, vol. 32, no. 1, pp. 88–96, 2011, doi: 10.1016/j.matdes.2010.06.030.

[73] T. Mori, H. Shimanuki, and M. M. Tanaka, "Effect of UIT on fatigue strength of web-gusset welded joints considering service condition of steel structures," *Weld. World*, vol. 56, no. 9–10, pp. 141–149, 2012.

[74] E. Mikkola, M. Doré, G. Marquis, and M. Khurshid, "Fatigue assessment of high-frequency mechanical impact (HFMI)-treated welded joints subjected to high mean stresses and spectrum loading," *Fatigue Fract. Eng. Mater. Struct.*, 2015, doi: 10.1111/ffe.12296.

[75] Eurocode 1, "Actions on structures - Part 2: Traffic loads on bridges." European Committee for Standardization, 2003.

[76] Eurocode 3, "Design of steel structures - Part 2: Steel bridges." European Committee for Standardization, 2006.

[77] G. M. Guðjónsdóttir, "Cost and Environmental Benefits of Fatigue Enhancement of Bridges: A Case Study of a Highway Bridge," Master's thesis, Chalmers University of Technology, 2016.

[78] ISO standard, "Welding – Fusion-welded joints in steel, nickel, titanium and their alloys (beam welding excluded) – Quality levels for imperfections (ISO 5817:2014)." European Committee for Standardization, 2014.

[79] U. Bremen, "Amélioration du comportement à la fatigue d'assemblages soudés - étude et modélisation de l'effet de contraintes résiduelles (Thesis No. 787)," PhD thesis, Ecole Polytechnique Fédérale de Lausanne (EPFL), Switzerland, 1989.

[80] A. Chattopadhyay, G. Glinka, M. El-Zein, J. Qian, and R. Formas, "Stress Analysis and Fatigue of welded structures," *Weld. World*, vol. 55, no. 7–8, pp. 2–21, Mar. 2013, doi: 10.1007/BF03321303.

[81] R. Goyal and G. Glinka, "Fracture mechanics-based estimation of fatigue lives of welded joints," *Weld. World*, vol. 57, no. 5, pp. 625–634, Sep. 2013, doi: 10.1007/s40194-013-0060-4.

[82] O. Vosikovsky and R. Bell, "Fracture mechanics assessment of fatigue life of welded plate T-joints, including thickness effect," in *Proc. 4th Intern. Conf. on Behaviour of Offshore Structures (BOSS '85)*, Delft, the Netherlands, 1985, pp. 453–465.

[83] T. Stenberg, E. Lindgren, and Z. Barsoum, "Development of an algorithm for quality inspection of welded structures," *Proc. Inst. Mech. Eng. Part B J. Eng. Manuf.*, vol. 226, no. 6, pp. 1033–1041, Jun. 2012, doi: 10.1177/0954405412439138.

[84] T. Ishikawa, M. Shimizu, H. Tomo, H. Kawano, and K. Yamada, "Effect of compression overload on fatigue strength improved by ICR treatment," *Int. J. Steel Struct.*, vol. 13, no. 1, pp. 175–181, 2013, doi: 10.1007/s13296-013-1016-7.

[85] L. Martinez and P. J. Haagensen, "Life Extension of Class F and Class F2 Details Using Ultrasonic Peening," *Int. Inst. Weld.*, pp. 1–9, 2006.

[86] M. M. Tai and P. C. Miki, "Improvement Effects of Fatigue Strength by Burr Grinding and Hammer Peening Under Variable Amplitude Loading," *Weld. World*, vol. 56, no. 7–8, pp. 109–117, 2012, doi: 10.1007/BF03321370.

[87] C. Miki and M. Tai, "Fatigue strength improvement of out-of-plane welded joints of steel girder under variable amplitude loading," *Weld. World*, vol. 57, no. 6, pp. 823–840, 2013, doi: 10.1007/s40194-013-0076-9.

[88] L. Martinez, Z. Barsoum, and A. Paradowska, "State-of-the-Art: Fatigue Life Extension of Offshore Installations," pp. 9–20, 2012, doi: 10.1115/OMAE2012-83044.

[89] M. Leitner, M. Ottersböck, S. Pußwald, and H. Remes, "Fatigue strength of welded and high frequency mechanical impact (HFMI) post-treated steel joints under constant and variable amplitude loading," *Eng. Struct.*, vol. 163, pp. 215–223, 2018, doi: 10.1016/j.engstruct.2018.02.041.

[90] L. Huo, D. Wang, and Y. Zhang, "Investigation of the fatigue behaviour of the welded joints treated by TIG dressing and ultrasonic peening under variable-amplitude load," *Int. J. Fatigue*, vol. 27, no. 1, pp. 95–101, 2005, doi: 10.1016/j.ijfatigue.2004.05.009.

[91] K. Ghahremani and S. Walbridge, "Fatigue testing and analysis of peened highway bridge welds under in-service variable amplitude loading conditions," *Int. J. Fatigue*, vol. 33, no. 3, pp. 300–312, 2011, doi: 10.1016/j.ijfatigue.2010.09.004.

[92] K. Ghahremani, S. Walbridge, and T. Topper, "High cycle fatigue behaviour of impact treated welds under variable amplitude loading conditions," *Int. J. Fatigue*, vol. 81, pp. 128–142, 2015, doi: 10.1016/j.ijfatigue.2015.07.022.

[93] J. Berg, N. Stranghoener, A. Kern, and M. Hoevel, "Variable amplitude fatigue tests at high frequency hammer peened welded ultra high strength steel S1100," *Procedia Struct. Integr.*, vol. 2, pp. 3554–3561, 2016, doi: 10.1016/j.prostr.2016.06.443.

[94] M. Leitner, S. Gerstbrein, M. J. Ottersböck, and M. Stoschka, "Fatigue Strength of HFMI-treated High-strength Steel Joints under Constant and Variable Amplitude Block Loading," in *Procedia Engineering*, 2015, vol. 101, pp. 251–258, doi: 10.1016/j.proeng.2015.02.036.

[95] C. Sonsino, "Principles of Variable Amplitude Fatigue Design and Testing," *J. ASTM Int.*, 2004.

[96] C. M. Sonsino, "Fatigue testing under variable amplitude loading," *Int. J. Fatigue*, vol. 29, no. 6, pp. 1080–1089, 2007, doi: 10.1016/j.ijfatigue.2006.10.011.

[97] F. Carlsson, "Modelling of Traffic Loads on Bridges Based on Measurements of Real Traffic Loads in Sweden," Structural Engineering, Lund University, Lund, Sweden, 2006.

[98] F. Carlsson, "Utredning av ekvivalent skadefaktor för utmattningsanalyser av stålbroar, baserad på mätningar av verkliga fordonslaster i Sverige," Structural Engineering, Lund University, Lund, Sweden, TVBK-3062, 2011.

[99] ASTM E1049-85 (2017), "Standard practices for cycle counting in fatigue analysis," *West Conshohocken PA ASTM Int.*, 2011, doi: DOI: 10.1520/E1049-85R17.

[100] T. Yonezawa, H. Shimanuki, and T. Mori, "Influence of cyclic loading on the relaxation behavior of compressive residual stress induced by UIT," *Weld. World*, Nov. 2019, doi: 10.1007/s40194-019-00821-1.

[101] H. Shimanuki, T. Mori, and M. Tanaka, "Study of a Method for Estimating the Fatigue Strength of Welded Joints Improved by UIT," *IIW Doc. XIII-2495*, 2013.

Appendix A

Properties of the case-study bridges

Loads

Calculated self-weight loads per I-beam

Bridge	Steel [kN/m]	Concrete [kN/m]	Pavement [kN/m]
1	3.7	22	6.15
2	5.0	40	11.5
3	2.8	26	8.90
4	4.4	43	10.1

Proportion of traffic load going to investigated beam

The load distribution factor (LDF) is calculated as the ratio of the dimensions A to B. A is the distance between the centre of vehicle/lane to the far beam. B is the distance between the investigated beam and the far beam.

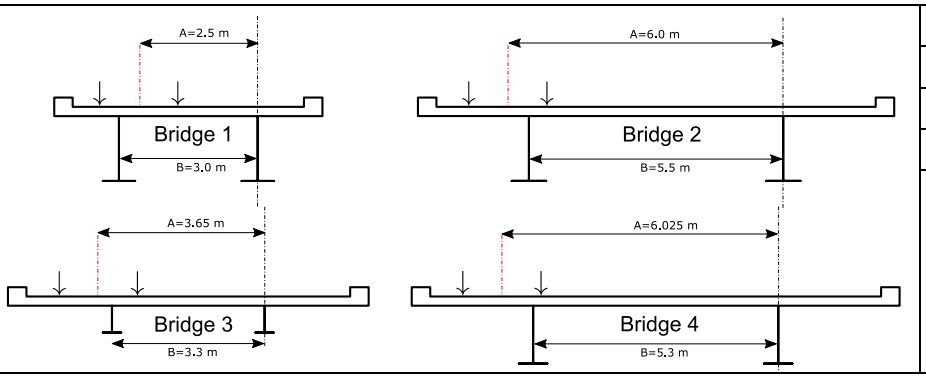

Bridge	LDF
1	0.833
2	1.090
3	1.106
4	1.140

Cross section constants

This part provides the calculated moment of inertia along the bridges considering the variations in steel sections, cracking of concrete and shear lag (effective width of concrete). The values consider short-term effects, i.e. traffic loads. No creep effect is therefore included in the calculations.

Bridge 1

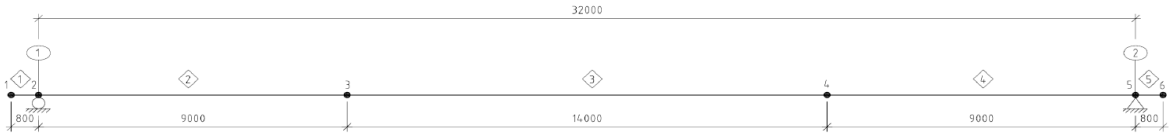

Moment of inertia (short-term)

Coordinate [m]	I [m^4]
0-9	0.0427
9-23	0.0495
23-32	0.0427

Bridge 2

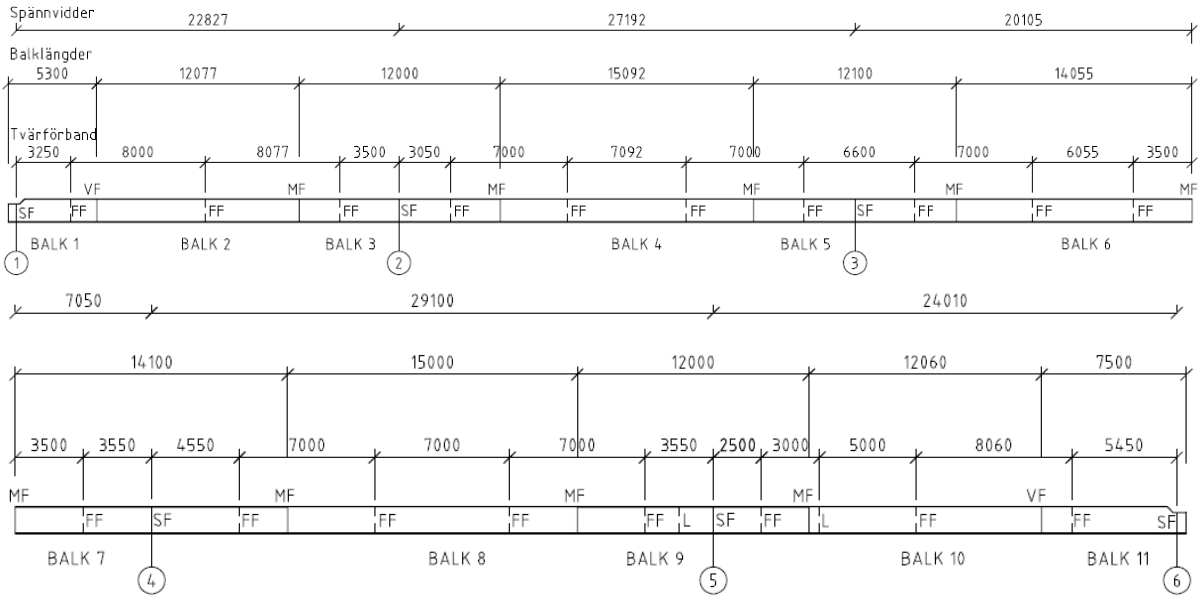

Support coordinates

Support	Coordinate [m]
1	0
2	22.827
3	50.019
4	77.174
5	106.274
6	130.284

Moment of inertia (short-term)

Coordinate [m]	I [mm^4]	Element length
0-4.85	5.94E+10	4.85
4.85-16.927	6.97E+10	12.077
16.927-19.415	7.04E+10	2.488
19.415-28.927	3.23E+10	9.412
28.927-29.677	7.00E+10	0.75
29.677-44.019	7.34E+10	14.242
44.019-45.954	7.24E+10	1.935
45.954-56.119	3.39E+10	10.065
56.119-56.869	7.42E+10	0.75

Coordinate [m]	I [mm^4]	Element length
56.869-70.424	7.68E+10	13.455
70.424-73.109	7.28E+10	2.685
73.109-84.524	3.37E+10	11.065
84.524-99.274	7.39E+10	14.65
99.274-101.909	7.21E+10	2.635
101.909-111.274	3.47E+10	9.265
111.274-112.324	7.07E+10	1.05
112.324-123.334	7.39E+10	11.01
123.334-130.284	7.53E+10	6.45

Bridge 3

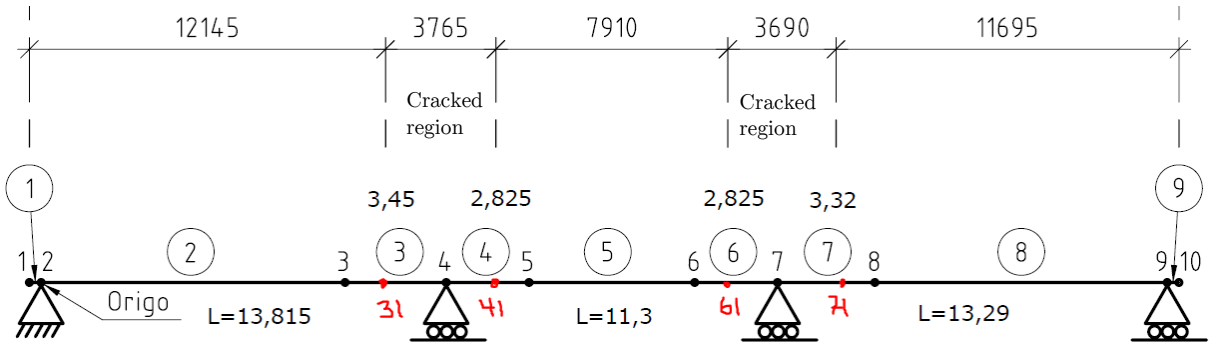

Node coordinates

Node	2	3	31	4	41	5	6	61	7	71	8
Coordinate	0	10.365	11.745	13.815	15.51	16.64	22.29	23.42	25.115	27.11	28.435

Moment of inertia (short-term)

Element	2	3/4	3/4 cracked	5	6/7	6/7 cracked	8
I [m^4]	0.010	0.008	0.003	0.009	0.008	0.003	0.009

Bridge 4

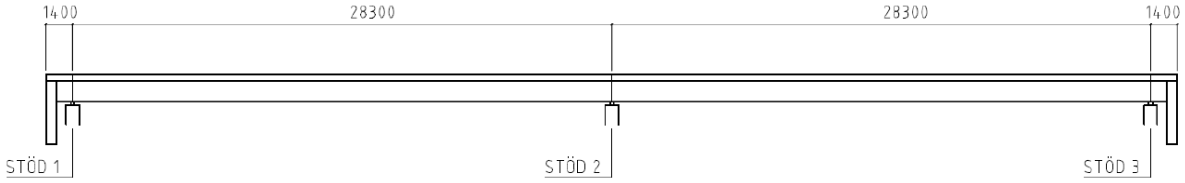

Moment of inertia (short-term)

Coordinate	0-7m	7-24m	24-32.6m	32.6-49.6	49.6-56.6
I [m^4]	0.049	0.055	0.026	0.055	0.049

Section moduli

The section moduli are calculated for the steel sections alone, composite sections with no creep (short-term) and composite sections with long-term creep. Only values for bottom flanges are given here for simplicity. These values were calculated for the bottom of the bottom flanges.

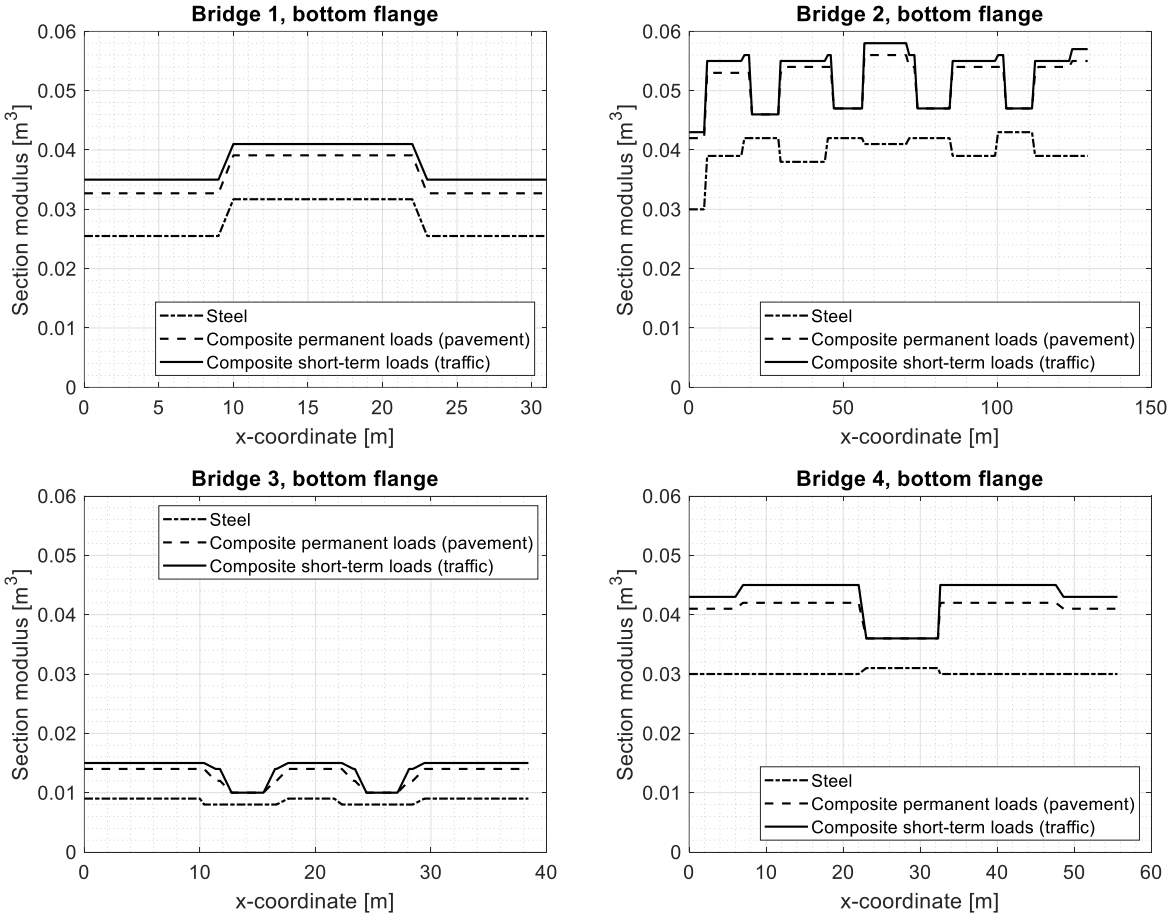

Influence lines

All the produced influence lines are shown here. The influence lines at the damage-critical locations are distinguished with thicker red lines.

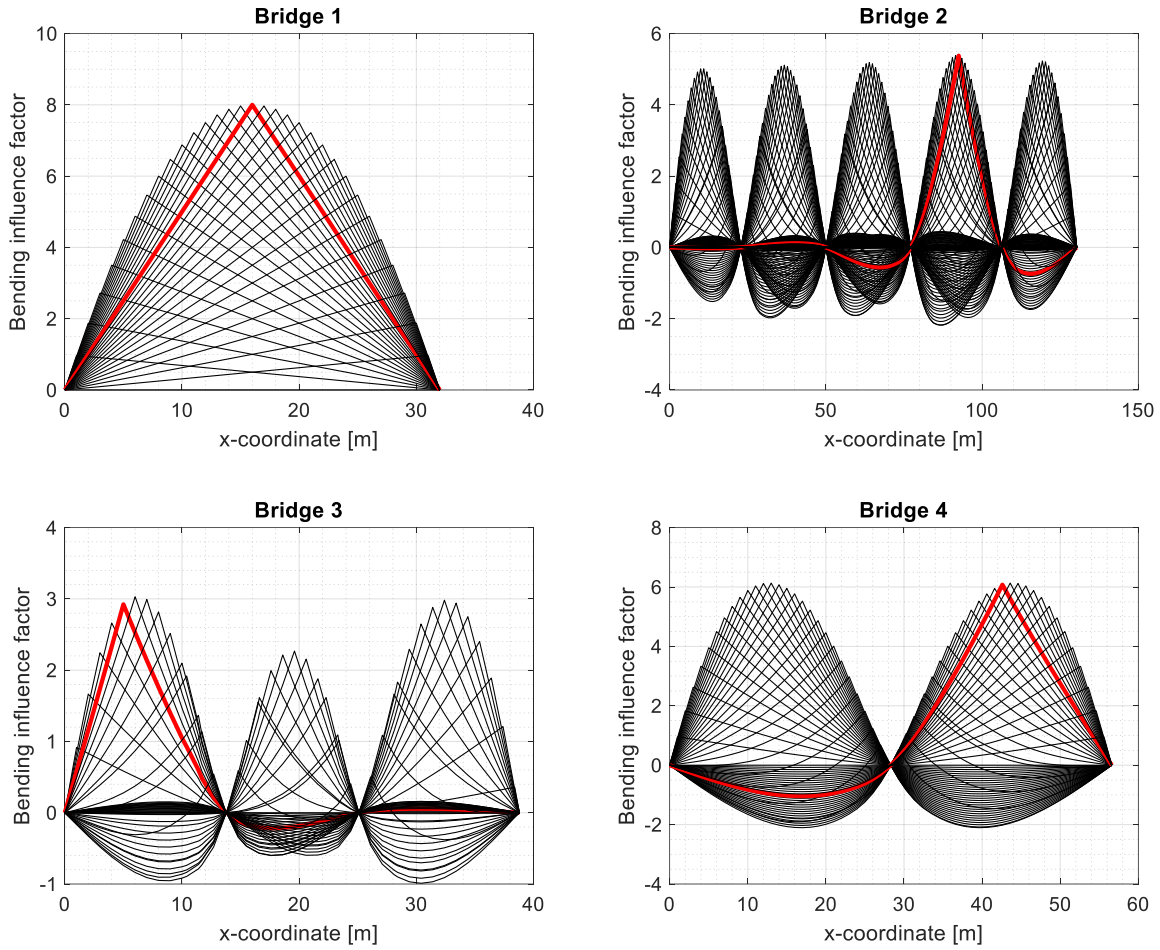

Some stresses

Self-weight stresses

The weight of the steel and the concrete is carried by the steel alone, whereas the weight of the pavement is carried by the composite section (long-term). In this way, the bending moment of each self-weight was divided by the corresponding section modulus and summed together to produce the self-weight stresses shown here.

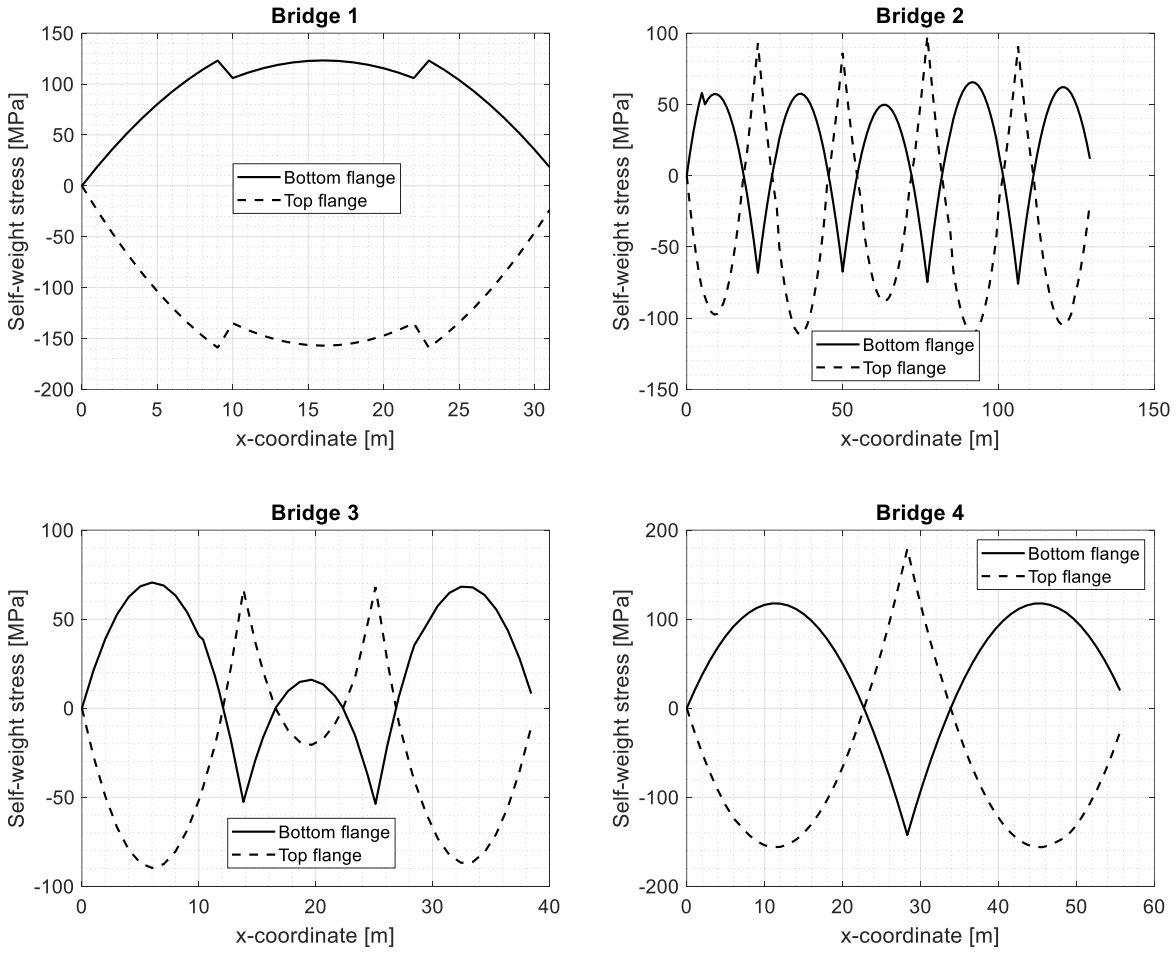

Maximum stress ranges from FLM3

The stress range used in the fatigue design is taken as the maximum stress range produced by the FLM3, ΔS_p. This stress range is depicted here.

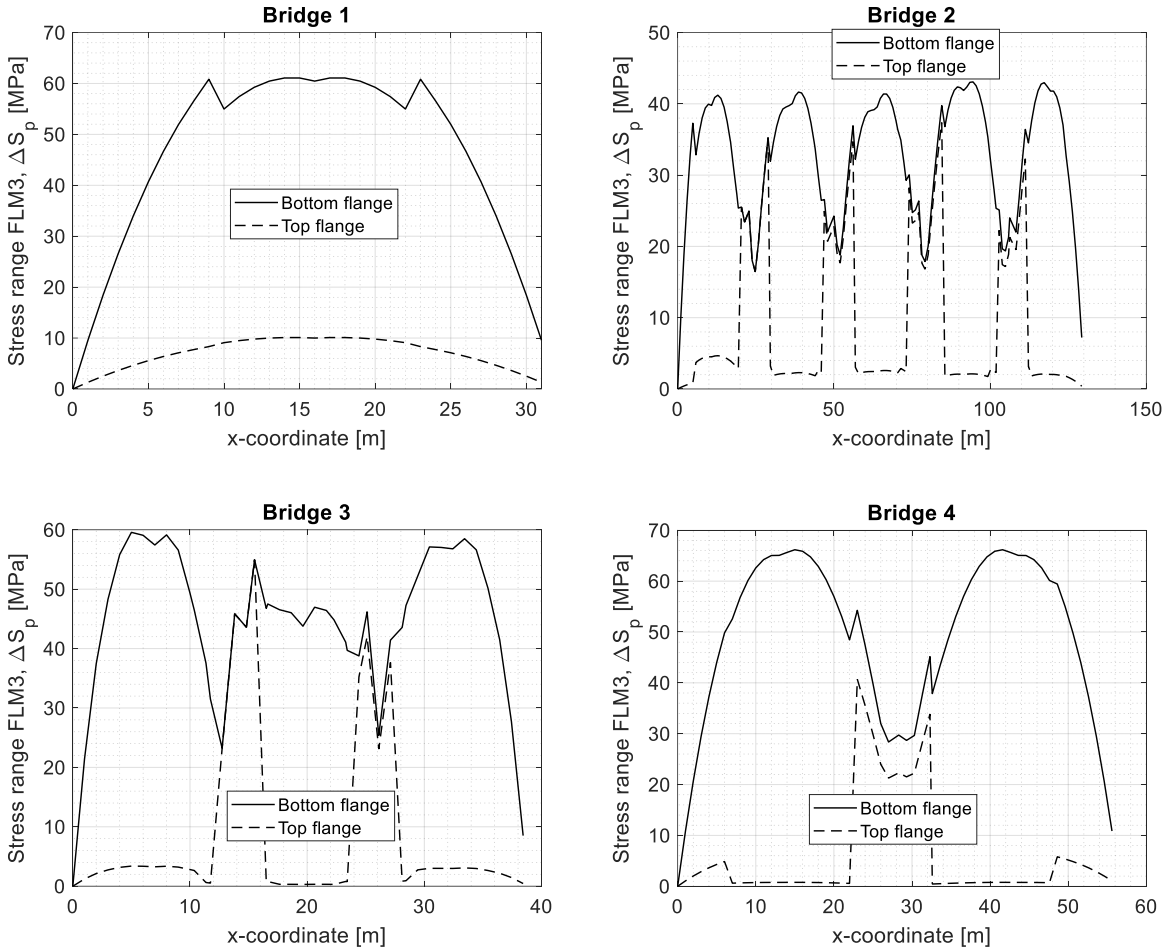

Fatigue design

Some of the involved parameters for the fatigue design of the original bridges is provided here. The λ_1 values are given for the locations with highest ΔS_p.

Bridge	Design life [yrs]	γ_{Mf}	γ_{Ff}	N_{obs}	$\lambda_{1,span}$	$\lambda_{1,supp}$	λ_2	λ_3	λ_4
1	80	1.35	1.0	50,000	2.33	-	0.39	0.96	1.00
2	120	1.35	1.0	50,000	2.36	1.73	0.54	1.04	1.00
3	80	1.35	1.0	50,000	2.51	2.26	0.39	0.96	1.00
4	80	1.35	1.0	50,000	2.37	1.73	0.42	0.96	1.00

Appendix B

Modelling stochastic traffic events

The effect of transverse position of traffic was simply modelled as a random variable from a normal distribution with a standard deviation of 0.23 m. Hence, each vehicle passage was provided a random transverse position.

For simultaneous trucks on bridges, two scenarios were considered; caravans and meetings. First, the number of such events per year was calculated according to Carlsson [97]. For caravan frequencies, Carlsson found that approximately 20% of all heavy trucks travel in caravans of at least two vehicles [97]. The determination of the portion of caravans that were short enough to occur within the lengths of the case study bridges was a difficult task however. As a simplification in this thesis, it was assumed that 15% of all caravans would result in simultaneous trucks on the case study bridges, irrespective of bridge length. This corresponded to 3% of all heavy traffic, i.e. 1500 caravans per year. Assuming a low travel speed of $v = 30$ km/h, the free distance between trucks for each caravan event could be modelled as a random variable from a beta distribution as described by Carlsson [97]. For each caravan event in the Monte Carlo simulation, two random vehicles were chosen from the database and depending on the distance between them, a time-shift was placed on their individual stress-time histories before they were superimposed.

Meeting frequency on the bridges was determined by assuming the same travel speed in both directions of travel, $v = 30$ km/h. The time interval during which a vehicle is on the bridge is $t_{bridge} = L_{bridge}/v$ if the vehicle length is neglected, where L_{bridge} is the total bridge length. In a year, the probability that a heavy vehicle is present on the bridge at any given time interval, t_{bridge}, is $P(1) = N_{obs} \times t_{bridge}/t_{year}$, where t_{year} is the number of seconds in a year. This regards the presence of a vehicle per slow lane. The probability that two heavy vehicles are present on the bridge is $P(2) = P(1)^2 = (N_{obs} \times t_{bridge}/t_{year})^2$ at any given time interval of t_{bridge}, assuming the same traffic intensity in both directions. In one year, there are t_{year}/t_{bridge} number of such time intervals so the number of times two heavy vehicles are on the bridge simultaneously during a year becomes $P(2) \times t_{year}/t_{bridge} = {N_{obs}}^2 \times t_{bridge}/t_{year}$. Meeting trucks were only relevant for Bridge 2 and 4 for which the number of meetings per year was calculated to 1240 and 538, respectively. For each meeting event in the Monte Carlo simulation, two vehicles were randomly selected from the database and a meeting point on the bridge was determined from a uniform probability distribution. The meeting location determined the degree of time-shift between the individual stress-time histories of the trucks which were superimposed.

Appendix C

λ_{HFMI} in the case-study bridges

In section 6.4 of this thesis, the proposed Φ-λ_{HFMI} design curves for mid-span and mid-support sections were compared with just a few cross-sections of each bridge. This appendix provides the real λ_{HFMI} values along the whole bridges, calculated as the actual value, $\Delta S_{eq,R}/\Delta S_{eq}$, and compares these with estimated λ_{HFMI} values, which were obtained with the expressions provided in section 7.2. It can be observed in the figures of this appendix that the proposed design framework predicts conservative λ_{HFMI} values in almost all bridge cross-sections.

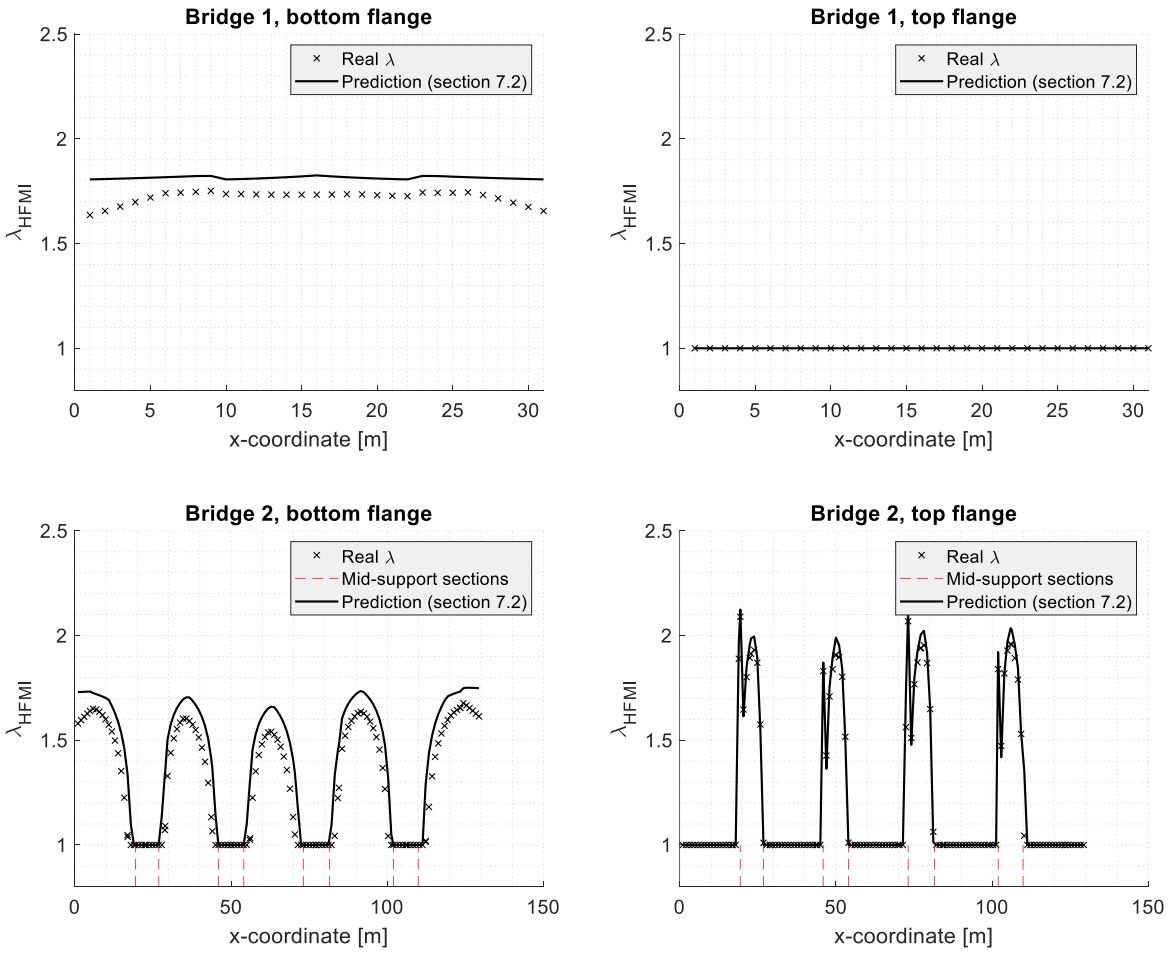

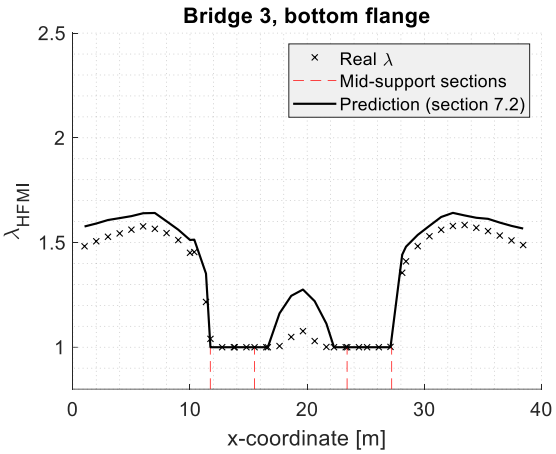
Bridge 3, bottom flange
Real λ
Mid-support sections
Prediction (section 7.2)
λHFMI
x-coordinate [m]

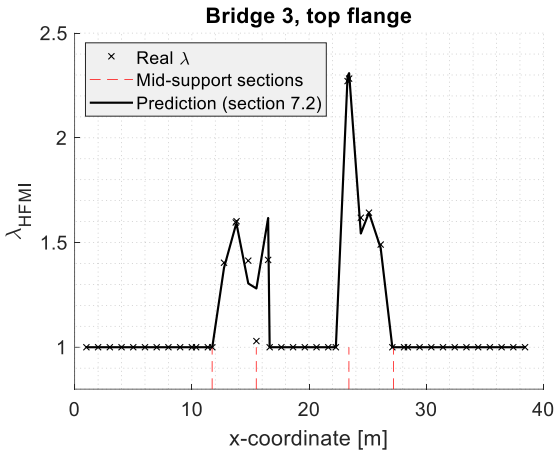
Bridge 3, top flange
Real λ
Mid-support sections
Prediction (section 7.2)
λHFMI
x-coordinate [m]

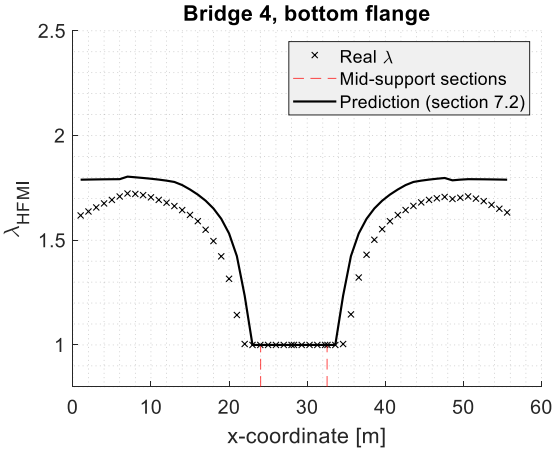
Bridge 4, bottom flange
Real λ
Mid-support sections
Prediction (section 7.2)
λHFMI
x-coordinate [m]

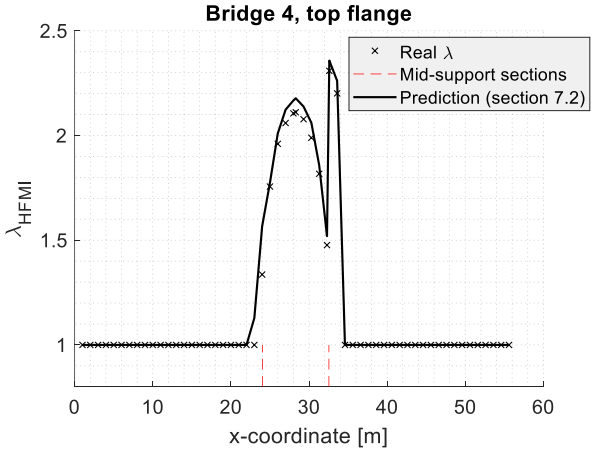
Bridge 4, top flange
Real λ
Mid-support sections
Prediction (section 7.2)
λHFMI
x-coordinate [m]

Appendix D

Prediction of HFMI fatigue strengths

In section 7.1 of this thesis, Equation (17) was used to predict 767 fatigue test results which were collected from the literature. This appendix provides an overview of additional data which were included in the prediction (Table D1). Also, detailed figures with more information is given.

Table D1. Summary of additional data with stress ratios outside the interval of $0 \leq R \leq 0.1$.

Ref	*Authors*	*Detail*	f_y *[MPa]*	R	t *[mm]*	k
[42]	Weich, 2008	B	434, 719	0.5	16	45
[43]	Deguchi et al., 2012	C	355	0.3, 0.5	16	6
[48]	Okawa et al., 2012	C	520	-1.0, 0.5	20	6
[55]	Lihavainen et al., 2004	L	355	0.3, 0.5	5, 8	11
[56]	Marquis and Björk, 2008	L	969	-1.0	6	11
[58]	Vanrostenberghe et al., 2015	L	690 - 960	0.5	5 - 20	34
[59]	Wu and Wang, 2012	L	272	-1.0, 0.5	8	11
[101]	Shimanuki et al., 2013	L	575, 753	0.3 – 0.8	12	61
B = butt weld, C = double-sided transverse attachment, T = single-sided transverse attachment, L = longitudinal attachment, t = main plate thickness, k = number of specimens						

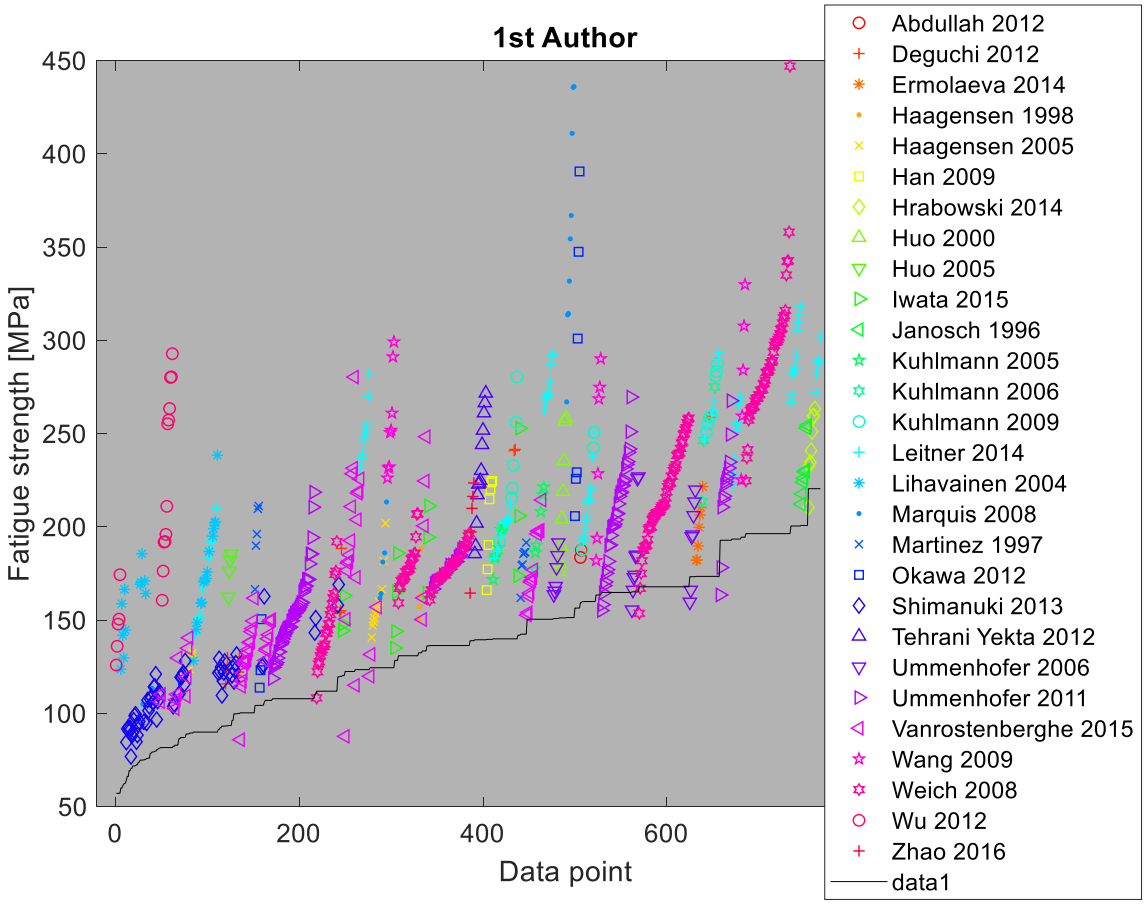

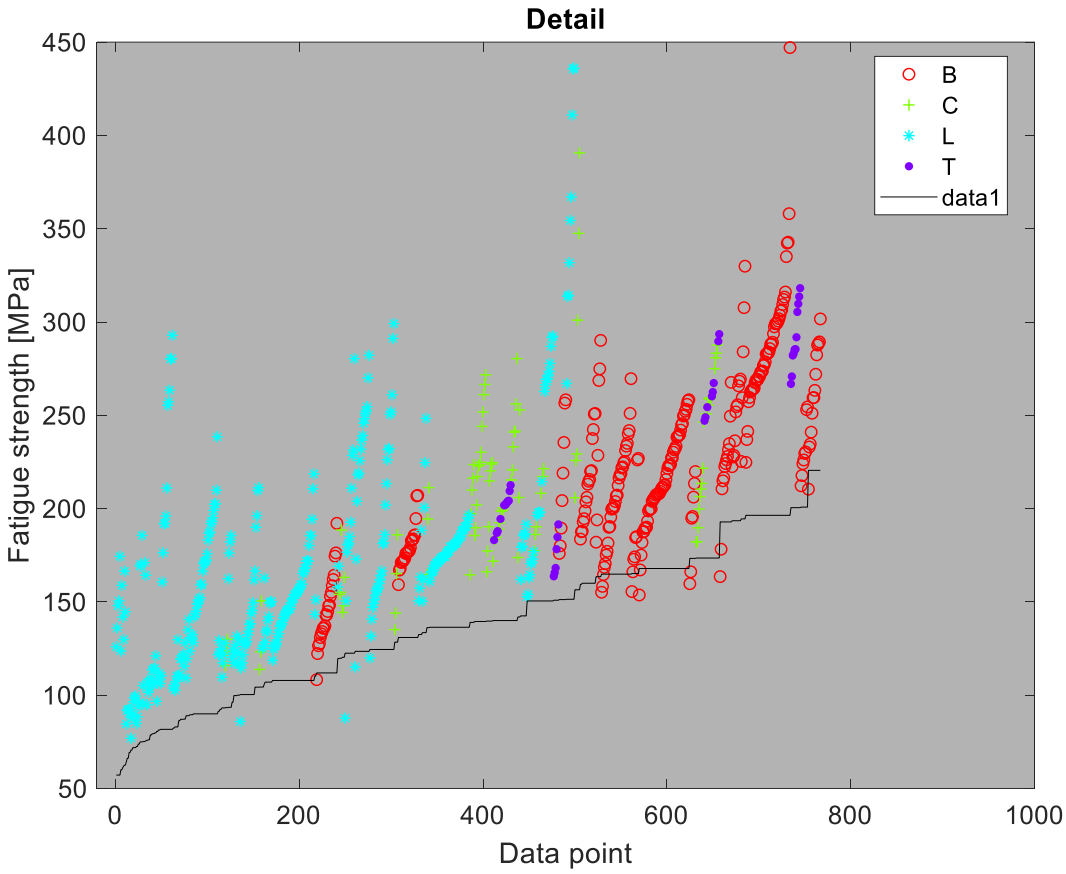
Detail
Fatigue strength [MPa]
Data point
B
C
L
T
data1

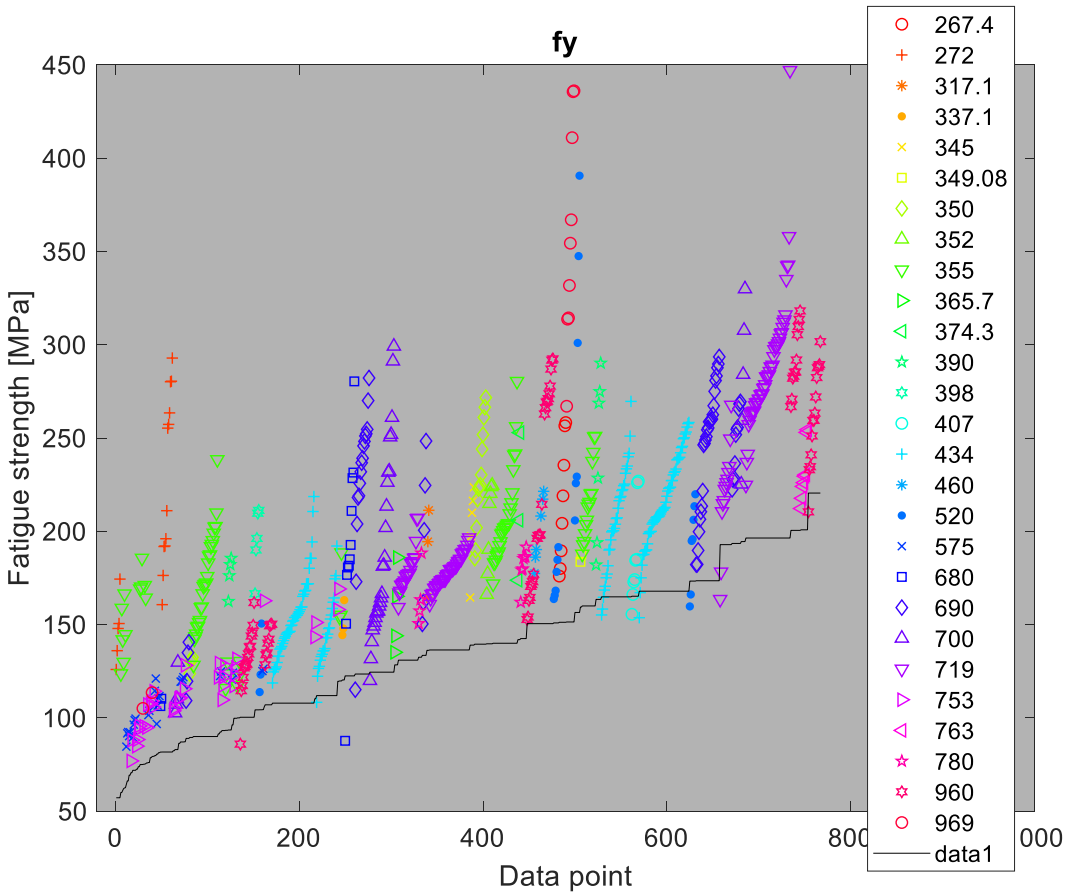
fy
Fatigue strength [MPa]
Data point
267.4
272
317.1
337.1
345
349.08
350
352
355
365.7
374.3
390
398
407
434
460
520
575
680
690
700
719
753
763
780
960
969
data1

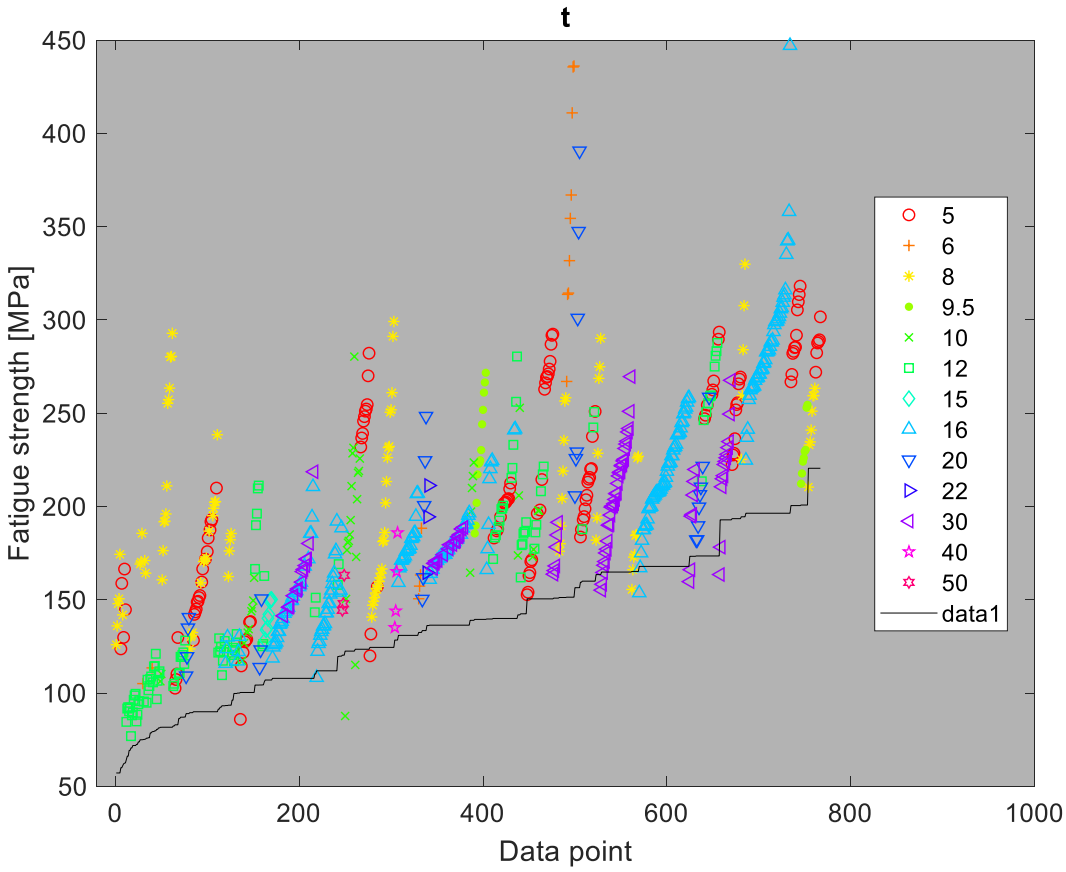
t
Fatigue strength [MPa]
Data point
5
6
8
9.5
10
12
15
16
20
22
30
40
50
data1

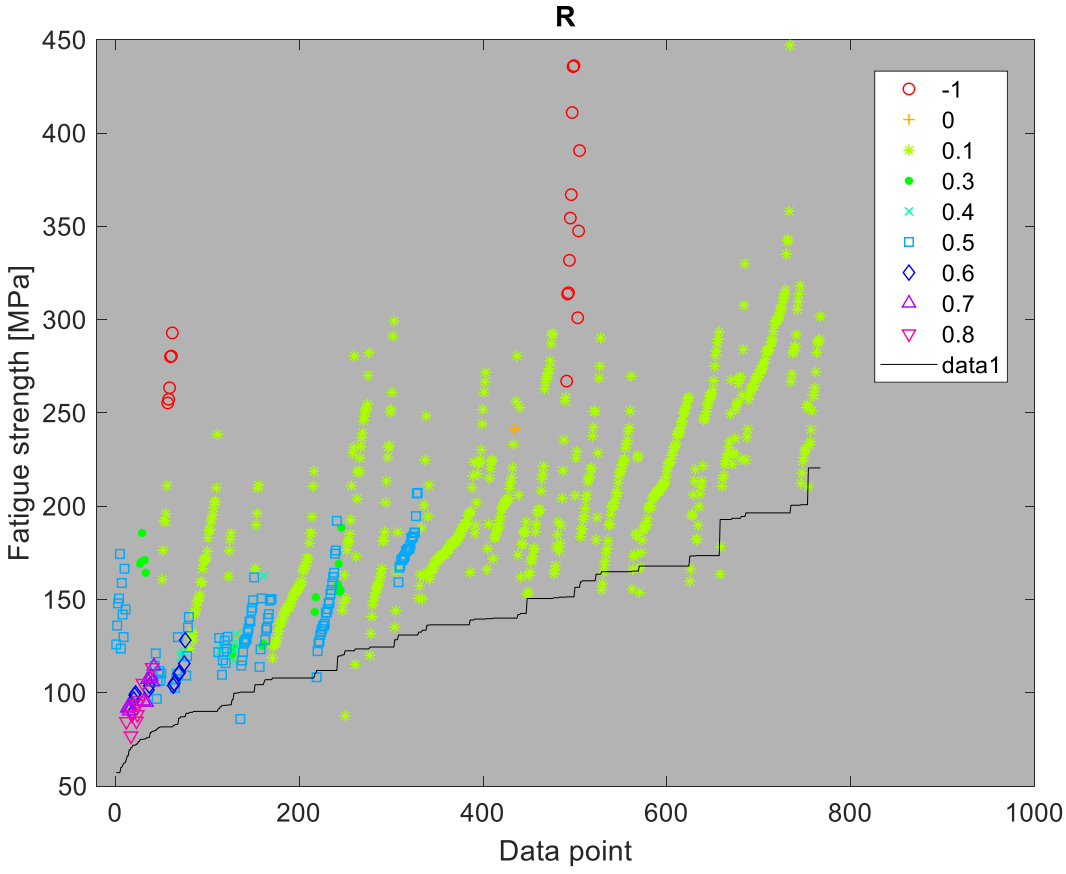
R
Fatigue strength [MPa]
Data point
-1
0
0.1
0.3
0.4
0.5
0.6
0.7
0.8
data1

Appended papers